Regulation of the Endothelial Cell Glycocalyx and its Role in Mechanotransduction

Scott Cooper

Department of Chemical Engineering

McGill University

Montreal, Quebec, Canada

January 2018

A thesis submitted to McGill University in partial fulfillment of the requirements of the degree of Doctor of Philosophy

“Life is like riding a bicycle- in order to keep your balance, you must keep moving forward”

-Albert Einstein

Acknowledgements

I would like to thank my supervisor Richard Leask for his guidance and support throughout my university career. He taught me the intricacies of sound research and his vast knowledge helped propel my studies.

Thank you to Karli McDonald who helped design and initiate research into the glycocalyx in our lab. Without her help, this thesis would have never gotten off the ground. To Alexander Emmott, your help and support was invaluable and made this adventure a lot more fun. To the rest of the Leask lab; Lisa Danielczak, Paul Jonak, Marc-Antoine Campeau, thank you for aiding in experiments and analysis throughout my studies.

I'd like to thank Paulo Saldanha for his mentorship and for opening countless doors to me during my time in Montreal. I owe a huge amount of gratitude to all of the other cherished friends that have been there to support me along the way.

Finally, I'd like to thank my family for their never-ending support, no matter how crazy my dreams may have become. Without you, I would not have had the same confidence to succeed.

Funding: The work in this thesis was supported by grants from the Canadian Institutes of Health Research (CHIR) and the National Sciences and Engineering Council (NSERC). I would like to also thank the McGill Engineering Doctoral Award (MEDA) and the Vadasz Family Foundation and the Eugenie Ulmer Lamothe Fund (EUL) for the scholarships I have received during my studies.

Abstract

Atherosclerosis is an inflammatory disease of the endothelium which is focally concentrated to regions of complex blood flow in the vasculature. Flow fields created in different vascular geometries, such as curvature and bifurcations, result in spatial wall shear stress gradients (WSSGs) which have been found to cause an inflammatory phenotype in endothelial cells (ECs). ECs sense these forces and elicit a biochemical response, a process termed mechanotransduction. Although the specific pathways are still unclear, a dynamic cell-surface proteoglycan layer called the glycocalyx is hypothesized to play a significant role in EC mechanotransduction.

The work in this thesis investigates the regulation of the glycocalyx in regions of WSSGs to better define its role in mechanotransduction. Heparan sulphate, a major component of the glycocalyx, was chosen as a target for degradation to impair the function of the glycocalyx and quantify shedding of the structure. *In vitro* cell culture models mimicking physiologically relevant regions of curvature and vessel stenosis were used in flow experiments to determine their relation to EC health. It was found that in both geometries, WSSGs resulted in an inflammatory EC response including cellular rounding and increased leukocyte adhesion. Enzymatic degradation of heparan sulphate attenuated the morphological response and adhesion patterns in these regions, demonstrating the role of the glycocalyx as a mechanotransducer. In these regions, increased activity of matrix metalloproteinases (MMPs) was also observed and this correlated with shedding of glycocalyx components, suggesting a mechanism by which this structure is regulated when exposed to complex flow.

A sodium-glucose transport protein inhibitor, empagliflozin (EMPA), used to treat hyperglycemia in diabetics, was also tested in flow experiments to investigate its potential pleiotropic effect on EC health. ECs treated with EMPA demonstrated an anti-inflammatory phenotype marked by cellular elongation, decreased leukocyte adhesion and decreased cellular adhesion molecule (CAM) expression. Further, EMPA treatment was shown to improve glycocalyx health and restore heparan sulphate expression following enzymatic degradation. This renewed the mechanotransduction response of ECs to shear stress, helping explain the pleiotropic benefits of EMPA. EMPA therefore presents a clinically relevant strategy to improve glycocalyx health. Together, these results demonstrate the important role that the glycocalyx plays in EC mechanotransduction and regulation in regions of complex flow.

Resumé

L'athérosclérose est une maladie inflammatoire de l'endothélium que l'on retrouve dans les régions où le flux sanguin est irrégulier. Les champs d'écoulement créés selon différentes géométries vasculaires, caractérisées par des courbures et des bifurcations, induisent des gradients dans la contrainte de cisaillement à la paroi (WSSGs). Il a été démontré que ces gradients provoquent un phénotype inflammatoire des cellules endothéliales (ECs). De plus, ces gradients amorcent une réponse biochimique des ECs, soit une réponse de mécanotransduction. Les voies de signalisation de cette réponse demeurent actuellement inconnues. Il est cependant plausible de postuler que le mécanisme de mécanotransduction des ECs réside dans le rôle que joue le glycocalyx, une couche dynamique de protéoglycanes de surface cellulaire.

Dans cette thèse, nous avons étudié la régulation du glycocalyx dans les régions caractérisées par des WSSGs afin de mieux définir son rôle dans les réponses de mécanotransduction. La dégradation du sulfate d'héparane, un composant majeur du glycocalyx, a permis d'altérer la fonction du glycocalyx et de quantifier l'excrétion de sa structure. Des modèles *in vitro* imitant la physiologie de courbure et de sténose vasculaire ont été utilisés dans des expériences de perfusion afin de déterminer comment le flux hydrodynamique affecte les ECs. Il a été démontré que dans les deux types de géométrie, les WSSGs provoquent une réponse inflammatoire des ECs via l'arrondissement cellulaire et l'augmentation de l'adhésion des leucocytes. La dégradation enzymatique du sulfate d'héparane a atténué la réponse morphologique et l'adhésion de leucocytes dans les modèles *in vitro,* ce qui démontre le rôle du glycocalyx comme étant un mécanotransducteur. Dans ces modèles, l'augmentation de l'activité des

métaloprotéases matricielles (MMPs) a été observée et corrélée avec la perte des composantes du glycocalyx suggérant un mécanisme d'action par lequel la structure est régulée suivant une exposition à un flux irrégulier.

Un inhibiteur du transporteur sodium-glucose, l'empagliflozine (EMPA), utilisé pour traiter l'hyperglycémie chez les diabétiques, a été appliqué dans les expériences de perfusion afin d'élucider son effet pléiotropique potentiel sur les ECs. Les ECs traitées avec l'inhibiteur EMPA ont démontré un phénotype anti-inflammatoire caractérisé par une élongation cellulaire, une diminution de l'adhésion des leucocytes et une diminution de l'expression des molécules d'adhésion cellulaire (CAM). De plus, le traitement avec l'EMPA a amélioré l'état du glycocalyx via la restauration de l'expression du sulfate d'héparane suivant la dégradation enzymatique. Cette amélioration de l'état du glycocalyx a permis de rétablir les réponses de mécanotransduction des ECs en réponse aux contraintes de cisaillement sur la paroi. Ces évènements pourraient expliquer les bénéfices pléiotropiques de l'EMPA et pourraient représenter une stratégie clinique afin d'augmenter l'état de santé du glycocalyx.

Finalement, ces résultats démontrent le rôle important que le glycocalyx joue dans la mécanotransduction des ECs et la régulation du glycocalyx dans différents modèles exposés à un flux irrégulier.

Table of Contents

Acknowledgements ..... **iii**

Abstract ..... **iv**

Resumé ..... **vi**

Table of Contents ..... **viii**

List of Figures ..... **x**

List of Abbreviations ..... **xiv**

Thesis Preface ..... **xv**

Contribution of Authors ..... **xvi**

Summary of Original Contributions ..... **xvii**

Chapter 1: Introduction and Hypothesis **1**

1.1 Introduction 1

1.2 Hypothesis 2

Chapter 2: Background and Literature Review **3**

2.1 The Cardiovascular System 3

2.1.1 Components of the Vasculature 3

2.1.2 Atherosclerosis 4

2.1.3 Arterial Hemodynamics 5

2.1.4 Structure of the Endothelial Cell Glycocalyx 9

2.2 Endothelial Cells and the Response to Flow 10

2.2.1 Response to Wall Shear Stress 10

2.2.2 Leukocyte Adhesion 11

2.2.3 Matrix Metalloproteinases (MMPs) 12

2.2.4 Glycocalyx Regulation 13

2.2.5 Mechanotransduction pathways in Endothelial Cells 15

2.3 Diabetes and SGLT-2 Inhibitors 17

Chapter 3: Stenosis hemodynamics disrupt the endothelial cell glycocalyx by MMP activity creating a proinflammatory environment **19**

3.1 Preface Article 19

3.2 Introduction 21

3.3 Materials and Methods 22
3.4 Results 28
3.5 Discussion 34
3.6 Acknowledgements 39
Chapter 4: Increased MMP activity in curved geometries disrupts the endothelial cell glycocalyx creating a proinflammatory environment 40
4.1 Preface Article 40
4.2 Introduction 42
4.3 Materials and Methods 43
4.4 Results 48
4.5 Discussion 56
4.6 Acknowledgements 62
Chapter 5: Empagliflozin promotes glycocalyx health in vitro demonstrating a mechanism for the decreased risk of cardiovascular disease following treatment in type 2 diabetics 63
5.1 Preface Article 63
5.2 Introduction 67
5.3 Materials and Methods 68
5.4 Results 71
5.5 Discussion 76
Chapter 6: Discussion 80
Chapter 7: Conclusions 86
Chapter 8: Future Work 87
References 89

List of Figures

Figure 2-1: CFD velocity plot cross section of flow in a curved vessel demonstrating Dean's vortices (velocity in m/s)..... 8

Figure 3-1: A) velocity contour normalized to inlet velocity of three dimensional, 50% asymmetric stenosis model with regions identified, B) WSS plot across stenosis model at inlet WSS of 10 dyne/cm^2 23

Figure 3-2: A) Morphological response (quantified by shape index) for both static and 24 hour presheared (inlet WSS of 10 dyne/cm^2) cultures, and HS-degraded (DEG) and control (CTL) conditions (n=3). In the inlet and outlet regions, CTL-presheared HAAECs had a significantly lower shape index (Bonferroni post-hoc text, P<0.001) than all other conditions. Representative images of stained HAAECs for the B) CTL-presheared and C) DEG-presheared experiments..... 28

Figure 3-3: Firm leukocyte adhesion of NB4 cells circulating at an inlet WSS of 1 dyne/cm^2 for 1 hour following 24 hours of preshearing (inlet WSS of 10 dyne/cm^2) (n=3). Results for HS-degraded (DEG) and control (CTL) HAAECs are normalized to the inlet location. There was a significant effect on adhesion by location and degradation (two way ANOVA, P<0.00025 and P<0.001, respectively). There was significantly higher adhesion in the acceleration and deceleration regions in control HAAECs (Bonferroni post-hoc test, P<0.01 and P<0.001, respectively)..... 30

Figure 3-4: Firm leukocyte adhesion of NB4 cells statically incubated for 1 hour following 24 hours of preshearing (inlet WSS of 10 dyne/cm^2) (n=3). Results for HS-degraded (DEG) and control (CTL) HAAECs are normalized to the inlet location. There was a significant effect on adhesion by location and degradation (two way ANOVA, P<0.001 and P<0.001, respectively). There was significantly higher adhesion in the deceleration region in control compared to HS-degraded HAAECs (Bonferroni post-hoc test, P<0.001) 31

Figure 3-5: Heparan sulphate (HS) immunofluorescence intensity in control (CTL) and MMP inhibited (GM 6001) HAAECs following 24 hours of preshearing (inlet WSS of 10 dyne/cm^2). HS is significantly down-regulated in the deceleration and outlet regions compared to the inlet in control, presheared models (Bonferroni post-hoc test, P<0.05, n=4). Furthermore, there is a significant decrease in control, presheared HAAEC HS intensity when compared to cultures treated with a general MMP inhibitor (Bonferroni post-hoc test, P<0.05, n=4)..... 32

Figure 3-6: Firm leukocyte adhesion of NB4 cells circulating at an inlet WSS of 1 dyne/cm^2 for 1 hour following 24 hours of preshearing (inlet WSS of 10 dyne/cm^2) (n=3). A general MMP inhibitor (GM6001) was included for presheared HAAECs (GM 6001-Presheared) and compared to control statically cultured and presheared HAAECs, with all values normalized to the inlet location. Preshearing resulted in significantly higher adhesion in the deceleration region in control HAAECs however this response was abolished when GM 6001 was present (Bonferroni post-hoc test, P<0.01, n=3) 33

Figure 4-1: A) WSS plot normalized to inlet WSS of 10 dyne/cm^2 with 3 defined regions of curvature, B) schematic drawing of 180^o curve model with regions of curvature annotated and C) Cross-sectional velocity plots at different positions along the curve demonstrating secondary flows and fluid momentum shift (right: inner wall, left: outer wall) 44

Figure 4-2: Flow diagram of experimental protocol. For all experiments, HAAECs were first grown to confluence for 48hr in the *in vitro* model. If HS degradation was included in an experiment, this was done immediately before experimentation. 24hr preshearing was then performed in an incubator (TNF-α stimulation was done simultaneously for adhesion assays). Models were then either prepared for analysis or exposed to a suspension of NB4 cells which had previously been stimulated with ATRA for 48hr. Following the 1hr adhesion assay, models were prepared for analysis 46

Figure 4-3: A) Analysis of shape index of HAAECs on the inner and outer walls of curvature following 24hr of preshearing at an inlet WSS of 10dyne/cm^2 (n=3, mean SI ± SEM). The inlet wall in the Dean's flow region had a significantly higher SI than the inlet inner wall (Bonferroni post-hoc test, P<0.05). The developing and Dean's flow regions also exhibited a significantly higher SI on the inner wall compared to the outer wall in the same region (Bonferroni post-hoc test, P<0.05 and P<0.05, respectively). Representative images used for analysis from Developing Flow region, with direction of flow indicated, in the B) inner wall of curvature and C) outer wall of curvature 50

Figure 4-4: A) Angle of orientation (absolute value) of HAAECs on the inner and outer walls of curvature following 24hr of preshearing at an inlet WSS of 10dyne/cm^2 (n=3, mean angle ± SEM). Both the inner and outer walls of the inlet were significantly more oriented in the direction of axial flow when compared to static controls (Bonferroni post-hoc test, P<0.01), however, perfused HAAECs were significantly less oriented across the longitudinal axis in the developing flow region (Bonferroni post-hoc test, P<0.01). In both the inner and outer wall of the Developing and Dean's flow regions, HAAECs were significantly less oriented along the vessel axis when compared to their respective inlet control (Bonferroni post-hoc test, P<0.01).

B) Representative cartoon of the angle of orientation (θ) of the longitudinal cell axis with 0° being axial and 90° being circumferential to the channel 51

Figure 4-5: Average position of adhered NB4s relative to the centreline of the with the inner wall in the negative direction and outer wall in the positive direction A) Both circulated (inlet WSS of 1 dyne/cm^2) and non-circulated (no WSS) adhesion assays for statically cultured control (CTL) and HS-degraded (DEG) HAAECs (n=3, mean average position ± SEM). The developing flow region of the circulated adhesion assay showed a significant bias towards the inner wall compared to static controls (Bonferroni post-hoc test, P<0.05). B) Mean average position of circulated (inlet WSS of 1 dyne/cm^2) adhesion assays following 24hr preshearing (inlet WSS of 10 dyne/cm^2). Controls exhibited a significant bias in adhesion to the inner wall in the developing flow region relative to HS-degraded HAAECs (Bonferroni post-hoc test, P<0.01). Representative images used for analysis from the Dean's Flow region with the inner wall on the bottom of C) presheared HAAECs demonstrating inner wall adhesion bias and D) statically cultured HAAECs demonstrating no adhesion bias, where the round cells are the adhered NB4 cells 53

Figure 4-6: Following 24hr of preshearing (inlet WSS of 10 dyne/cm^2), mean fluorescence intensity (n=3, mean intensity ± SEM). of A) of HS which showed a significant decrease in mean intensity in the Dean's flow region relative to the inlet (Bonferroni post-hoc test, P<0.05) and B) Syndecan-1 which also showed a significant decrease in mean intensity in the Dean's flow region relative to the inlet (Bonferroni post-hoc test, P<0.05) 54

Figure 4-7: A) Regional MMP activity quantified by *in situ* gel zymography following treatment of HAAEC with DQ gelatin showing a trend for increased activity throughout the curve and B) Regional MMP activity quantified by *ex situ* gel zymography showing a significant increase in MMP-9 activity in the curve and outlet regions of the model when compared to the inlet (Bonferonni post-hoc test, P<0.05). (n=3, mean intensity ± SEM) 56

Figure 4-8: Flow diagram demonstrating mechanism of increased leukocyte adhesion. Regions of WSSGs elicit an inflamed HAAEC phenotype which includes an increase in MMP activity, causing shedding of the GCX. This shedding decreases the steric hindrance of leukocytes from adhering to the EC surface, and in conjunction with other changes in EC phenotype, results in increased adhesion in these regions 57

Figure 5-1: Analysis of shape index of HAAECs following 24hr of perfusion at a WSS of 10dyne/cm^2 with and without EMPA treatment (n=3, mean SI ± SEM). EMPA significantly elongated cells under static conditions (Bonferroni post-hoc test, P<0.05) 72

Figure 5-2: Total adhered NB4 cells after 24hr exposure to a WSS of 10dyne/cm^2 or statically cultured (n=3, mean ± SEM). EMPA treated HAAECs exhibited decreased NB4 adhesion under both static and perfused conditions (Bonferroni post-hoc test, P<0.01 and P<0.001, respectively). Further, following 24hr exposure to shear, both control and EMPA treated HAAECs exhibited significant lower NB4 adhesion (Bonferroni post-hoc test, P<0.001 and P<0.05, respectively) 73

Figure 5-3: HAAEC surface A) VCAM-1 and B) ICAM-1 expression was quantified through imuunofluorescent imaging following 24hr of exposure to flow at a WSS of 10dyne/cm^2 with and without EMPA treatment (n=3, mean SI ± SEM). For both VCAM-1 and ICAM-1, a significant decrease in IF intensity was observed following perfusion on EMPA treated HAAECs (Bonferroni post-hoc test, P<0.05 and P<0.05, respectively) 74

Figure 5-4: HS immunofluorescence intensity of HAAECs in either static culture or following exposure to 24hr of flow (WSS of 10dyne/cm^2) (n=3, mean IF intensity ± SEM). Experiments were performed on HAAECs immediately following HS-degradation (DEG), immediately following HS-degradation with EMPA treatment during flow conditioning/ static culture (DEG + EMPA) and controls (CTL) and EMPA treated (EMPA) cells. Both EMPA and EMPA+DEG HAAECs exhibited a significantly higher intensity than DEG in static culture (Bonferroni post-hoc test, P<0.05 and P<0.05, respectively) and following flow treatment (Bonferroni post-hoc test, P<0.05 and 0.001, respectively). After flow treatment, CTL HAAECs also exhibited a higher HS intensity than DEG (Bonferroni post-hoc test, P<0.001) 75

Figure 5-5: Shape index (SI) and NB4 adhesion following 24hr of exposure to flow (WSS of 10dyne/cm^2) on HAAECs immediately following HS-degradation (DEG), immediately following HS-degradation with EMPA treatment during flow conditioning/ static culture (DEG + EMPA) and controls (CTL). A) In static cultures, DEG+EMPA HAAECs exhibited a significantly lower SI than both CTL (Bonferroni post-hoc test, P<0.05) and DEG cultures (Bonferroni post-hoc test, P<0.001) (n=3, mean SI ± SEM). Both CTL and DEG+EMPA cultures exhibited a significantly lower SI than DEG HAAECs (Bonferroni post-hoc test, P<0.001). B) NB4 cells were circulated for 1hr (WSS of 1dyne/cm^2) following 24hr flow treatment CTL and DEG+EMPA HAAECs exhibited significantly lower adhesion than DEG cultures (Bonferroni post-hoc test, P<0.001) (n=3, total adhered NB4 ± SEM) 76

List of Abbreviations

ATRA: All-trans retinoic acid
D_N: Dean Number
EC: Endothelial cell
E-Selectin: Endothelial cell-leukocyte adhesion molecule 1
EMPA: Empagliflozin
eNOS: Nitric oxide synthase
ERK: Extracellular signal-regulated kinases
GAG: Glycosaminoglycan
GCX: Glycocalyx
HAAEC: Human abdominal aortic endothelial cell
HS: Heparan sulphate
ICAM-1: Intracellular adhesion molecule 1
M-CPF: Macrophage colony stimulating factor
MMP: Matrix metalloproteinase
NF-κB: Nuclear factor kappa beta
Ox-LDL: oxidized low-density lipoprotein
ρ: density
Re: Reynolds Number
RhoA: Ras homolog gene family, member A
Synd-1: Syndecan-1
T2D: Type 2 diabetes
TGF-β: Transforming growth factor beta
TIMPs: Tissue inhibitors of metalloproteinases
TNF-α: Tumor necrosis factor alpha
μ: Kinematic viscosity
VCAM-1: Vascular cell adhesion molecule 1
VE-Cadherin: Vascular endothelial-cadherin
WSS: Wall shear stress
WSSG: Wall shear stress gradients

Thesis Preface

This is a manuscript-based thesis which consists of the following three manuscripts:

1) **Stenosis hemodynamics disrupt the endothelial cell glycocalyx by MMP activity creating a proinflammatory environment**

   Cooper, S., McDonald, K., Burkat, D., Leask, R.L.

   Ann Biomed Eng. 2017 Sep;45(9):2234-2243. doi: 10.1007/s10439-017-1849-0

2) **Increased MMP activity in curved geometries disrupts the endothelial cell glycocalyx creating a proinflammatory environment**

   Cooper, S., Emmott, A., McDonald, K., Campeau, M.A., Leask, R.L.

   Manuscript accepted with revisions in Annals of Biomedical Engineering

3) **Empagliflozin promotes glycocalyx health in vitro demonstrating a mechanism for the decreased risk of cardiovascular disease following treatment in type 2 diabetics**

   Cooper, S., Hwee, T., Quan, A., Verma, S., Leask, R.L.

   Manuscript prepared to be submitted to Molecular and Cellular Biochemistry

Contribution of Authors

I was first author on all three of the manuscripts presented in this thesis. I performed experiments, acquired and analyzed the subsequent data and wrote the manuscripts. Richard L. Leask was the principle investigator on all three manuscripts and helped conceptualize and design the studies and edited the manuscripts. Subudh Verma and Adrian Quan helped conceptualize the experiments in Chapter 5. The 50% asymmetric stenosis model used in Chapter 3 was previously developed by Leonie Rouleau and the 180^{o} curved model used in Chapter 4 was developed by myself. Enzymatic degradation protocols were developed with Karli McDonald and Lisa Danielczak provided technical help in experiments.

In the manuscript presented in Chapter 3, Daniel Burkat performed the CFD simulations for Figure 3-1. In Chapter 4, Marc-Antoine Campeau and Paul Jonak ran the CFD simulations for Figure 4-1, Alexander Emmott performed experiments and collected data for Figures 4-2 and 4-3 with my help and Karli McDonald ran experiments for the data presented in Figure 4-6a.

Summary of Original Contributions

- Regions of wall shear stress gradients (in an asymmetric 50% stenosis and 180^{o} curve), which are susceptible to disease, lead to an inflammatory endothelial cell phenotype characterized by altered patterns of leukocyte adhesion and rounded morphology, suggesting an area to target for treatment and screening of pathologies.
- Regions of wall shear stress gradients (in an asymmetric 50% stenosis and 180^{o} curve) cause shedding of heparan sulphate and syndecan-1 from the surface of endothelial cells, impairing the glycocalyx and affecting pathways of mechanotransduction.
- Local glycocalyx shedding in regions of wall shear stress gradients (in an asymmetric 50% stenosis and 180^{o} curve) is causally linked to increased activity of matrix metalloproteinases.
- Empagliflozin elicits an anti-inflammatory phenotype in both statically cultured and flow-conditioned endothelial cells characterized by decreased leukocyte adhesion and elongated morphology suggesting a pleiotropic effect that explains the decrease in cardiovascular disease observed clinically.
- Empagliflozin treatment promotes endothelial cell glycocalyx health by increasing surface heparan sulphate expression in static cultures and returns expression to basal levels following enzymatic degradation. This improvement in glycocalyx health can explain the apparent anti-inflammatory phenotype exhibited following empagliflozin treatment.

- Empagliflozin treatment returns normal endothelial cell response to flow following enzymatic degradation of heparan sulphate, further supporting the hypothesis that empagliflozin's effect on glycocalyx health promotes an anti-inflammatory endothelial cell phenotype, decreasing the risk of cardiovascular disease.

Chapter 1: Introduction and Hypothesis

1.1 Introduction

Atherosclerosis, an inflammatory disease, is a leading cause of death in North America and the world [1]. The disease is characterized by the build up of fatty plaques and is observed focally in areas of complex blood flow such as bifurcations and regions of curvature [2]. Endothelial cells (ECs) which line the vasculature respond to hemodynamics and exhibit an inflammatory or "atheroprone" phenotype through upregulation of inflammatory pathways in areas characterized by spatial wall shear stress gradients (WSSGs) [3]. This inflammation is an early step in the progression of atherosclerotic lesions.

In vitro experiments using parallel plate flow chambers and three-dimensional models have studied the EC response to WSS [4]. These models have generated a thorough body of knowledge describing the effect of steady and dynamic WSS on ECs, helping to investigate the connection between hemodynamics and atherosclerosis. Attention has now turned to uncovering the mechanism in which ECs sense these shear fields and transmit this stimulus into biochemical responses within the cell, a process termed mechanotransduction. An extracellular layer called the glycocalyx (GCX), which lines the endothelium, has become a key structure in these studies [5-7].

A comprehensive understanding of the development of atherosclerosis is dependent on a better understanding of GCX regulation and the associated mechanotransduction pathways in ECs. The overall objectives of this thesis were: i) identify the role that the GCX plays in EC mechanotransduction, ii) how the GCX structure is regulated by biomolecules and mechanical

forces and iii) identify the potential therapeutic benefits to the GCX from empagliflozin (EMPA). Three-dimensional tissue culture models with physiologically relevant, complex geometries were utilized to facilitate flow experiments.

1.2 Hypothesis

Experiments to address the objectives of this thesis tested the hypotheses that:

1) The GCX plays a pivotal role in the mechanotransduction of WSSGs
2) The GCX is focally shed in regions of WSSGs
3) EMPA pleiotropically promotes an anti-inflammatory EC phenotype by improving GCX health

By testing these hypotheses, this thesis provides a better understanding of the progression of atherosclerosis in complex vascular geometries and its relationship to GCX health. This work will help researchers and clinicians more efficiently target and screen for disease. Further, understanding how EMPA reduces the risk of cardiovascular disease can help lead to the development of strategies to improve GCX health and help prevent and control disease progression.

Chapter 2: Background and Literature Review

2.1 The Cardiovascular System

2.1.1 Components of the Vasculature

The circulatory system is comprised of a network of arteries, arterioles and arterial capillaries which support the flow of oxygenated blood to the body's tissues, and venous capillaries, venules and veins which return deoxygenated blood from these tissues back to the lungs. This dynamic system supports the transfer of blood and nutrients (electrolytes, proteins, carbohydrates, etc.) while acting as a semi-permeable membrane separating blood from surrounding tissues. The entire vasculature, besides capillaries, is comprised of three layers or "tunics": the intima, media and adventitia [8]. The inner-most layer is the intima which is in contact with blood flow and is comprised of a monolayer of ECs. This layer is the barrier between blood and other tissues and imparts the selective qualities of the vessel membrane. There is also a subendothelial layer which supports the ECs and is comprised of smooth muscle cells and collagen.

The media is the middle layer found immediately below the intima and the adventitia is the final layer encompassing the artery. The media layer is comprised of smooth muscle cells and an extracellular matrix of elastic fibres. This layer is responsible for many of the mechanical properties of vessels and its constriction and dilation are responsible for vasoconstriction and vasodilatation, respectively [9].

2.1.2 Atherosclerosis

Atherosclerosis is pathologically relevant in large and medium sized arteries [10, 11]. It is initiated by dysfunction of the endothelium and the earliest signs of the disease are mediated by the inflammatory cascade. Endothelial dysfunction involves many phenotypical changes including increases in pro-inflammatory cytokines such as tumor necrosis factor alpha (TNF-α). Nuclear factor kappa B (NF-κB) is a regulator of inflammatory and immune genes, apoptosis, and cell proliferation that is activated in atherosclerosis [12, 13]. Translocation of NF-κB to the nucleus regulates inflammatory protein expression such as, intracellular and vascular adhesion molecules (ICAM-1) and (VCAM-1), as well as selectins such as E-selectin [14-17]. Regulation of CAMs induces recruitment of leukocytes, specifically monocytes and T cells, from the blood to the inflamed endothelium. After these cells penetrate the endothelium, macrophage colony stimulating factor (M-CSF) will then induce most migrated leukocytes to behave like macrophages while increasing macrophage proliferation in the intima. M-CSF also activates Ox-LDL receptors on the macrophages and they will eventually form foam cells [18]. Their accumulation leads to the formation of a "fatty streak", the earliest visible sign of atherosclerosis [19, 20]. Clinically, a change of diet or lifestyle can decrease LDL levels and reverse the disease at this early stage [20].

The uptake of Ox-LDLs continues to increase until the macrophages are unable to absorb anymore. Ox-LDLs will then begin accumulating in the macrophages and become toxic to the cells, causing them to rupture and release lipids which then form a developing plaque's lipid core [20].

The body's response is to try to isolate this growing plaque by forming a fibrous cap over the lesion which acts as a barrier between it and the blood flow [19]. T cells release MMPs which disrupt the extracellular matrix in the intima providing the necessary constituents to build the fibrous cap [18]. These enzymes can also degrade other cellular structures, including the glycocalyx (GCX), impairing the health of the surrounding cells.

As the plaque continues to grow, vessel remodelling is inevitable. Negative remodelling occurs when the growing plaque expands into the arterial lumen, restricting blood flow and forming a stenosis [20]. When this stenosis is disturbed, clinically significant manifestations of atherosclerosis occur. Two of the most dangerous of these events are plaque destabilization which exposes the thrombogenic subendothelium to blood, forming clots, or detachment of pieces of the plaque which migrate downstream with the flowing blood. Once mobile, they can potentially be degraded by the fluid flow, preventing pathological events, or they can remain intact and become lodged and fully impede a smaller artery. This will inevitably lead to tissue necrosis due to oxygen no longer being delivered to the area. This can cause severe pathologies such as gangrene, myocardial infarction or stroke in cerebral vessels [20].

2.1.3 Arterial Hemodynamics

The compliance of arteries as well as the pulsatile nature of blood flow complicate the flow profiles in the vessels and without assumptions, would be very difficult to determine. To simplify the fluid dynamics for *in vitro* models, researchers commonly assume blood flow through medium arteries to be steady, incompressible and Newtonian with a no-slip boundary

condition [21]. Determination of laminar flow can be validated using the Reynolds Number, Re, which is the ratio between viscous and inertial forces in a fluid:

$$Re = \frac{\rho V D}{\mu}$$

Where ρ is the density of the fluid, V is the average velocity, D is the vessel diameter and μ is the kinematic viscosity of the fluid. A Reynolds Number below 2300 indicates laminar flow in straight, rigid tubes with steady flow. The average values for the coronary artery fall between 150-300 demonstrating the flow is well within the laminar regime [21, 22].

With these assumptions, the Navier-Stokes Equation, which governs fluid flow, can be solved to yield a solution in the form of Hagen-Poiseulle Flow. This simplifies to a fully developed hemodynamic velocity profile, v, as a function of the arterial radius, r:

$$v(r) = 2\left(\frac{Q}{\pi R^2}\right)\left[1 - \left(\frac{r}{R}\right)^2\right]$$

Where Q is the volumetric flow rate and R is the vessel radius.

WSS is the tangential force per unit area that a flowing fluid imposes on the wall of a vessel. For a material with a constant dynamic viscosity, termed a Newtonian fluid, the WSS, τ_w, evaluated at the wall can be presented as:

$$\tau_w = \mu\gamma|_{r=R}$$

Where γ is the shear rate. Various components of blood such as red blood cells tend to make blood act as a Non-Newtonian fluid for shear rates less than 100-200 1/s [9]. However, from the relatively high shear rates caused by flow throughout the vasculature, blood is commonly

assumed to be in the Newtonian regime and maintains a constant viscosity of around 3.5cP for shear rates above this threshold [22].

For Hagen-Poiseulle Flow the shear rate can be defined as:

$$\gamma|_{r=R} = \left.\frac{dv(r)}{dr}\right|_{r=R} = \frac{4Q}{\pi R^3}$$

By combining the above equations, the WSS within an artery can be approximated as:

$$\tau_w = \mu\frac{4Q}{\pi R^3}$$

WSS values have been shown to vary between 5-70 dyne/cm^2, *in vivo,* however average values within the coronary artery have been found to be approximately 15 dyne/cm^2 [23, 24]. Spatial WSS gradients (WSSGs) at the vessel wall can be calculated by the change in WSS given a distance along the vessel, L:

$$WSSG = \frac{d\tau_w}{dL}$$

In curved vessels, fluid momentum creates complex spatial WSSGs and this phenomenon was first described by Dean in the 1920s [25, 26]. Centrifugal forces cause the bulk fluid motion to shift to the outer wall of curvature, creating a differential WSS between the inner and outer wall of curvature, with lower values observed on the inner wall. Secondary flows sweep fluid flow to the outer wall of curvature through the centre of the channel which is redistributed to the inner wall along the circumference of the channel. This results in two counter-rotating vortices, termed Dean vortices, which are a hallmark of fully developed Dean flow, Figure 2-1.

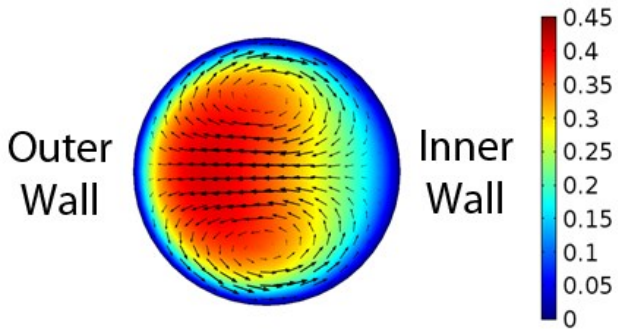

Figure 2-1: CFD velocity plot cross section of flow in a curved vessel demonstrating Dean vortices (velocity in m/s).

These complex flows create an M-shaped velocity profile as opposed to the aforementioned parabolic profile which describes flow in a straight vessel [27].

The dimensionless parameter, Dean Number (D_N), is used to describe laminar flow through curved vessels. It takes into consideration the ratio of the channel radius, R, to the radius of curvature, A, using the curvature ratio, δ, is defined as:

$$\delta = \frac{R}{A}$$

Consequently, D_N can be described as:

$$D_N = \sqrt{\delta} \cdot Re$$

This parameter can be applied to laminar blood flow in curved arteries. *In vivo*, D_N values range from 10 to 700 throughout different regions of the vasculature, with the highest values occurring in the aortic arch [9]. As the D_N increases, both the axial velocity and the velocity of the secondary vortices increases. This is accompanied by an increased fluid flow bias to the outer wall of curvature[28].

2.1.4 Structure of the Endothelial Cell Glycocalyx

The GCX is a layer of membrane-bound macromolecules which lines the apical side of the endothelium and is approximately 150-400nm thick, *in vivo* [29]. Its extension into the vessel is dependent on pH and the protein content of its environment. For example, sphingosine-1-phosphate is a component of plasma which binds to albumin and its reduction can result in up to a 20% drop in GCX coverage, *in vitro* [30]. Similarly, the concentration of various cations has been shown to drastically affect GCX extension [31-35]. A less extended GCX is commonly found *in vitro* compared to that of an *in vivo* endothelium, making it a difficult structure to investigate. It is debated whether this is a consequence of imaging techniques or a change in expression due to the cellular environment [36].

The major components of the GCX include: glycoproteins, syndecans, proteoglycans and glycosamioglycans (GAGs). The net negative charge of the GCX is largely due to glycoproteins which bear oligosaccharides containing terminal sialic acids. Syndecans are a family of transmembrane proteins containing membrane-bound glypicans and the basement matrix-associated perlecans. Linker molecules bind the cytoplasmic tails of the syndecans to the EC cytoskeleton and this allows them to distribute forces throughout the cell. Syndecans contain binding sites for various GAGs and important biomolecules like glypican-1 which contains caveolae housing signalling molecules such as nitric oxide synthase (eNOS). Proteoglycans are bound to corresponding GAGs which impart a negative charge due to their polyanionic constituents. Heparan sulphate (HS), chondroitin sulfate and hyaluronic acid are GAGs associated with the GCX with HS accounting for 50-90% of total GAGs in ECs [37].

The actin filaments of the cytoskeleton construct an intricate network under the plasma membrane called the actin cortical web which anchors the GCX. The "bush like" structure allows the GCX to act as a permeability barrier restricting the transport of inflammatory cells and molecules to the EC surface. The EC surface is also insulated from shear forces by the GCX as the WSS is dissipated mainly in the tips of the structure [38]. As a result of the inefficiency of force penetration, negligible shear acts on the apical EC surface.

2.2 Endothelial Cells and the Response to Flow

2.2.1 Response to Wall Shear Stress

The inflammatory nature of atherosclerosis has led to a focus on EC phenotype and the role of WSS. Steady, uniform WSS at physiologically relevant values promotes an anti-inflammatory morphology characterized by cellular elongation and orientation in the direction of flow which is believed to help reduce shear gradients along the cell surface [39]. This morphological adaptation is accompanied by a reorganization of F-actin filaments into bundles of stress fibres which also align in the direction of flow [40]. Numerous biomolecules that help promote a healthy, anti-inflammatory phenotype are modulated by uniform WSS including the upregulation of eNOS, increasing vascular levels of NO [41] and superoxide dismutases [42].

Conversely, in situations of complex hemodynamics characterized by WSSGs and unsteady flow, ECs exhibit an inflammatory phenotype. This includes a more rounded, cobblestone-like morphology [43], increased proliferation rate and increased migration speed [44]. Disturbed flow also increases expression and activation of pro-inflammatory biomolecules such as MCP-1, NADPH oxidase and MMPs [45].

There are several key transcription factors that are regulated in response to WSS and alter gene expression. These can be activated by pro-inflammatory cytokines such as TNF-α and Interleukin-1 and β which can be produced from activated macrophages and other inflammatory and vascular cells [46]. NF-κB, a member of the Rel family of DNA binding proteins, plays a key role in the inflammatory response. It has been shown to exhibit increased activity in atherosclerotic lesions and has been linked to the upregulation of genes implicated in the EC inflammatory response including E-selectin, ICAM-1, VCAM-1 [47] and MMP-9 [48]. This is crucial as NF-κB is activated in regions of WSSGs [49, 50].

2.2.2 Leukocyte Adhesion

Leukocyte adhesion, a hallmark of the early progression of atherosclerosis, is also modulated in response to WSS. A cascade of events leads to firm leukocyte adhesion beginning with "tethering and rolling" of leukocytes along the endothelium which is induced by P- and E-selectin [51]. In ECs, P-selectin is constitutively expressed and released upon stimulation whereas E-selectin is synthesized and expressed in direct response to stimulation. These molecules interact with L-selectin which is expressed on leukocytes resulting in weak bonds forming and subsequently breaking, as leukocytes roll across the endothelium. Chemokines are secreted by circulating leukocytes as well as ECs which increases integrin expression on the surface of leukocytes. Increases in chemokine expression have been found to be antagonized by WSS acting on ECs [52]. Certain integrins such as β_2-integrins bind to ICAM-1 and others such as $\alpha_4\beta_1$-integrins bind to VCAM-1. Leukocytes tethering and rolling across the endothelium will eventually slow, allowing the formation of integrin-CAM binding complexes and firm adhesion [53]. This process is closely regulated in response to flow with uniform WSS, downregulating

VCAM-1 at the protein transcript level subsequently decreasing adhesion. Inversely, VCAM-1, is upregulated, increasing adhesion in regions of WSSGs [4].

2.2.3 Matrix Metalloproteinases (MMPs)

MMPs are a group of over 20 zinc-dependent proteolytic enzymes. They can be categorized into 4 major sub groups: collagenases (MMP-1, -8, -13 and -14), gelatinases (MMP-2 and -9), stromelysins (MMP -3, -10 and -11) and a final miscellaneous group. They play a pivotal role in the regulation of human tissue and are implicated in extracellular matrix remodelling which can be either beneficial or pathological. The majority of MMPs are secreted proteins, being released from cells in either their pro- or latent form in response to stimuli[54]. There are however there are 6 so called membrane-bound/ membrane-type MMPs (MT-MMPs) which have transmembrane domains. In vascular biology, the gelatinases, MMP-2 and MMP-9, are the focus of many studies, however, several other MMPs are commonly implicated in vascular remodelling. These MMPs are secreted in a latent pro-form containing a cysteine switch which can be activated through chemical agents and reactive oxygen species, *in vitro*, and through serine proteinases and even other MMP molecules *in vivo* [54, 55]. Tissue inhibitors of metalloproteinases (TIMPs) are a class of endogenous inhibitors of MMPs and once the pro-domain of the secreted MMPs is cleaved, TIMPs can further regulate activity through the binding of their N-terminal region to the catalytically active site of MMPs [56]. There are four members of the TIMP family and TIMPs 1 and 2 are commonly regarded as the most potent inhibitors of MMPs [57].

Many factors including inflammatory cytokines (such as TNF-α), hormones, growth factors and oncogenes can induce MMP expression [57, 58]. Most members of the MMP family share similar elements in their promoters resulting in frequent co-expression even though they have distinct expression pathways. Groupings of MMPs based on their regulation mechanisms link the majority into a single group (MMP-1, -3, -7, -9, -12, -13 and -19) and split most of the remaining into two smaller groups [59]. Expression can occur through many pathways, for example, cell-cell contact in ECs has been shown to downregulate MMP-2 and MMP-9 expression, coinciding with an increased expression of VE-cadherin [60].

MMPs have been directly related to activation of various pathways which can become pathologically relevant. MMP-2 and MMP-9 can release TGF-β from an extracellular complex increasing activity and can therefore alter cell migration [61]. Furthermore, TGF-β has been shown to increase the half life of mRNA which codes for MMPs such as MMP-9, demonstrating their positive feedback relationship. Synd-1 sequesters many chemokines, which can play a key role in leukocyte adhesion and subsequent migration through the endothelium, and consequently shedding of these proteoglycans through the action of MMPs can release these molecules, increasing cellular mobility [62].

2.2.4 Glycocalyx Regulation

Uniform WSS promotes the health and extension of the EC GCX. Regions of steady, laminar WSS elicit an increased expression of GCX components such as HS whereas WSSGs have been shown to shed HS [63]. This shedding can lead to an impaired response to WSS in ECs, including a more rounded morphology and increased leukocyte adhesion [64]. The regulation of GCX

components has also been linked closely with MMP expression. Magid *et al* found that oscillatory WSS significantly upregulated MMP-9 expression and resulted in a 10-fold increase in activity compared to controls exposed to steady WSS while not affecting expression of its regulatory inhibitor, TIMP-1 [65]. In a simulated bifurcation *in vitro* model, Wang et al observed upregulation and increased activity of MMP-2 and MMP-9 in regions of WSSGs [66]. A cobblestone-like, rounded morphology characteristic of regions of WSSGs has been linked with increased MMP-2 expression in ECs [67] and studies have linked MMP expression with NF-κB activity [48]. Although the mechanisms of GCX shedding are not fully understood, a variety of MMPs have been linked to its different components such as: MMP-9 cleaving HS [68], MMP-1 and MT1-MMP (MMP-14) cleaving synd-1 preferentially at the Gly^{245}-Leu^{246} peptide bond [69, 70], MMP-2, MMP-7, MMP-9 cleaving chondroitin sulphate [71] and a correlation*, in vivo*, between MMP-2 expression and atherosclerosis [72].

In vivo, observations of increased GCX shedding have been linked to numerous conditions including both acute and chronic hyperglycemia in diabetics [29, 73], atherosclerosis [74, 75], ischemia/ reperfusion [76-78] and patients with severe burns [79] and other trauma [80]. Shedding in such conditions can be mediated by a variety of factors. For example, reactive oxygen species and nitrogen species have been observed to directly cleave HS, hyaluronic acid and chondroitin sulphate. They have also been shown to activate MMPs and inactivate endogenous protease inhibitors further potentiating the proteolysis of the GCX [81]. In type 2 diabetes, GCX impairment has been linked to increased glucose concentration (without a causal mechanism being identified) [73] as well as altered HS biosynthesis [82].

Currently there are very few clinical strategies to promote GCX health but the suggested use of antithrombin III and the infusion of human plasma albumin are being investigated as ways to stabilize the GCX structure and direct inhibition of TNF-α has been proposed to limit degradation of GCX components [83]. Further, drugs such as sulodexide have been developed which introduce exogenous HS to improve GCX health [84, 85].

2.2.5 Mechanotransduction Pathways in Endothelial Cells

Observing the changes in EC phenotype in response to flow has garnered interest in mechanotransduction pathways. This process involves several sequential steps initiated first by deformation of components at the cell surface, followed by transmission of stress into and through the cell. Next, changes in chemical activity in response to the mechanical force will initiate downstream biochemical activity [86]. Although certain pathways can bypass intracellular stress transmission [87] most shear-mediated signalling highlights the role of the cytoskeleton in the transmission of forces leading to a “decentralized” model of mechanotransduction. This model proposes that most cell signalling occurs after the forces acting on structures at the apical surface of the cell are transmitted intracellularly through the actin network that comprises the cell cytoskeleton. The cytoskeleton is held under tension to provide cell stiffness and maintain the shape of the cell. The importance of this integrity has been highlighted by Malek et al who showed that even small interferences in cytoskeletal assembly can inhibit flow responses [88]. Although several regulators of actin cytoskeletal remodelling exist, RhoA is an important molecule because of its role in the formation of actin stress fibres [89]. Specifically, RhoA translocates to the membrane in response to WSS and subsequently activates important transcription factors through c-Jun NH2-terminal kinases

which mediate the EC shear response [90]. Studies have shown that inhibiting Rho blocks cellular responses to WSS, highlighting its role in mechanotransduction [90, 91]. One particular area of interest in cytoskeletal force transmission is at focal adhesion sites where the initiation of mechanically stimulated signals can occur as well as rapid responses from shear sensitive proteins such as platelet EC adhesion molecule 1 (PECAM-1) [92]. In general, junctional sites tend to be abundant in adaptor proteins, enzymes and cofactors which elicit mechanotransduction responses [93]. Other signalling molecules such as VE-cadherin [94] and stretch activated cation and K+ channels [95] are regulated at these junctions.

The GCX as a location of mechanotransduction for ECs has been increasingly supported and an analogy has been made as blood flow being the "wind in the trees" of this structure. Simply explained, wind (blood flow) is sensed by the branches (GAGs) and this force is transmitted to the ground (membrane and/or cytoskeleton) through the tree trunk (core proteins) [96]. Weinbaum *et al* found that a near zero fluid velocity is found at the cell membrane (0.2% of centerline velocity [38]) which helps strengthen the hypothesis that the GCX is transmitting signals to the rest of the cell. Theoretical calculations have suggested that the GCX can attenuate the WSS felt by the apical cell surface with some claiming that no WSS reaches the plasma membrane [97]. Further studies found that the "bush like" structures help increase the force felt by the core proteins allowing these core proteins (with a relatively high flexural rigidity of 700pN-nm^2) to act as cantilever beams which can exert a torque on the cytoskeleton [38]. This force transmission relates to several “decentralized” pathways of mechanotransduction including: FAK activation in response to changes in cytoskeleton tension [98], sensing of flow direction through cytoskeletal torque acting on basal syndecan-4 [99, 100]

and focal adhesion site activation through platelet endothelial cell adhesion molecule 1 (PECAM-1), vascular endothelial cadherin (VE-Cadherin) and connexions (Cx40 and Cx43) due to cytoskeletal force transmission [101, 102]. Although these models highlight the potential importance of the GCX, other studies have recorded deformation of the cell surface at the onset of WSS, calling into question the validity of these calculations [103]. Other "centralized" pathways of mechanotransduction do not act through the cytoskeleton. For example, eNOS activation has been related to glypican-1 bound HS on the cell surface due to the localization of caveolae in these structures [104]. Despite the current advances, the role the EC GCX plays in mechanotransduction of WSS is still not fully understood and this knowledge is vital in better understanding the maintenance of cellular homeostasis and initiation of EC dysfunction.

2.3 Diabetes and SGLT-2 Inhibitors

Sodium-glucose cotransporters (SGLTs) are a group of six membrane bound proteins that control the transfer of glucose against concentration gradients. This class of molecule is found throughout many cell types but is most prominent in the renal control of blood glucose levels. To control a tight homeostasis of blood glucose, the renal glomeruli filters approximately 160-180g of glucose per day out of the blood where it is then reabsorbed in the proximal convoluted tubule [105, 106]. SGLTs are active cotransporters of which SGLT-1 and -2 are considered the most important with SGLT-2 accounting for up to 90% of renal glucose reabsorption [107].

Type 2 diabetes is characterized by hyperglycemia due to impaired insulin action and/ or secretion. It can lead to a wide range of both acute and vascular conditions including

retinopathy, nephropathy, heart attack, stroke and an increased risk or cardiovascular disease [108]. C-glucoside SGLT inhibitors such as Empagliflozin (EMPA) have been developed to stop glucose reabsorption causing it to be eliminated in urine to treat hyperglycemia in type 2 diabetics. Clinical trials have shown that it decreases blood glucose levels without increasing the risk for hypoglycemia and also decreases both blood pressure and weight [109-112]. EMPA also significantly reduces cardiovascular disease morbidity and related hospitalizations by up to a third [113]. Despite this interesting finding, little research has been able to explain this pleiotropic effect. The most highly investigated hypothesis is that hyperglycemia increases the risk of cardiovascular disease, however, studies have not been able to support that glycemic control reduces this risk [114-116]. Studies have shown that SGLT-2 inhibitors are capable of attenuating SNP-induced membrane hyperpolarization [117]. This could potentially lead to changes in the actin cortical skeleton in ECs, affecting mechanotransduction and cell signalling, however this link has not yet been established.

Chapter 3: Stenosis hemodynamics disrupt the endothelial cell glycocalyx by MMP activity creating a proinflammatory environment

3.1 Preface Article

Due to its structure and location, the GCX is commonly implicated in the mechanotransduction of WSS in ECs [7, 104, 118]. Disruption of this proteoglycan layer has been observed *in vivo* [63], focally occurring in regions of complex flow. Little research has investigated regulation of the GCX in regions of WSSGs, *in vitro*, and how it relates to mechanotransduction. In the current study, we utilized a three-dimensional tissue culture model to simulate the fluid dynamics occurring at a 50% asymmetric stenosis. Flow experiments demonstrated an inflammatory response by HAAECs in regions of WSSGs through morphological rounding and increased leukocyte adhesion. Interestingly, after disruption of the GCX layer, this inflammatory response was attenuated. Further, decreased abundance of the GCX components HS and synd-1 was observed in regions of WSSGs as well as downstream of these regions. This suggested that these flow fields resulted in GCX shedding. Through experiments blocking MMP activity, it was concluded that increased MMP activity and expression in regions of WSSGs resulted in the observed GCX shedding.

This manuscript has been published: Annals of Biomedical Engineering, 2017 Sep;45(9):2234-2243. doi: 10.1007/s10439-017-1849-0

Stenosis hemodynamics disrupt the endothelial cell glycocalyx by MMP activity creating a proinflammatory environment

Cooper, S[1]., McDonald, K[1]., Burkat, D.[1], Leask, R.L.[1,2]

[1]Department of Chemical Engineering, McGill University, Montreal, Quebec, Canada

[2]Montreal Heart Institute, Montreal, Quebec, Canada

Abstract and key terms

Hemodynamic forces are known to be able to induce an inflammatory phenotype in endothelial cells (ECs). The EC glycocalyx (GCX) is a dynamic structure which is regulated in response to different stimuli and hypothesized as an important contributor to the mechanotransduction of wall shear stresses (WSS). In this work, we used a three-dimensional *in vitro* EC culture model with a 50% asymmetric stenosis to investigate degradation of the GCX by increased matrix metalloproteinase (MMP) activity in regions of WSS gradients and how this degradation might create a proinflammatory environment. Experiments showed GCX degradation was observed in regions of WSSGs created by a 50% asymmetric stenosis. Furthermore, inhibition of MMP activity abolished this regional degradation. The integrity of the GCX altered EC morphological elongation to flow and leukocyte adhesion patterns. These results help strengthen the hypothesis that the EC GCX is involved in the mechanotransduction of hemodynamic forces and that the GCX is regulated by MMP activity in regions of WSSGs.

Key Words: Atherosclerosis, Mechanotransduction, Inflammation

3.2 Introduction

Inflammation is pivotal in the initiation and progression of atherosclerosis and can affect plaque stability in its later stages. The disease is focal in nature leading to the hypothesis that disturbed flow causes endothelial cell (EC) dysfunction and initiation of atherosclerosis [119]. ECs respond to the wall shear stress (WSS) imparted by fluid flow [120, 121] with steady, uniform WSS resulting in an anti-inflammatory phenotype and wall shear stress gradients (WSSGs) eliciting an inflammatory phenotype characteristic of plaque development [122]. Morphology, cell alignment and firm adhesion can be altered by WSS [4, 45, 123] and are implicated in the focal inflammation which can occur with atherosclerosis [2] .

How ECs sense WSS to produce a biochemical response, a process termed mechanotransduction, is still poorly understood. The glycocalyx (GCX), a layer of membrane-bound macromolecules lining the endothelium, has been investigated as a prime location for mechanotransduction. This layer is comprised of glycoproteins, syndecans, proteoglycans and glycosaminoglycans and has been found to extend on the scale of 0.5-4.5µm into the vessel, *in vivo* [31, 75, 124]. Heparan sulfate (HS), chrondroitin sulfate and hyaluronic acid are the glycosaminoglycans associated with the GCX with HS being the most plentiful, accounting for 50-90% of them [37]. Because of its relative abundance in the GCX, HS has become a common target for flow studies investigating the GCX's role in mechanotransduction.

The GCX is constantly shed and regrown and its integrity is vital to vascular health [30]. Numerous studies have found that shedding of the GCX is linked to atherosclerosis and diabetes [29, 125, 126]. This shedding is suggested to be the result of matrix metalloproteinases

(MMPs) which are comprised of over 20 zinc-dependent proteases responsible for tissue remodelling with MMP-2 and MMP-9 (gelatinases), MMP-1 (interstitial collagenase), MT1-MMP (MMP-14) and MMP-12 being the most investigated in vascular research. MMP expression and activity has been documented to increase in regions of complex flow both *in vivo* [127] and *in vitro* [66].

Ultimately, disruption of components of the GCX results in negative effects on EC health including increased leukocyte adhesion and abolition of other mechanotransduction responses [7]. Building on this understanding, we sought to investigate how the GCX was modulated in the presence of a stenosis and how this affected the inflammatory response of ECs. Previous work in our lab showed ECs in regions of spatial WSSGs, created by a three dimensional, 50% asymmetric stenosis, have an inflammatory phenotype and exhibit increased leukocyte adhesion [4]. In this study we investigated the role of the EC GLX in this inflammatory response to stenosis hemodynamics and local degradation of the GLX by MMP activity.

3.3 Materials and Methods

Three Dimensional Tissue Models

In vitro experimentation was performed in three dimensional tissue culture models. The models were made of Sylgard®184 (Dow Corning), prepared as previously described [128]. CFD simulations were conducted in Comsol Multiphysics 5.0 (Comsol Inc. Burlington, MA) to determine the WSS profile in the 50% asymmetric stenosis tissue culture model. The acceleration region which occurs on the inlet shoulder of the stenosis produces a positive WSSG and the deceleration region on the distal side of the stenosis can cause flow recirculation at

larger Reynolds numbers, Figure 1. In both the inlet and outlet of the model, uniform WSS is established. More detailed descriptions have been previously published [3].

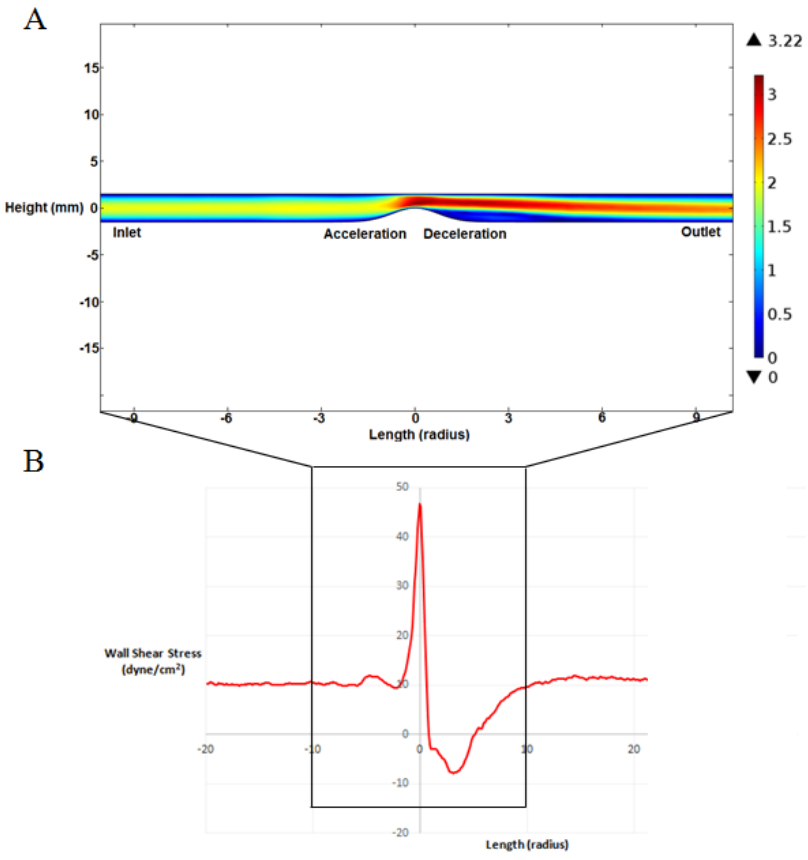

Figure 3-1: A) velocity contour normalized to inlet velocity of three dimensional, 50% asymmetric stenosis model with regions identified, B) WSS plot across stenosis model at inlet WSS of 10 dyne/cm^2.

Cell Culture

Human abdominal aortic endothelial cells (HAAECs, Coriell, AG09799) were cultured and grown to confluence in 0.01% gelatin-coated T-175 flasks in incubators (37°C, 100% humidity and 5% CO_2) over 48 hours. The HAAECs were grown in EC media (PromoCell, C-22010) with 10% fetal bovine serum (Invitrogen, 26140-079) and 1% penicillin-streptomycin (Invitrogen, 15140-122).

The Sylgard®184 models were coated with 40 µg/mL fibronectin (Sigma Aldrich, F2006-5X5MG) for 12 hours prior to cell seeding. The cultured HAAECs were removed from the T-175 flasks using a trypsin solution (0.25% Trypsin/EDTA, Invitrogen) and seeded into the *in vitro* models at a density of $1x10^6$ cells/mL. The HAAECs were cultured for 48 hours prior to each flow experiment, with a fresh media change after 24 hours, allowing them to establish a confluent monolayer on the models' luminal surface.

NB4 cells, a human promyelocytic cell line, have been previously used to simulate leukocyte adhesion to the endothelium [3, 129]. NB4 cells were cultured in suspension in T-75 flasks with RPMI Media (Global Cell Solutions, 89140-464) containing 10% fetal bovine serum (Invitrogen, 26140-079) and 1% penicillin-streptomycin (Invitrogen, 15140-122). Prior to experimentation, NB4 cells were treated with RPMI media spiked with 10^{-6} M all-trans retinoic acid (ATRA) (Life Sciences, 89158-732) for 48 hours. Brown et al observed that stimulation of NB4 cells with ATRA results in a differentiation into neutrophil-like cells characterized by increased expression of β1 and β2 integrins on the cell surface [130].

After ATRA stimulation, the NB4 cells were suspended in HAAEC media at a cell density of $1x10^6$ cells/mL and split into 40mL aliquots to act as perfusion loop media reservoirs.

HS Degradation

To compromise the integrity of the GCX, selective degradation of a single GCX component, heparan sulphate (HS), was performed by heparinase III (Sigma Aldrich, H8891-10UN) treatment using an adapted protocol from studies carried out by Florian et al [7]. Prepared EC media (PromoCell, C-22010) without added serum (SFM) was spiked with 180mU/mL

heparinase III and acted as the enzyme solution. Digestions consisted of adding the spiked SFM to the *in vitro* models in the 2 hours immediately prior to perfusion experiments. This resulted in a significant decrease in HS intensity of 33±4%, with no loss in cell viability, as previously shown [131]. At the start of the experiments, standard EC media was reintroduced into the models.

Perfusion Experiments

Perfusion experiments were maintained in an incubator at standard cell culture conditions (37^{o}C, 100% humidity and 5% CO_2) in a sterilized closed-loop setup as previously described [128]. The flow rate was maintained to impart an inlet WSS of 10 dyne/cm^2 in morphology and preshearing experiments and 1 dyne/cm^2 in circulating leukocyte adhesion assays.

Morphological Quantification

The shape index (SI), as previously used by Nerem et al [123], was determined by staining 1% paraformaldehyde-fixed ECs with Crystal Violet and imaging the 4 defined sections of the *in vitro* model, Figure 1, using an inverted light microscope (DC300, Leica Microsystems, Canada) at 80x total magnification. The images were processed by a MatLab® protocol developed by Farcas et al which determines the SI of the stained nuclei of at least 10 cells per image [128].

NB4 Quantification

Leukocyte adhesion to the endothelium was investigated by introducing a neutrophil-like cell line (ATRA stimulated NB4 cells) to the *in vitro* cell culture models both statically and through circulation [4]. Both control and HS-degraded models were presheared for 24 hours at an inlet

WSS of 10 dyne/cm^2 and were stimulated with 10 ug/mL of the cytokine TNF-α for 24 hours to increase the adhesive "stickiness" of the ECs [17]. Following this treatment, a 1x10^6 NB4 cells/mL suspension was either statically added to the models or circulated through at an inlet WSS of 1 dyne/cm^2. The lower flow rate helped facilitate an increase in firm adhesion of the NB4 cells as demonstrated by Lawrence et al who found that above low values of shear (0.5-4 dyne/cm^2), little to no adhesion occurs *in vitro* as the circulating cells have too much momentum [132]. Following the 1 hour exposure to the NB4 cell suspension, the models were fixed using a 1% paraformaldehyde solution and imaged under an inverted light microscope (DC300, Leica Microsystems, Canada) at 40x total magnification.

Immunofluorescence Quantification of Glycocalyx

Immediately following experiments, ECs were fixed with a 1% paraformaldehyde solution and subsequently probed with a monoclonal antibody specific to HS (Millipore, MAB2040) and an alexflour® 488 secondary antibody (Invitrogen, A31570). Using a laser scanning confocal microscope (Zeiss Exciter), the ECs were excited with an argon laser (AS 488nm) and images were taken. An average intensity of at least 10 cells per image was used and all values were normalized to the inlet of the statically cultured controls.

Inhibition of Matrix Metalloproteinases

During perfusion experiments, a potent inhibitor of collagenases, GM 6001 (Santa Cruz Biotechnology, 203979), was used to inhibit MMP function. GM6001 has been proven to inhibit a wide range of MMPs including: MMP-1, MMP-2, MMP-3, MMP-7, MMP-8, MMP-9, MMP-12,

MT-MMP-1 (MMP-14) and MMP-26 [133]. During the 24hr preshearing protocol, GM 6001 was included in flow loops or in statically cultured models at a concentration of 25μM.

Statistical Analysis

All results were expressed as mean ± standard mean and experiments were performed at least in triplicates. Analysis of results was completed using Graphpad Prism 5 software (Graphpad Software, La Jolla, CA). One-way and Two-way ANOVAs were used for comparisons when needed and were accompanied by multiple comparisons tests (Bonferroni post-hoc tests). Differences between means were considered significant at $P<0.05$.

3.4 Results

Glycocalyx degradation leads to an impaired morphological response to WSS

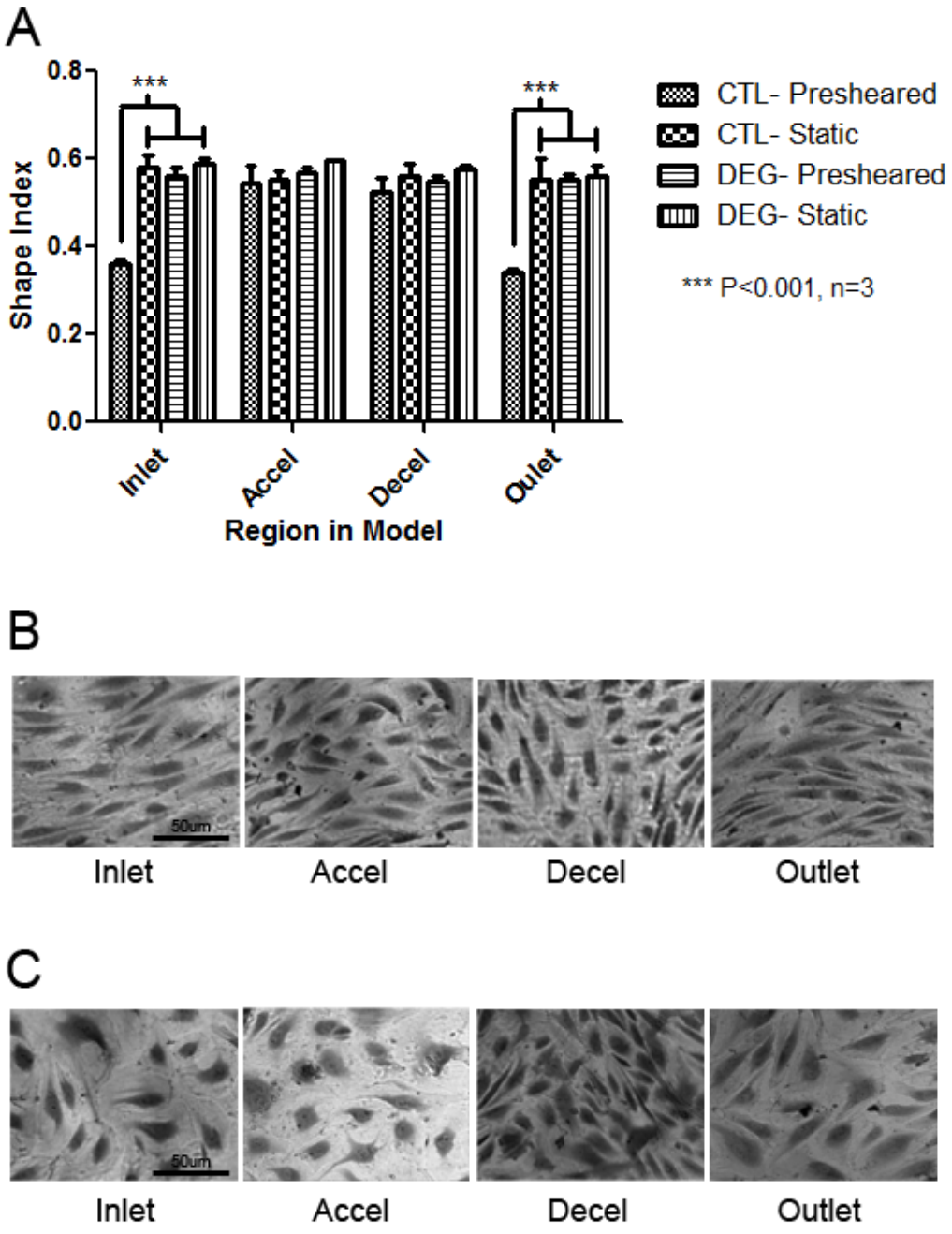

Figure 3-2: A) Morphological response (quantified by shape index) for both static and 24 hour presheared (inlet WSS of 10 dyne/cm^2) cultures, and HS-degraded (DEG) and control (CTL)

conditions (n=3). In the inlet and outlet regions, CTL-presheared HAAECs had a significantly lower shape index (Bonferroni post-hoc text, P<0.001) than all other conditions. Representative images of stained HAAECs for the B) CTL-presheared and C) DEG-presheared experiments.

ECs statically cultured exhibited no significant regional differences in SI (two way ANOVA, P>0.05), whereas preshearing resulted in significant differences (P<0.0001, two way ANOVA), Figure 2. Control ECs in the inlet and outlet regions were elongated compared to the statically grown cells (Bonferroni post-hoc test, P<0.001) whereas in regions of WSSGs, no elongation was observed. This different morphological response to uniform WSS in the inlet/ outlet versus spatial WSSGs has previously been shown [3].

Following HS degradation, ECs in regions of uniform WSS (inlet/outlet) had significantly higher SI than the control ECs in the same regions (Bonferroni post-hoc test, P<0.01). In regions of spatial WSSGs, no difference was observed between the HS-degraded or control EC morphology.

Glycocalyx degradation leads to altered patterns of regional NB4 adhesion

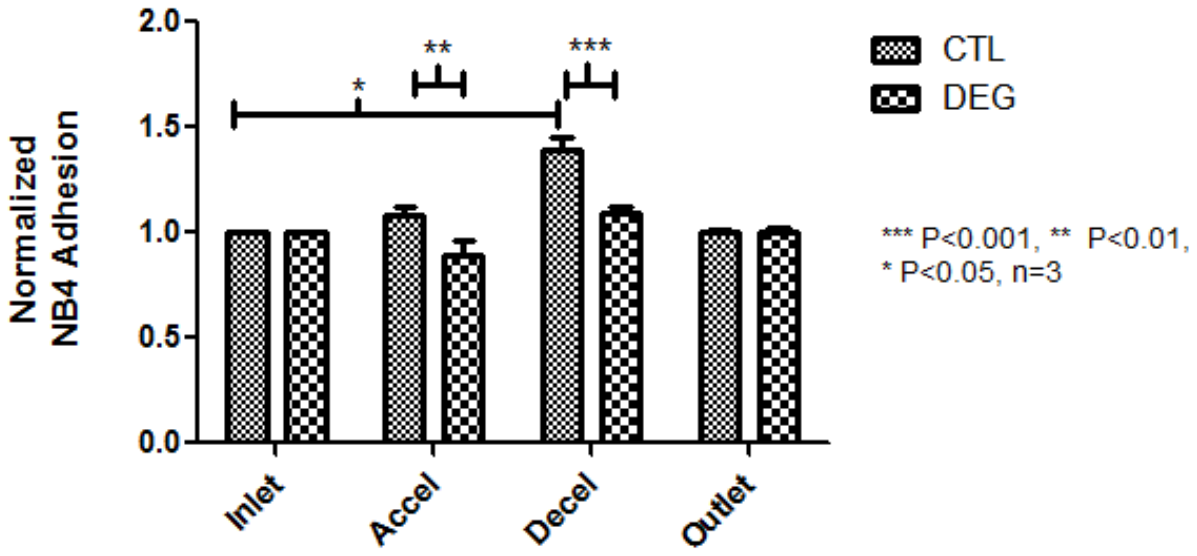

Figure 3-3: Firm leukocyte adhesion of NB4 cells circulating at an inlet WSS of 1 dyne/cm^2 for 1 hour following 24 hours of preshearing (inlet WSS of 10 dyne/cm^2) (n=3). Results for HS-degraded (DEG) and control (CTL) HAAECs are normalized to the inlet location. There was a significant effect on adhesion by location and degradation (two way ANOVA, P<0.00025 and P<0.001, respectively). There was significantly higher adhesion in the acceleration and deceleration regions in control HAAECs (Bonferroni post-hoc test, P<0.01 and P<0.001, respectively).

The firm adhesion of circulated NB4 cells to presheared ECs demonstrated a significant dependence on HS degradation and model region (two way ANOVA, P<0.00025 and P<0.001, respectively), Figure 4. In control ECs, a significant increase in normalized adhesion was observed in the deceleration region when compared to the inlet (Bonferroni post-hoc test, P<0.05), as previously shown [4]. There were no significant regional differences in normalized adhesion in HS-degraded ECs, however, there was significantly lower normalized adhesion in the acceleration (Bonferroni post-hoc test, P<0.05) and deceleration (Bonferroni post-hoc test, P<0.001) regions in HS-degraded ECs when compared to controls, Figure 3.

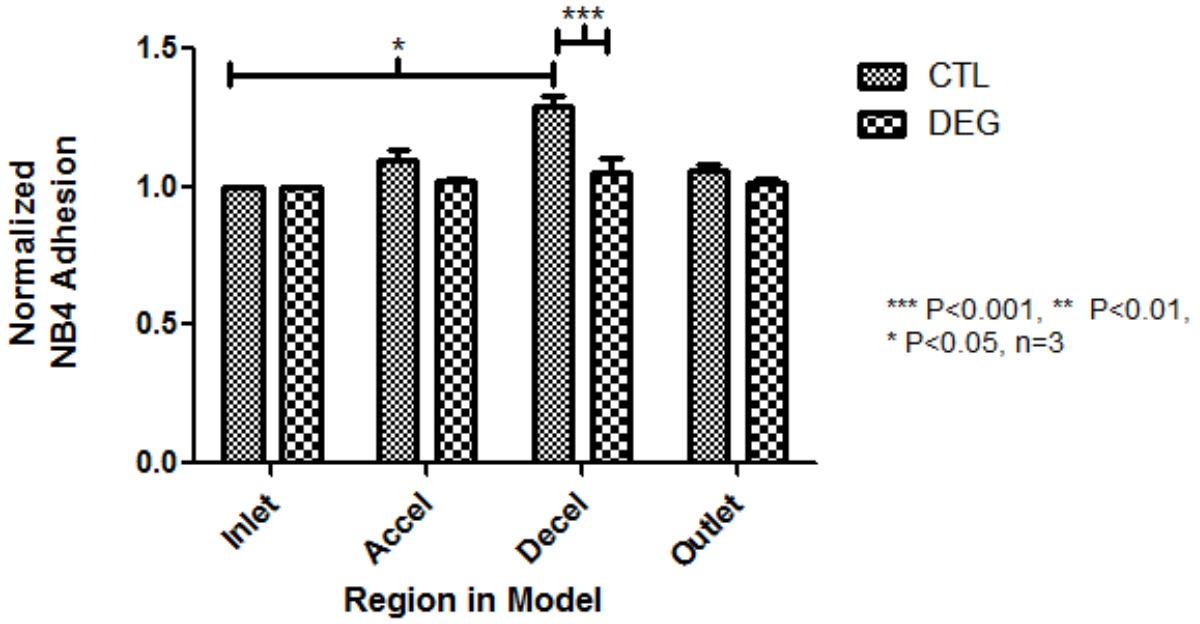

Figure 3-4: Firm leukocyte adhesion of NB4 cells statically incubated for 1 hour following 24 hours of preshearing (inlet WSS of 10 dyne/cm^2) (n=3). Results for HS-degraded (DEG) and control (CTL) HAAECs are normalized to the inlet location. There was a significant effect on adhesion by location and degradation (two way ANOVA, P<0.001 and P<0.001, respectively). There was significantly higher adhesion in the deceleration region in control compared to HS-degraded HAAECs (Bonferroni post-hoc test, P<0.001).

Static adhesion assays following preshearing demonstrated the firm adhesion of NB4 cells was dependent on HS degradation and model region (two way ANOVA, P<0.001 and P<0.001, respectively), Figure 4. Similar to the circulated adhesion assays, there was an increased pattern of adhesion in regions of spatial WSSGs, with a significant increase in the deceleration region (Bonferroni post-hoc test, P<0.05). In HS-degraded ECs, no significant difference in regional normalized adhesion was found. There was a significantly lower normalized adhesion in the deceleration region (Bonferroni post-hoc test, P<0.001) in HS-degraded ECs when compared to controls

Overall adhesion was assessed by comparing the absolute number of adhered cells in the inlet regions of each assay. HS degradation significantly increased total adhesion, however, assay condition showed no significant effect (two way ANOVA, $P<0.05$) (data not shown).

Fluid dynamics of a stenosis lead to disruption of GCX components

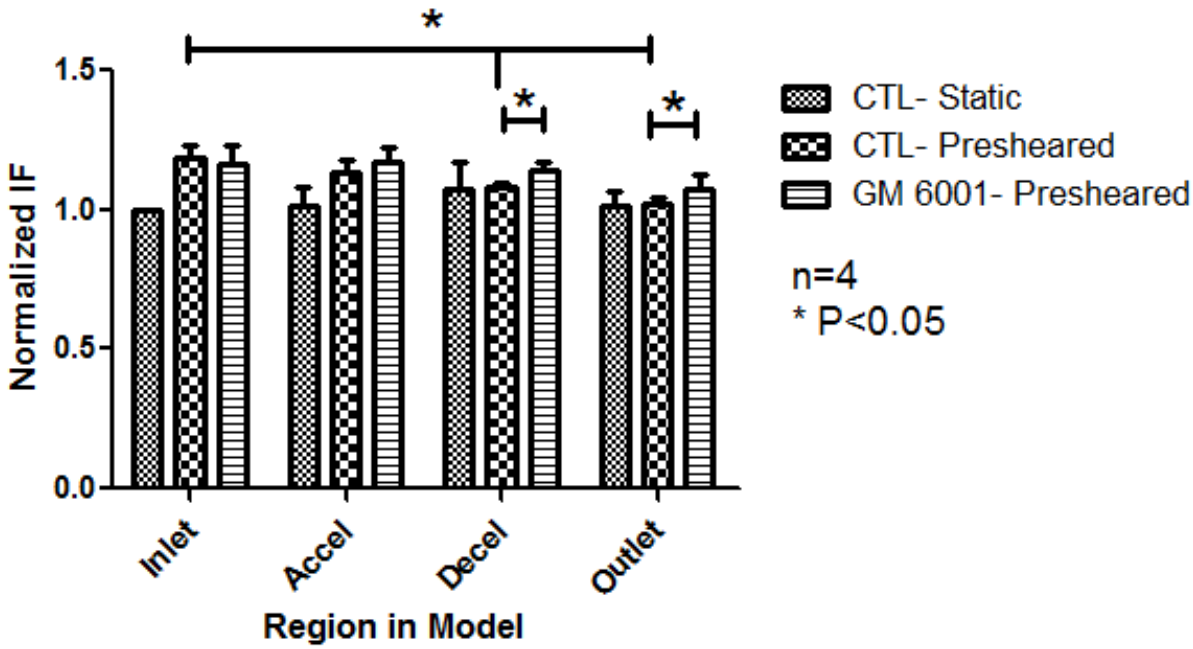

Figure 3-5: Heparan sulphate (HS) immunofluorescence intensity in control (CTL) and MMP inhibited (GM 6001) HAAECs following 24 hours of preshearing (inlet WSS of 10 dyne/cm^2). HS is significantly down-regulated in the deceleration and outlet regions compared to the inlet in control, presheared models (Bonferroni post-hoc test, $P<0.05$, $n=4$). Furthermore, there is a significant decrease in control, presheared HAAEC HS intensity when compared to cultures treated with a general MMP inhibitor (Bonferroni post-hoc test, $P<0.05$, $n=4$).

GCX health in ECs was compared between presheared and statically cultured ECs showing HS intensity was increased with preshearing and dependent on model region (two way ANOVA, $P<0.01$). Statically cultured ECs exhibited no regional differences in HS intensity, however, following 24 hours of preshearing, there was a significant decrease in HS intensity in both the

deceleration and outlet regions of the model compared to the inlet (Bonferroni post-hoc test, $P<0.05$), Figure 5.

Inhibition of MMP activity mitigates regional differences in HS abundance

Perfusion experiments spiked with a general MMP activity inhibitor, GM 6001, demonstrated HS intensity was dependent on MMP inhibition (two way ANOVA, $P<0.01$), Figure 5. Following MMP inhibition, there were no regional decreases in HS intensity. Notably, there was a significantly higher HS intensity in both the deceleration and outlet regions following MMP inhibition when compared to presheared controls (Bonferroni post-hoc test, $P<0.05$).

General inhibition of MMP activity abolishes regional patterns of NB4 adhesion

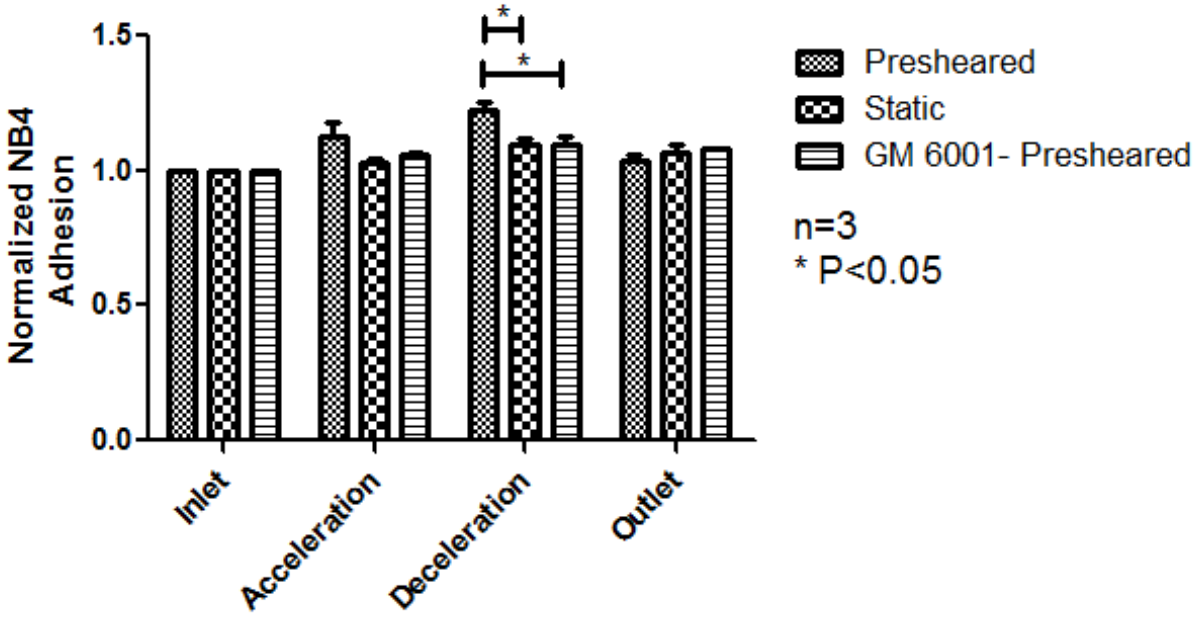

Figure 3-6: Firm leukocyte adhesion of NB4 cells circulating at an inlet WSS of 1 dyne/cm^2 for 1 hour following 24 hours of preshearing (inlet WSS of 10 dyne/cm^2) (n=3). A general MMP inhibitor (GM6001) was included for presheared HAAECs (GM 6001-Presheared) and compared to control statically cultured and presheared HAAECs, with all values normalized to the inlet location. Preshearing resulted in significantly higher adhesion in the deceleration region in

control HAAECs however this response was abolished when GM 6001 was present (Bonferroni post-hoc test, P<0.01, n=3).

Adhesion assays were performed showing that the attachment of NB4 cells was dependent on MMP inhibition and model region (two way ANOVA, P<0.05and P<0.01, respectively). MMP inhibition abolished the patterns of increased normalized adhesion in regions of WSSGs observed in control conditions (Bonferroni post-hoc test, P<0.05), Figure 6.

3.5 Discussion

It has been previously established that EC GCX degradation disrupts mechanotransduction in ECs exposed to steady, uniform WSS [7, 134]. The present study demonstrated that WSS patterns created by a 50% asymmetric stenosis caused regional disruption of the GCX which was dependent on MMP activity, resulting in an altered inflammatory response in ECs.

Morphological Response to WSS

Disturbed flow regions characterized by WSSGs can elicit an inflammatory phenotype including a morphological rounding of ECs [3] and inversely, cellular elongation is observed in response to uniform, steady WSS [45]. This study demonstrated an elongated EC morphology in the uniform inlet and outlet regions and rounding in the disturbed acceleration and deceleration regions, agreeing with previous findings [3].

Following HS degradation, there was no difference in SI in any region of the models, suggesting the cells did not morphologically respond to WSS, Figure 2. This result supports the hypothesis proposed by Thi et al that after eliminating a significant proportion of the HS, the GCX may not be able to transmit enough torque upon the actin cytoskeleton to initiate actin reorganization

[134]. In response to WSSGs proximal and distal to the stenosis, steady flow failed to elongate either control or HS-degraded ECs.

Similar studies have looked at other HS dependant EC responses to WSS such as NO production[7], cell alignment[5] and NF-κB nuclear localization [131] but few studies have looked at morphological changes in shape. Ebong et al showed a significant decrease in EC elongation, through quantification of the cells' aspect ratio, with respect to uniform steady WSS in HS-degraded samples when compared to controls [104]. These findings demonstrate that changes in EC morphology in response to flow are dependent on the integrity of the GCX.

Firm adhesion of NB4 cells is mediated by mechanotransduction via HS

With the GCX present, there was an increased occurrence of normalized adhesion of circulating NB4 cells in regions of WSSGs, Figure 3, agreeing with previous studies [3, 135]. However, following GCX disruption, there were no significant regional differences in normalized adhesion. This demonstrated that in ECs, WSS regulated pathways involving leukocyte adhesion are mitigated in part by HS.

A static NB4 adhesion assay was performed demonstrating the same adhesive patterns as in the circulating adhesion assays with no regional differences between static and circulating assays, Figure 4. This suggests that phenotypical EC changes, not the hydrodynamic forces circulating the NB4 cells, are responsible for the observed adhesion patterns.

The overall quantity of adhesion was found to significantly increase following HS degradation demonstrating that disruption of the GCX can increase adhesion, as previously shown [131]. This increase can be linked to a decrease in steric hindrance normally present due to the size of

the GCX [136]. Mulivor et al attributed increased adhesion in heparinase III treated ECs to a size limitation of adhesion molecules [120]. Molecules such as ICAM-1 extend approximately 20 nm past the cell surface [137], which is significantly shorter than the GCX extension of 20-1000 nm, *in vitro* [120, 138]. Constantinescu et al also found that in mouse cremaster venules, thickness of the GCX was inversely correlated to leukocyte adhesion *in vivo* [64]. Therefore, when the GCX is intact, it may cause steric hindrance between the EC surface ICAM-1 and binding sites on circulating leukocytes, limiting adhesion.

MMP activity focally mediates degradation of HS

Numerous studies have linked degradation and/ or shedding of HS with EC dysfunction [139, 140]. The current study found that following 24hrs of flow, there was a decreased level of HS on the distal shoulder and downstream of the stenosis demonstrating the detrimental effect WSSGs have on EC GCX health, Figure 5. Similar *in vivo* findings have shown that HS and other GCX components are focally shed in regions of disturbed flow [63, 141, 142]. It is hypothesized that altered expression and activity of MMPs in response to the complex flow regimes in the stenosis model were responsible for the observed GCX disruption. Supporting this hypothesis, Magid et al found that oscillatory WSS significantly upregulated MMP-9 expression and also resulted in a 10-fold increase in activity compared to steady flow treated controls while not affecting expression of its regulatory inhibitor, TIMP-1 [65]. In a simulated bifurcation *in vitro* model, Wang et al observed upregulation and increased activity of MMP-2 and MMP-9 in regions of WSSGs [66]. Furthermore, studies have linked MMP expression with NF-κB activity [48] and NF-κB activity has previously been observed in areas of WSSGs [49, 50]. Although the mechanisms are not fully understood, a variety of MMPs have been linked to shedding of

different components of the GCX such as MMP-9 cleaving HS [68] and MMP-1 and MT1-MMP (MMP-14) cleaving the HS proteoglycan syndecan-1 [69, 70]. Furthermore, an *in vivo* link between MMP-2 expression and atherosclerosis has been established [72].

A general MMP inhibitor was used to test the hypothesis that MMPs played a key role in the observed regional shedding. GM6001 is a cell permeable inhibitor of collagenases that has been proven to inhibit a wide range of MMPs including: MMP-1, MMP-2, MMP-3, MMP-7, MMP-8, MMP-9, MMP-12, MT-MMP-1 (MMP-14) and MMP-26 [133]. It has been previously used in experiments and has been shown to affect GCX shedding and leukocyte adhesion [143]. It was observed that inhibition with GM6001 significantly increased the quantity of HS in the deceleration and outlet regions of the model, helping to strengthen the hypothesis that MMP activity affects GCX degradation in regions of WSSGs.

A disrupted GCX in the regions of WSSGs was an expected finding however it was interesting to see this trend continue into the outlet region of the model where uniform SS had redeveloped. It was hypothesized that a “wash down” effect explains this finding whereby the increased activity of MMPs in the regions surrounding the stenosis were carried downstream of these regions by the fluid flow, degrading HS in the outlet region.

MMP Activity Mediates Adhesion in Regions of WSSGs

To further investigate the role MMPs play in the inflammatory cascade and progression of atherosclerosis, NB4 adhesion assays were run while inhibiting MMP activity. MMP inhibition abolished the regional patterns of adhesion in control cultures. In fact, following inhibition, presheared ECs showed the same adhesive patterns as statically cultured ECs.

MMP inhibition improved HS abundance while decreasing adhesion in the deceleration region, supporting the hypothesis that the GCX introduces a steric hindrance to adhesion. In control cells, disruption of the GCX by MMPs in regions of WSSGs resulted in a less dense GCX, allowing for easier access to binding sites on circulating NB4 cells. However, when MMP activity was inhibited, the GCX was left unimpeded in these regions, and therefore posed a physical barrier to firm adhesion. This was demonstrated *in vivo* by Mulivor et al as they found inhibition of MMPs with doxycycline resulted in less GCX shedding and leukocyte-endothelial adhesion [144]. Similarly, Lipowsky et al found that limiting GCX shedding *in vivo* resulted in decreased leukocyte adhesion in regions of WSSGs [143]. This exemplifies the complex interplay between MMPs and glycocalyx shedding and the further consequences on the inflammatory cascade in ECs.

Model Limitations

It should be noted that this *in* vitro model does not take into account cellular interactions which would be observed *in vivo* between the intima and adventitia of an artery. Further, perfusions were run under steady flow which is not representative of the pulsatile nature of blood flow.

The current study demonstrated that HS plays a key role in the modulation of EC morphology and leukocyte adhesion patterns in response to WSSGs. By using a three-dimensional tissue culture model containing a 50% asymmetric stenosis, it was observed that elongation of HAAECs did not occur following degradation of HS in regions of steady WSS. Furthermore, regional leukocyte adhesion patterns near WSSGs in control HAAECs were also abolished following HS degradation.

This study found that HS was focally disrupted in regions of WSSGs which can be attributed to increased MMP activity. MMP activity was also linked to NB4 regional adhesion patterns, strengthening the hypothesis that the GCX sterically hinders firm adhesion to ECs.

Together, these findings demonstrate the dynamic nature of the EC GCX's health in different flow regimes and highlight its role in mechanotransduction in regions of WSSGs.

3.6 Acknowledgements

The authors do not wish to make any further acknowledgements.

Chapter 4: Increased MMP activity in curved geometries disrupts the endothelial cell glycocalyx creating a proinflammatory environment

4.1 Preface Article

Building on the findings of the previous chapter, we next investigated GCX regulation and its role in mechanotransduction in a different physiological geometry. First, a 180^{o} curved cell culture model was developed to match dimensionless parameters describing *in vivo* regions of curvature. It was observed that the inner wall of curvature exhibited an inflammatory phenotype marked by morphological rounding of HAAECs and loss of alignment with flow and a bias of increased leukocyte adhesion towards the inner wall. After enzymatic degradation, the leukocyte adhesion bias was attenuated demonstrating the role that the GCX plays in mechanotransduction of WSSGs. Further, in regions of curvature, decreased abundance of both HS and synd-1 was observed, suggesting GCX shedding in response to WSSGs. This shedding correlated with increased activity of MMPs in these regions as determined by both *in situ* and *ex situ* gel zymography. Specifically, MMP-9 and not MMP-2 demonstrated increased activities in these regions suggesting it could be responsible for the observed shedding.

This manuscript is: Accepted with revisions in Annals of Biomedical Engineering

Increased MMP activity in curved geometries disrupts the endothelial cell glycocalyx creating a proinflammatory environment

Cooper, S[1]., Emmott, A[1,2], McDonald, K[1]., Campeau, M.A.[1], Leask, R.L.[1,2]

[1]Department of Chemical Engineering, McGill University, Montreal, Quebec, Canada

[2]Montreal Heart Institute, Montreal, Quebec, Canada

Abstract and Key Terms

Wall shear stress gradients (WSSGs) induce an inflammatory phenotype in endothelial cells (ECs) which is hypothesized to be mediated by mechanotransduction through the EC glycocalyx (GCX). We used a three-dimensional *in vitro* cell culture model with a 180^{o} curved geometry to investigate if WSSGs created by curvature can cause EC inflammation and disruption of the GCX. The hydrodynamics of the model elicited a morphological response in ECs as well as a pattern of leukocyte adhesion towards the inner wall of curvature that was attenuated with enzymatic removal of GCX components. GCX degradation was also observed in regions of curvature which corresponded to increased activity of MMPs. Together, these results support the hypothesis that the EC GCX is involved in mechanotransduction of WSSGs and that components of the GCX are regulated by MMP activity in regions of curvature.

Key Words: Atherosclerosis, Mechanotransduction, Inflammation

4.2 Introduction

The localization of atherosclerosis to regions of disturbed flow is hypothesized to be caused by endothelial cell (EC) dysfunction in response to the wall shear stress (WSS) patterns in these areas [119]. ECs are sensitive to WSS and are known to exhibit an anti-inflammatory phenotype in response to steady, uniform WSS and a pro-inflammatory phenotype including cellular rounding and increased leukocyte adhesion when exposed to wall shear stress gradients (WSSGs) [45, 88, 122, 123, 145]. Curved arteries exhibit WSSGs which are prone to focal inflammation and atherosclerosis [146].

The mechanotransduction of WSS is poorly understood in ECs, however, the apical glycocalyx (GCX) layer is commonly implicated [6, 7]. The GCX extends 0.5-4.5µm into the vessel *in vivo* [31, 75, 124] and is comprised of a variety of components including glycosaminoglycans of which heparan sulfate (HS) is the most abundant [37]. It is a dynamic structure [30] whose disruption has been linked to atherosclerosis and diabetes [29, 125, 126]. Shedding of GCX components has been linked to matrix metalloproteinases (MMPs) expression and activity, which has been documented to increase in regions of complex flow both *in vivo* [127] and *in vitro* [66].

We investigated how the hydrodynamics of a curved vessel related to the inflammatory response of ECs and the regulation of GCX health. Using a novel *in vitro* cell culture model, it was observed that cell morphology and leukocyte adhesion patterns were dependent on GCX integrity and that enzymatic degradation of GCX components resulted in a loss of these observed patterns. We hypothesized that the hydrodynamic forces created by a curved geometry were responsible for regional GCX degradation which was linked to MMP regulation.

Together these findings can explain the observed focal inflammation observed in regions of vessel curvature.

4.3 Materials and Methods

Three-Dimensional Cell Culture Models

In vitro models were made of Sylgard®184 (Dow Corning), prepared similarly to previously described methods [128]. A polished metal rod was bent to match the radius of curvature then cast in a mold with Sylgard®184. Once the elastomer was fully cured, the metal rod was removed and connectors for perfusion tubing were added to the inlet and outlet of the model. Dimensionless analysis matched the model dynamics to regions of arterial curvature. The Dean's Number (D_N) is the most relevant of these parameters and is defined as:

$$D_N = Re_N \times [D/2R_{Curv}]^{1/2}$$

which takes into account the Reynolds Number (Re_N) and the curvature ratio ($D/2R_{Curv}$) of a curved cylindrical vessel [147]. The model had a vessel diameter (D) of 2 mm and a radius of curvature (R_{Curv}) of 25.4 mm and the cell culture media had a viscosity and density of 9.75×10^{-4} Pa·s and 994.3 kg/m^3, respectively. By controlling the media flow rate, a Dean's Number of 104 was achieved which falls in the physiological range (10-700 *in vivo*, [148]) and corresponds with a relevant inlet WSS of 10 dyne/cm^2 and Reynolds Number of 543. Under these conditions, fluid momentum caused differential WSS profiles between the inner and outer wall of curvature, Figure 1A.

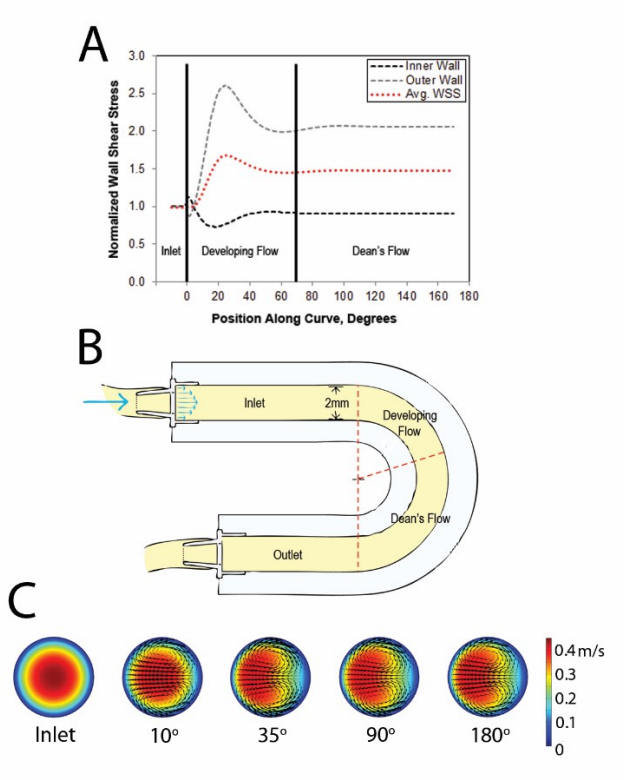

Figure 4-1: A) WSS plot normalized to inlet WSS of 10 dyne/cm^2 with 3 defined regions of curvature, B) schematic drawing of 180^o curve model with regions of curvature annotated and C) Cross-sectional velocity plots at different positions along the curve demonstrating secondary flows and fluid momentum shift (right: inner wall, left: outer wall).

The WSS profile was used to segment the model into 3 distinct flow regions for analysis: the uniform WSS inlet region (inlet), a developing flow region (developing flow) and a fully developed Dean's flow region (Dean's flow), Figure 1B.

Computational Fluid Dynamics

CFD simulations were conducted in Comsol Multiphysics 5.0 (Comsol Inc. Burlington, MA) to determine the WSS profile in the cell culture model. Simulations were run at an inlet Reynolds number of 543 to achieve an inlet WSS of 10 dyne/cm^2 and a Dean's Number of 104. Wall effects from cells were assumed to be negligible due to their much smaller size compared to the channel diameter. WSS was calculated from the near wall velocity gradient using a mesh

independent laminar solver for steady, incompressible, Newtonian flow with a zero-pressure outlet condition.

Tissue Culture

Human abdominal aortic endothelial cells (HAAECs, Coriell, AG09799) were cultured and grown to confluence in 0.1% gelatin-coated T-175 flasks in incubators (37^{o}C, 100% humidity and 5% CO_2) over 48 hours. The HAAECs were grown in EC media (PromoCell, C-22010) with 10% fetal bovine serum (Invitrogen, 26140-079) and 1% penicillin-streptomycin (Invitrogen, 15140-122). The Sylgard®184 models were coated with 40 μg/mL fibronectin (Sigma Aldrich, F2006-5X5MG) for 24 hours prior to cell seeding. The cultured HAAECs were removed from the T-175 flasks using a trypsin solution (0.25% Trypsin/EDTA, Invitrogen) and seeded into the *in vitro* models at a density of $1x10^6$ cells/mL. The HAAECs were cultured for 48 hours prior to each flow experiment, with a fresh media change after 24 hours, allowing them to establish a confluent monolayer on the models' luminal surface.

NB4 cells, a human promyelocytic cell line, were used to simulate leukocyte adhesion to the endothelium [3, 129]. NB4 cells were cultured in suspension in T-75 flasks with RPMI Media (Global Cell Solutions, 89140-464) containing 10% fetal bovine serum (Invitrogen, 26140-079) and 1% penicillin-streptomycin (Invitrogen, 15140-122). Prior to experimentation, NB4 cells were treated with RPMI media spiked with 10^{-6} M all-trans retinoic acid (ATRA) (Life Sciences, 89158-732) for 48 hours to differentiate them into neutrophil-like cells exhibiting increased expression of β1 and β2 integrins, as previously described [4]. Following ATRA stimulation, the NB4 cells were suspended in HAAEC media at a cell density of $1.67x10^6$ cells/mL and then used in adhesion assays.

HS Degradation

To impair the structure of the GCX, degradation of HS was performed by heparinase III (Sigma Aldrich, H8891-10UN) treatment [7, 149]. Briefly, serum free media (PromoCell, C-22010) was spiked with 180mU/mL heparinase III and incubated with ECs for 2 hours immediately prior to perfusion experiments. This resulted in a significant decrease in HS intensity of 33±4%, with no loss in cell viability, as previously shown [131]. At the start of experiments, standard EC media was reintroduced into the models.

Perfusion Experiments

Perfusion experiments were performed in an incubator at standard cell culture conditions (37^{o}C, 100% humidity and 5% CO_2) in a sterilized closed-loop as previously described [128]. The flow rate was maintained to achieve an inlet WSS of 10 dyne/cm^2 in morphology and preshearing experiments and 1 dyne/cm^2 in circulating adhesion assays. A flow diagram of perfusion protocol can be referred to in Figure 2.

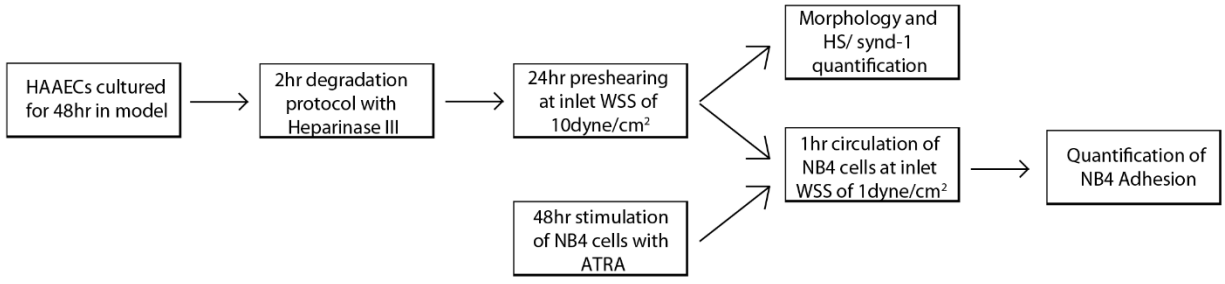

Figure 4-2: Flow diagram of experimental protocol. For all experiments, HAAECs were first grown to confluence for 48hr in the in vitro model. If HS degradation was included in an experiment, this was done immediately before experimentation. 24hr preshearing was then

performed in an incubator (TNF-α stimulation was done simultaneously for adhesion assays). Models were then either prepared for analysis or exposed to a suspension of NB4 cells which had previously been stimulated with ATRA for 48hr. Following the 1hr adhesion assay, models were prepared for analysis.

EC Morphology

The shape index (SI), which describes the ratio of a cell's perimeter to its area [123], was determined by staining ECs with Crystal Violet and imaging the 3 defined sections of the *in vitro* model. The images were processed by a MatLab® protocol to determine the SI of the stained nuclei of at least 10 cells per image [128].

Immunofluoresence Quantification of Glycocalyx

Immediately following the completion of an experiment, ECs were fixed with a 1% paraformaldehyde solution and subsequently probed with a monoclonal antibody specific to HS (Millipore, MAB2040) or syndecan-1 (Santa Cruz, SC-7099) and an Alexa Fluor® 488 secondary antibody (Invitrogen, A31570). Images were taken with a laser scanning confocal microscope (Zeiss Exciter) and an average intensity of at least 10 cells per image was used.

NB4 Adhesion Assays

Leukocyte adhesion to the endothelium was investigated using ATRA-stimulated NB4 cells. NB4 cells exhibit similar binding sites to leukocytes following ATRA stimulation and have thus been used in similar adhesion studies [4, 129, 150]. Models were presheared for 24 hours at an inlet WSS of 10 dyne/cm^2 and were simultaneously stimulated with 10 ug/mL of the cytokine TNF-α to increase total adhesion [17]. Following this treatment, a suspension of 1x10^6 NB4 cells/mL was either statically added to the models (non-circulated) or circulated at an inlet WSS of 1 dyne/cm^2 [132, 149]. Both the low WSS circulation and TNF-α stimulation were included in

adhesion assays to ensure measurable differences in cell adherence over the time scale accessible *in vitro.* Following a 1 hour exposure to the NB4 cell suspension, the models were fixed using a 1% paraformaldehyde solution and imaged.

In Situ Gel Zymography

HAAECs were fixed in 1% paraformaldehyde and rinsed with PBS. DQ gelatin (Molecular Probes, D12054) was diluted in Tris Zymo buffer (50mM Tris (pH 7.3), 15mM $CaCl_2$) at a concentration of 1:40. Cells were incubated with the solution for 16hr then washed and mounted before imaging.

Ex Situ Gel Zymography

Following experiments, HAAECs were removed from the models with a 0.25% Trypsin solution (0.25% Trypsin/EDTA, Invitrogen) and were treated with RIPA lysis buffer. Samples were prepared and run on acrylamide gels as previously described [151].

Statistical Analysis

All results were expressed as mean ± standard error of the mean and experiments were performed at least in triplicates. Analysis of results was completed using Graphpad Prism 5 (Graphpad Software, La Jolla, CA) software. One-way and Two-way ANOVAs were used for comparisons when needed and were accompanied by multiple comparisons tests (Bonferroni post-hoc tests). Differences between means were considered significant at $P<0.05$.

4.3 Results

Characterization of Fluid Dynamics of the In Vitro Model Using CFD Analysis

The WSS profile was obtained from CFD analysis using the experimental flow conditions, Figure 1. This profile was used to section the model into 3 regions where distinct WSS patterns were

observed. The inlet demonstrated a uniform parabolic velocity profile and was used as an internal control. The developing flow region was defined from 0 to approximately 70^{o} around the curve where the velocity profile changed in the axial direction. WSS gradients were observed on the inner and outer wall of curvature in this region. The Dean's flow region from 70^{o} to the curve outlet exhibited fully developed Dean's flow with a lower WSS on the inner wall of curvature which was similar in magnitude to the inlet and no spatial gradients in the axial direction.

Morphological Response of HAAECs to WSS

Analysis following 24 hours of preshearing demonstrated a significant dependence of EC morphology (SI) to both the side of the curve (two-way ANOVA, $P<0.01$) and model region (two-way ANOVA, $P<0.05$), Figure 3. There was also significant interaction between model region and side of the curve (two-way ANOVA, $P<0.05$). In the Dean's flow region, the inner wall of curvature demonstrated significant rounding when compared to the inlet (Bonferroni post-hoc test, $P<0.05$). Further, the inner wall of the developing and Dean's flow regions exhibited significant rounding when compared to their matched outer wall (Bonferroni post-hoc test, $P<0.05$ and $P<0.05$, respectively).

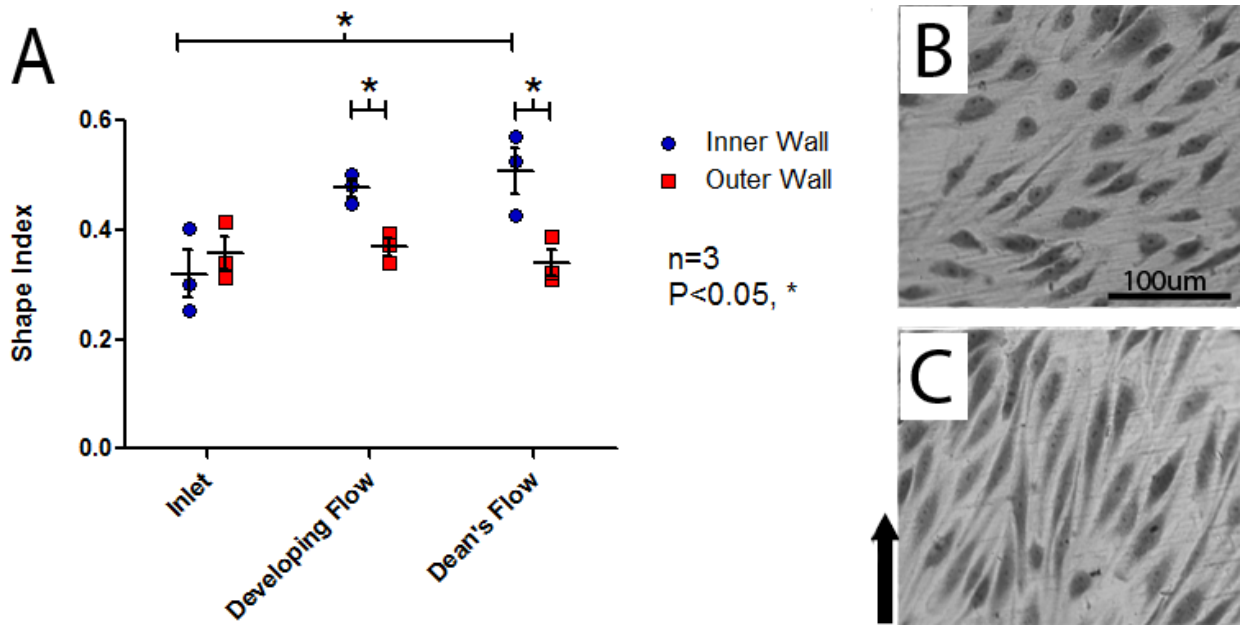

Figure 4-3: A) Analysis of shape index of HAAECs on the inner and outer walls of curvature following 24hr of preshearing at an inlet WSS of 10dyne/cm^2 (n=3, mean SI ± SEM). The inlet wall in the Dean's flow region had a significantly higher SI than the inlet inner wall (Bonferroni post-hoc test, P<0.05). The developing and Dean's flow regions also exhibited a significantly higher SI on the inner wall compared to the outer wall in the same region (Bonferroni post-hoc test, P<0.05 and P<0.05, respectively). Representative images used for analysis from Developing Flow region, with direction of flow indicated, in the B) inner wall of curvature and C) outer wall of curvature.

Angle of Orientation of HAAECs in Response to WSS

Following 24 hours of preshearing, the angle of orientation, defined as the absolute value of the angle of the longitudinal cell axis relative to the axial flow through the channel (0^o is perfectly along the axial direction and 90^o is perfectly circumferential), was significantly affected by the model region as well as the side of the curve (two-way ANOVA, P<0.001 and P<0.05, respectively), Figure 4. Both the inner and outer walls of the inlet region in presheared models demonstrated HAAECs which were significantly more oriented along the longitudinal axis of the model than static controls (Bonferroni post-hoc test, P<0.01). However, ECs in the developing and Dean's flow regions were less oriented along the longitudinal axis than static controls

(Bonferroni post-hoc test, both P<0.01). In both the inner and outer walls of presheared models, cells in the respective inlet were significantly more oriented along the longitudinal axis of the model than the developing and Dean's flow regions (Bonferroni post-hoc test, P<0.01).

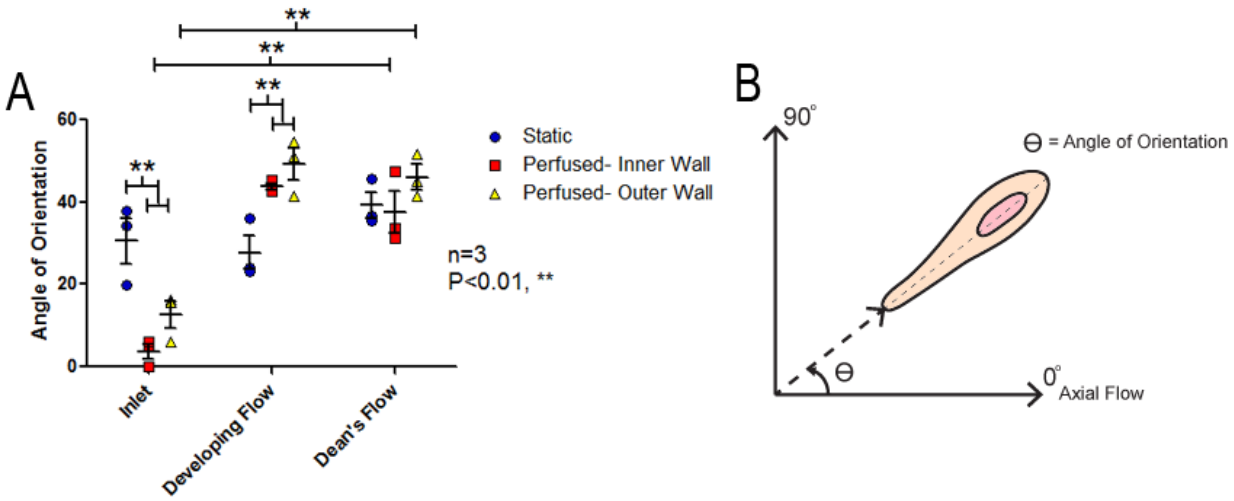

Figure 4-4: A) Angle of orientation (absolute value) of HAAECs on the inner and outer walls of curvature following 24hr of preshearing at an inlet WSS of 10dyne/cm^2 (n=3, mean angle ± SEM). Both the inner and outer walls of the inlet were significantly more oriented in the direction of axial flow when compared to static controls (Bonferroni post-hoc test, P<0.01), however, perfused HAAECs were significantly less oriented across the longitudinal axis in the developing flow region (Bonferroni post-hoc test, P<0.01). In both the inner and outer wall of the Developing and Dean's flow regions, HAAECs were significantly less oriented along the vessel axis when compared to their respective inlet control (Bonferroni post-hoc test, P<0.01). B) Representative cartoon of the angle of orientation (ϑ) of the longitudinal cell axis with 0^o being axial and 90^o being circumferential to the channel.

Distribution of Adhered NB4 Cells

Circulated and non-circulated adhesion assays were performed on both statically cultured and presheared HAAECs, with and without GCX degradation. Adhesion assays on statically cultured HAAECs were included to determine if any bias was attributed to the hydrodynamics in the model. Since the HAAECs were not exposed to the shear fields created in the model, there

would be no phenotypical changes in the cells and hence any patterns of adhesion could be attributed to hydrodynamics alone.

Static cultures demonstrated that the type of adhesion assay (circulated/ non-circulated) and model region both had a significant effect on adhesion (two-way ANOVA, $P<0.05$ and $P<0.05$), Figure 5A. In the developing flow region, there was a significant bias of adhesion towards the inner wall of curvature in circulated compared to non-circulated assays. There was no significant difference between adhesion distribution between control and degraded cultures. The adhesion assays were then repeated following 24 hours of preshearing. Both degradation and location had a significant effect on adhesion (two-way ANOVA, $P<0.001$ and $P<0.001$, respectively), Figure 5B. Following preshearing, adhesion was higher on the inner wall of curvature in the developing flow region when compared to statically cultured control (Bonferroni post-hoc test, $P<0.01$) and HS-degraded (Bonferroni post-hoc test, $P<0.01$) HAAECs. Preshearing following HS degradation resulted in no difference in adhesion pattern compared to both statically cultured control and HS-degraded HAAECs (data not shown).

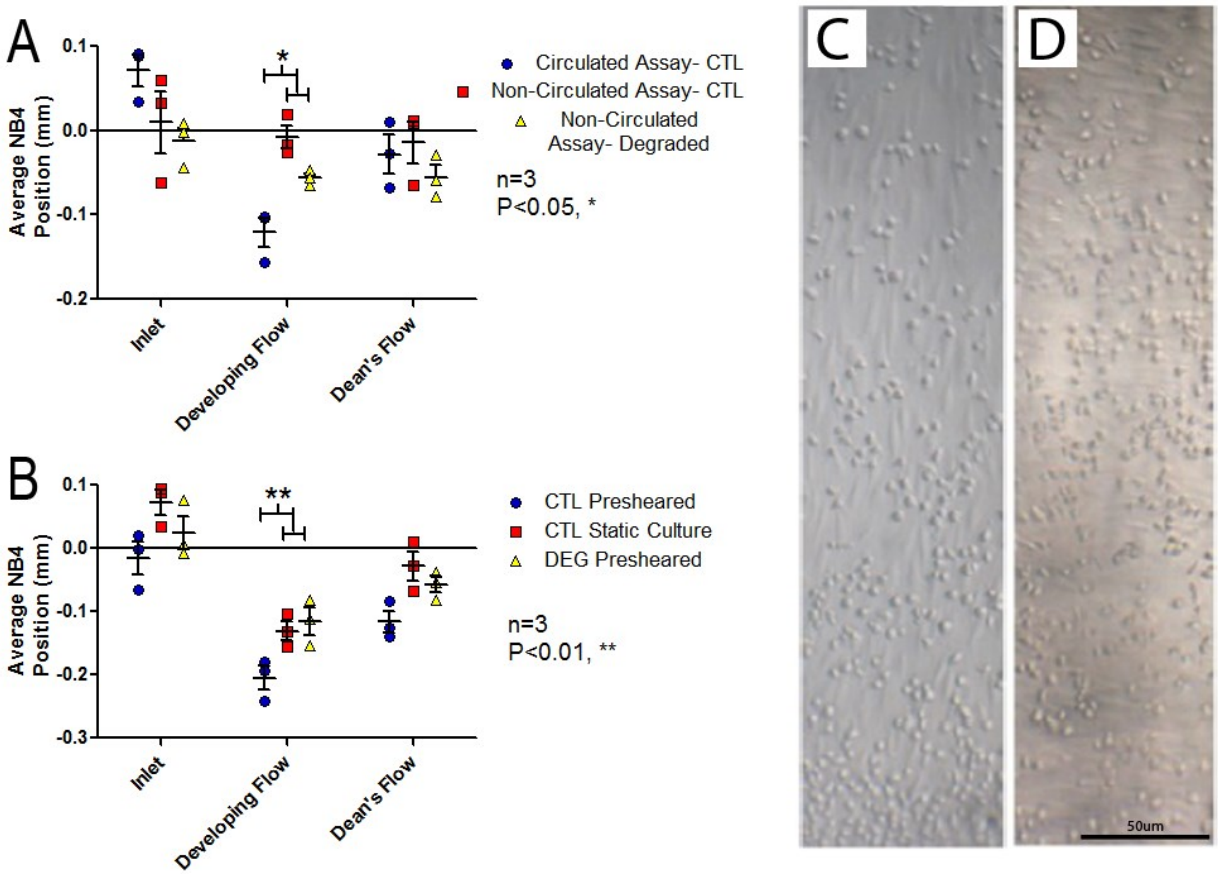

Figure 4-5: Average position of adhered NB4s relative to the centreline of the with the inner wall in the negative direction and outer wall in the positive direction A) Both circulated (inlet WSS of 1 dyne/cm^2) and non-circulated (no WSS) adhesion assays for statically cultured control (CTL) and HS-degraded (DEG) HAAECs (n=3, mean average position ± SEM). The developing flow region of the circulated adhesion assay showed a significant bias towards the inner wall compared to static controls (Bonferroni post-hoc test, P<0.05). B) Mean average position of circulated (inlet WSS of 1 dyne/cm^2) adhesion assays following 24hr preshearing (inlet WSS of 10 dyne/cm^2). Controls exhibited a significant bias in adhesion to the inner wall in the developing flow region relative to HS-degraded HAAECs (Bonferroni post-hoc test, P<0.01). Representative images used for analysis from the Dean's Flow region with the inner wall on the bottom of C) presheared HAAECs demonstrating inner wall adhesion bias and D) statically cultured HAAECs demonstrating no adhesion bias, where the round cells are the adhered NB4 cells.

HS and Syndecan-1 Expression

Following 24 hours of preshearing, the expression of HS was similar between the inner and outer wall, however there was significant variation in HS amongst the model regions (two-way

ANOVA, P<0.01), Figure 6A. A significant decrease in HS expression was observed in the Dean's flow region when compared to the inlet (Bonferroni post-hoc test, P<0.05).

Similarly, following 24 hours of preshearing, the side of the curve showed no effect on syndecan-1 expression, however expression varied significantly by model region (two-way ANOVA, P<0.01), Figure 6B. On the outer wall of curvature, there was a significant decrease in syndecan-1 expression in the Dean's flow region when compared to the inlet (Bonferroni post-hoc test, P<0.05).

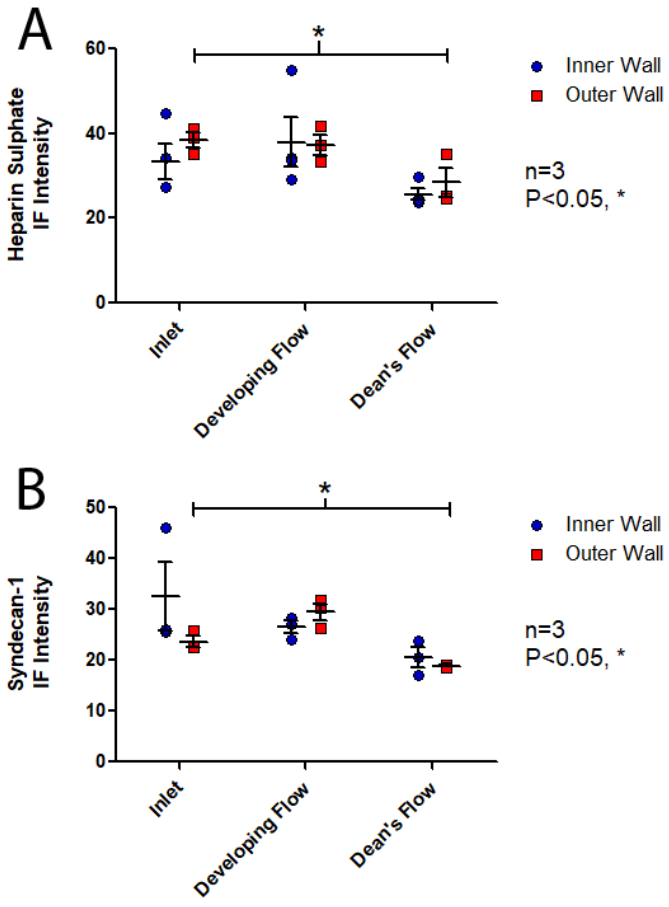

Figure 4-6: Following 24hr of preshearing (inlet WSS of 10 dyne/cm^2), mean fluorescence intensity (n=3, mean intensity ± SEM). of A) of HS which showed a significant decrease in mean intensity in the Dean's flow region relative to the inlet (Bonferroni post-hoc test, P<0.05) and B)

Syndecan-1 which also showed a significant decrease in mean intensity in the Dean's flow region relative to the inlet (Bonferroni post-hoc test, P<0.05).

MMP Activity

Following 24 hours of preshearing, *in situ* gel zymography demonstrated that MMP activity was significantly affected by model region (two-way ANOVA, P<0.05) but did not show dependence on the side of curvature, Figure 7A.

Ex situ gel zymography was performed and HAAECs were pooled from both the Developing Flow and Dean's Flow regions and labelled "Curved region" to ensure adequate protein concentrations for analysis. *Ex situ* gel zymography demonstrated that MMP activity was dependent on model region (one-way ANOVA, P<0.05). Significantly higher MMP-9 activity was observed in both the curve and the outlet when compared to the inlet of the model (Bonferroni post-hoc test, P<0.05), whereas no differences were observed for MMP-2, Figure 7B.

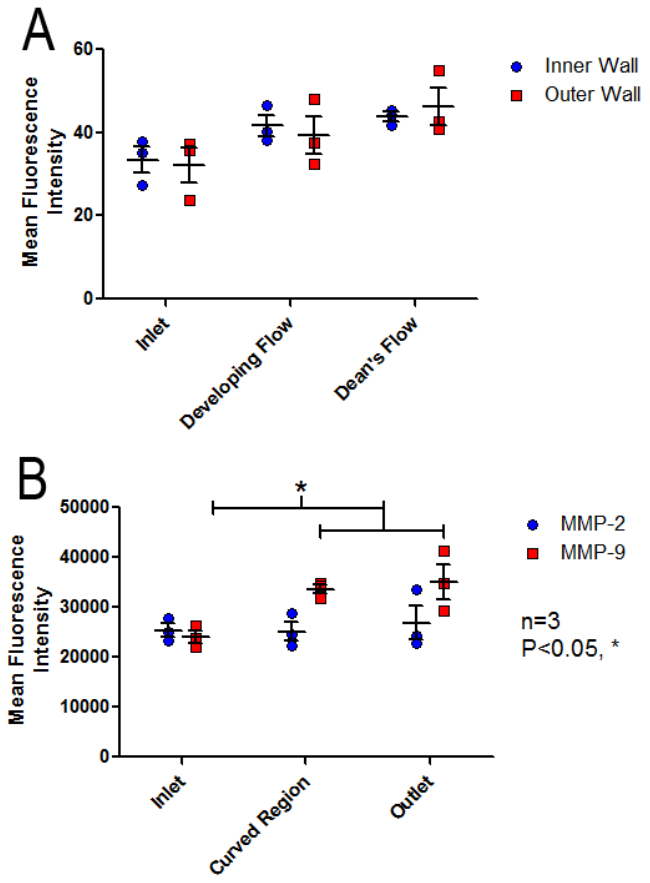

Figure 4-7: A) Regional MMP activity quantified by in situ gel zymography following treatment of HAAEC with DQ gelatin showing a trend for increased activity throughout the curve and B) Regional MMP activity quantified by ex situ gel zymography showing a significant increase in MMP-9 activity in the curve and outlet regions of the model when compared to the inlet (Bonferonni post-hoc test, P<0.05). (n=3, mean intensity ± SEM).

4.5 Discussion

In this study, we investigated the role of the EC GCX in cellular inflammation in regions of a 180^{o} curved vessel. Results demonstrated that the hydrodynamics of this geometry regionally degraded the EC GCX which correlated with increased MMP activity and altered patterns of leukocyte adhesion, Figure 8.

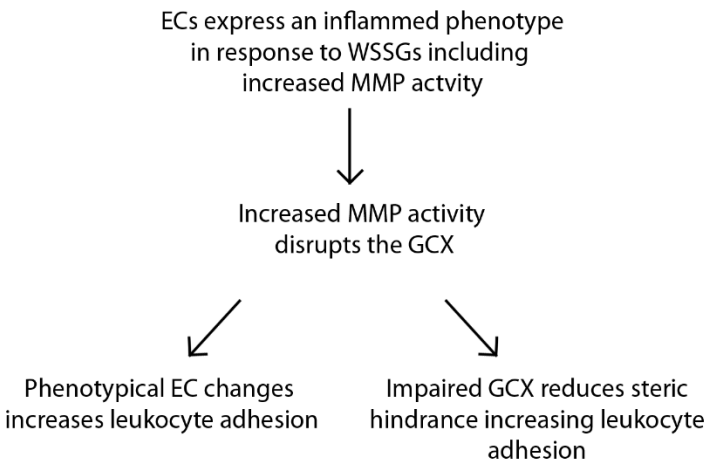

Figure 4-8: Flow diagram demonstrating mechanism of increased leukocyte adhesion. Regions of WSSGs elicit an inflamed HAAEC phenotype which includes an increase in MMP activity, causing shedding of the GCX. This shedding decreases the steric hindrance of leukocytes from adhering to the EC surface, and in conjunction with other changes in EC phenotype, results in increased adhesion in these regions.

CFD simulations suggested a spatially variable midline shear field with WSSGs along the model. The fluid dynamics of the model were found to significantly alter EC phenotype, with observed differences in morphology and orientation and leukocyte adhesion patterns in the different model regions. Degradation of HS and syndecan-1 was observed downstream of WSSGs, corresponding to regions of increased MMP activity, suggesting a link between GCX health and MMP regulation in curved vessels.

HAAECs Exhibited a Differential Morphological Response to WSS in Regions of Curvature

The model's hydrodynamics lead to an elongated morphology on the outer wall of curvature, with the developing and Dean's flow regions exhibiting significantly greater elongation than both the inlet and matched inner wall of the model, Figure 3. This can be correlated with a higher WSS on the outer wall due to momentum carrying the bulk flow to the outer curve.

Elongation of EC morphology is indicative of an "atheroprotective" phenotype [145], indicating the outer wall may be comparatively less prone to developing a pathological phenotype. Potter *et al* used an elongation index to show that ECs on the outer wall of curvature were elongated when compared to those found on the inner wall of porcine aortic endothelial cells in tissue culture models [152]. In contrast, Wang *et al* found increases in VCAM-1 and E-selectin, markers of EC inflammation, on the outer wall of curvature, but these results were confounded by having suspended red blood cells which they hypothesized “bombarded” the outer wall, causing more severe EC damage [153].

The angle of EC orientation demonstrated significantly less alignment with the direction of bulk flow on both sides of the flow channel when compared with static controls, Figure 4. Typically, WSS will result in alignment with the direction of bulk flow in regions of steady, uniform flow [145]. In contrast, complex fluid dynamics and WSSGs have been shown to cause a less organized orientation [145]. The lack of orientation along the vessel axis can also be attributed to the nature of Dean's flow. Dean's flow produces secondary flows in the circumferential direction which redistribute the increased momentum on the outer wall back towards the inner wall of curvature. Therefore, this flow will take a more circumferential than longitudinal path when compared to flow in a straight cylinder. The angle of orientation may have been offset from the longitudinal direction due to these secondary flows. Potter *et al* showed that *in vivo*, ECs in the aortic arch had increased variability in alignment when compared to static *in vitro* cultures [154]. Ghriallais *et al* found an increased alignment in the direction of flow compared to static controls in a curved model (without inner/ outer wall specificity) and noted less alignment in curved regions when compared to straight tube models [155]. Alloush *et al*

observed decreased alignment with flow in regions of curvature where complex fluid dynamics were present [156]. The observed changes in EC morphology contribute to the hypothesis that flow in curved arteries results in regional inflammation of the endothelium focused on the inner wall of curvature.

Differential NB4 Adhesion to ECs was Observed in Regions of Curvature

To determine the effect of the model's hydrodynamics on adhesion patterns, ECs were statically cultured before being exposed to a suspension of either circulated or non-circulated NB4 cells for 1hr. The 1hr circulation at a relatively low WSS was assumed to not elicit a phenotypical response in ECs, therefore, any adhesion patterns which differed between the circulated and non-circulated assays were assumed to be the result of the hydrodynamics acting on the NB4 cells. These experiments demonstrated the hydrodynamics caused a bias in adhesion towards the inner wall of curvature in the developing flow region, Figure 5A.

To determine the phenotypical response of ECs to curved vessel hydrodynamics, ECs were presheared for 24 hours prior to circulated adhesion assays. These assays demonstrated a significant bias of NB4 adhesion to the inner wall of curvature beyond the effect of the hydrodynamic forces acting on the circulated cells, Figure 5B. This bias can therefore be attributed to the WSS fields eliciting a phenotypical change in ECs in these regions. Suo *et al* demonstrated an increased expression of cellular adhesion molecules on the inner wall of curvature in mouse aortas which could help support this finding [157]. Similarly, increased adhesion has been linked to regions of WSSGs and lower WSS [158] and is indicative of EC inflammation. The observed adhesion patterns in this study are further supported by clinical

evidence of an increased prevalence of plaque development on the inner wall of curvature in arteries [159-161].

Disruption of the GCX Attenuates NB4 Adhesion Patterns in Regions of Curvature

Mechanotransduction of fluid forces through the GCX was hypothesized to be responsible for the WSS mediated phenotypical changes which lead to the NB4 adhesion bias. Supporting this hypothesis, presheared HS-degraded ECs did not exhibit the amplified adhesion bias to the inner wall of curvature seen in control cultures, Figure 5B. Cooper *et al* demonstrated a similar effect in a 50% stenosis model, where non-uniform regional NB4 adhesion patterns were attenuated following GCX degradation [149]. HS degradation also resulted in an overall increase in total NB4 adhesion (data not shown), agreeing with previous work which has linked the GCX to sterically hindering firm adhesion [64, 120, 131, 149].

Disruption of HS and Syndecan-1 Occurs in Regions of Curvature

In the Dean's flow region, significant decreases were observed in both HS and Syndecan-1 compared to the inlet, Figure 6, demonstrating that flow through regions of curvature negatively affected EC GCX health. Studies have found similar findings *in vivo*, reporting that GCX components, including HS, are focally shed in regions of disturbed flow [63, 141, 142]. The observed degradation was hypothesized to be the result of increased MMP activity in response to the complex of flow in the curved model. Studies utilizing oscillatory flow found upregulation of MMP-9 [65], bifurcation models increased activity of MMP-2 and MMP-9 in regions of WSSGs [66] and MMP expression has been linked to NF-κB activity which is regulated in response to WSSGs [49, 50, 154], all supporting this notion. A variety of MMPs have been linked

to GCX disruption, with MMP-9 cleaving HS [68] and MMP-1 and MMP-14 cleaving syndecan-1 [69, 70].

MMP Activity was Increased in Regions of Curvature

MMP activity was quantified by *in situ* and *ex situ* gel zymography, both demonstrating a correlation with MMP activity and GCX degradation. Although increased activity of the gelatinases (MMP-2 and MMP-9) was not observed in any distinct region with *in situ* analysis, there was still a significant overall effect of region on MMP activity. *Ex Situ* zymography showed significant increases in MMP-9 activity were observed in the curve and outlet when compared to the inlet. This correlated with decreased HS and syndecan-1 expression and was in agreeance with previous findings [49]. These results support the proposed hypothesis that WSSGs increase MMP activity which then degrade the GCX, eliciting an inflammatory response in ECs. Although increased activity was expected in the curve where WSSGs were found, it was unexpected to see higher MMP-9 activity in the outlet region where uniform flow was re-established. We hypothesize this to be from a "wash down" effect whereby MMP-9 activation in the curve is subsequently carried downstream of this region by the fluid flow. We have suggested a similar mechanism in a 50% stenosis model [149].

Overall, this study demonstrated that a curved vessel geometry elicits a differential inflammatory response in ECs. Specifically, experiments showed changes in morphology and NB4 adhesion patterns were tied to GCX health. Regional degradation of GCX components also correlated with increased MMP activity, suggesting MMP regulation in areas of WSSGs can significantly affect GCX health and lead to an inflammatory EC response.

4.6 Acknowledgements

The authors do not wish to make any further acknowledgements.

Chapter 5: Empagliflozin promotes glycocalyx health in vitro demonstrating a mechanism for the decreased risk of cardiovascular disease following treatment in type 2 diabetics

5.1 Preface Article

After determining the intimate link between GCX health and EC inflammation, a clinical application of this connection was investigated. Empagliflozin (EMPA) is a SGLT-2 inhibitor which has been successfully used for glycemic control in type 2 diabetes and has also demonstrated a pleiotropic effect, decreasing the risk of cardiovascular disease. We sought to determine if this effect was linked to an anti-inflammatory effect on ECs. This study demonstrated that EMPA promotes an anti-inflammatory phenotype which may be less prone to atherosclerosis. Specifically, EMPA treated HAAECs in static culture exhibited less cellular rounding than controls. Straight tube models were used to expose HAAECs to steady WSS to determine the baseline response before determining the cellular response to more complex models with WSSGs as was reported in chapters 3 and 4. Following exposure to steady WSS, EMPA treated HAAECs exhibited decreased leukocyte adhesion compared to controls. Also, expression of ICAM-1 and VCAM-1 was significantly reduced following exposure to steady WSS in EMPA treated HAAECs but not in controls. Interestingly, HS abundance was significantly increased in static cultures of EMPA treated HAAECs and after HS was enzymatically degraded, treating HAAECs for 24hr regained HS to control levels. This was also found to renew the morphological and leukocyte adhesion response which is typically attenuated by HS degradation. Together, these findings suggest that EMPA improves GCX health, promoting an

anti-inflammatory phenotype which could explain the decreased risk of cardiovascular disease in patients with type 2 diabetes taking this drug.

This manuscript is: Currently being finalized for submission to Molecular and Cellular Biochemistry

Empagliflozin promotes glycocalyx health in vitro demonstrating a mechanism for the decreased risk of cardiovascular disease following treatment in type 2 diabetics

Cooper, S[1]., Hwee, T.[3], Quan, A.[3,4], Verma, S.[3,4], Leask, R.L.[1,2]

[1]Department of Chemical Engineering, McGill University, Montreal, Quebec, Canada

[2]Montreal Heart Institute, Montreal, Quebec, Canada

[3]Keenan Research Centre for Biomedical Science, University of Toronto, Toronto, Ontario, Canada

[4]St Michaels Hospital, Toronto, Ontario, Canada

Abstract

Hyperglycemia in type 2 diabetes can be controlled with the sodium-glucose cotransporter protein inhibitor, empagliflozin (EMPA). Pleiotropically, EMPA has been shown to decrease the risk of cardiovascular disease, however, the mechanism of this effect has yet to be established. Endothelial cells (ECs) which line the arteries respond to fluid forces and their inflammation can initiate atherosclerosis. They sense the shear stress imparted by fluid flow, a term called mechanotransduction, in part by the surface proteoglycan layer, the glycocalyx. Flow experiments demonstrated that EMPA establishes an anti-inflammatory EC phenotype, *in vitro*. EMPA treatment altered EC phenotype with significant changes in morphology and leukocyte adhesion. Further, EMPA treatment improved glycocalyx expression and was able to restore components of this structure following enzymatic degradation. This resulted in a renewed

mechanotransduction response in ECs and presents a mechanism by which EMPA can improve vascular health.

5.2 Introduction

Type 2 diabetes (T2D) is characterized by impaired insulin secretion and action which leads to increased blood glucose levels in patients [162]. The disease can lead to both acute and chronic vascular complications on the microscale (such as retinopathy and nephropathy) and macroscale (such as heart attack and stroke) [108]. Sodium glucose cotransporters (SGLTs) are a class of molecules that mediate the reuptake of glucose from the kidneys to help control blood glucose levels in patients. SGLT-2 is a low affinity, high capacity glucose cotransporter which is responsible for the reabsorption of up to 90% of glucose filtered by the kidneys. Its inhibition has been shown to block the reabsorption of glucose in the kidney leading to glucose elimination through the urine reducing blood glucose levels [163]. This has lead to the development of C-glucoside SGLT-2 inhibitors, such as empagliflozin (EMPA), for the treatment of T2D. EMPA has demonstrated a high degree of selectivity for SGLT-2 over SGLT-1, 4, 5 and 6 compared to other C-glucoside SGLT-2 inhibitors [164]. Further, *in vitro* studies have demonstrated the inhibitory potency of EMPA [164] and clinical trials have confirmed its efficacy in lowering blood glucose levels, blood pressure and body weight in T2D patients without increasing the risk of hypoglycemia [109-112].

T2D results in up to a 5-fold increase in prevalence of heart failure and is responsible for an increased risk of developing cardiovascular disease [165]. Although it is postulated that increased glucose concentrations could lead to increased occurrence of cardiovascular disease, little proof supports that glycaemic control reduces this risk [114-116]. However, trials have shown that EMPA significantly reduces cardiovascular disease morbidity and related hospitalization by up to a third [113].

Endothelial cell (EC) inflammation is increased with T2D, notably resulting in degradation of the EC glycocalyx (GCX) [73, 166]. The GCX is a cell surface proteoglycan layer which has been linked to mechanotransduction of wall shear stress (WSS) and is implicated in the focal nature of atherosclerosis [73, 149]. Its structure is comprised of core proteins anchoring glycosaminoglycans of which heparan sulphate (HS) is the most abundant [37]. It is a dynamic structure which is constantly shed and regrown and compromising its integrity can detrimentally affect the vasculature.

This study investigated the effect EMPA had on EC health, *in vitro*. Through flow studies, markers of EC inflammation were evaluated in the presence of EMPA to determine whether it promotes an atheroprotective cellular phenotype. Further, EMPA's role in protecting and restoring the GCX was evaluated as a possible mechanism for observed changes in EC response and phenotype.

5.3 Materials and Methods

Cell Culture

Human abdominal aortic endothelial cells (HAAECs, Coriell, AG09799) were cultured for 48hr in 0.01% gelatin-coated T-175 flasks in incubators (37^{o}C, 100% humidity and 5% CO_2). The HAAECs were grown in EC media (PromoCell, C-22010) with 10% fetal bovine serum (Invitrogen, 26140-079) and 1% penicillin-streptomycin (Invitrogen, 15140-122).

In vitro experimentation was performed in straight tube, three-dimensional tissue culture models. The models were made of Sylgard®184 (Dow Corning), prepared as previously described [128]. Models were coated with 40 µg/mL fibronectin (Sigma Aldrich, F2006-5X5MG)

for 24 hours prior to a suspension of HAAECs being injected into the models at a density of $1x10^6$ cells/mL. The HAAECs were cultured for 48 hours, with a fresh media change after 24 hours, allowing them to establish a confluent monolayer on the models' luminal surface.

NB4 cells were cultured in suspension in T-75 flasks with RPMI Media (Global Cell Solutions, 89140-464) containing 10% fetal bovine serum (Invitrogen, 26140-079) and 1% penicillin-streptomycin (Invitrogen, 15140-122). NB4 cells were treated with RPMI media spiked with 10^{-6} M all-trans retinoic acid (ATRA) (Life Sciences, 89158-732) for 48hr prior to adhesion assays to promote differentiation into neutrophil-like cells characterized by increased expression of neutrophil specific integrins [130]. For adhesion assays, stimulated NB4 cells were suspended in EC media at a cell density of $1x10^6$ cells/mL.

Empagliflozin Stimulation

Stock solutions of EMPA (MedChem Express, HY-15409) were prepared as a 100mM solution and stored at -80^{o}C until use. During 24hr static culture or exposure to flow, EMPA was added to EC media to a final concentration of 50µM [107]. MTT assays identified no loss in cell viability from experimental EMPA concentration (data not shown).

HS Degradation

Heparan sulphate (HS) degradation was achieved by *heparinase III* (Sigma Aldrich, H8891-10UN) treatment as previously described [7, 149, 167]. Briefly, serum-free EC media was spiked with 180mU/mL *heparinase III* then introduced into the *in vitro* models for 2hr resulting in a decrease in HS of 33±4%, with no loss in cell viability [167]. Degradation was performed prior to

experimentation after which standard EC media with or without EMPA was reintroduced into the models.

Perfusion Experiments

Perfusion experiments were performed in a sterilized closed-loop in an incubator (37^{o}C, 100% humidity and 5% CO_2) as previously described [128]. Flow was controlled to maintain a uniform, steady WSS of 10 dyne/cm^2 in flow exposure experiments and 1 dyne/cm^2 in circulating NB4 adhesion assays.

Quantification of Cellular Morphology

Following perfusion experiments, ECs were stained with a 4% crystal violet (BD Biosciences) solution and imaged using an inverted light microscope (DC300, Leica Microsystems, Canada). A MatLab® protocol was used to analyze a minimum of 10 cells per image to determine the average shape index ($SI = \frac{4\pi * Area}{Perimeter^2}$), previously defined by Nerem et al [123].

NB4 Quantification

Leukocyte adhesion was investigated by circulating a neutrophil-like cell line (ATRA stimulated NB4 cells) through the *in vitro* models [4]. ECs were exposed to flow for 24 hours at a WSS of 10 dyne/cm^2 accompanied by stimulation with 10 ug/mL of the cytokine TNF-α to increase the adhesiveness of ECs [17]. Immediately after, a suspension of 1x10^6 NB4 cells/mL was circulated through the models at a WSS of 1 dyne/cm^2. Models were subsequently fixed using a 1% paraformaldehyde solution and imaged under an inverted light microscope (DC300, Leica

Microsystems, Canada) at 40x total magnification and adhered NB4 cells were manually counted.

Immunofluorescence Quantification

HAAECs were probed with a HS monoclonal antibody (Millipore, MAB2040), ICAM-1 monoclonal antibody (Santa Cruz, SC-8439) or VCAM-1 monoclonal antibody (Santa Cruz, SC-8304) and an alexflour® 488 secondary antibody (Invitrogen, A31570). Images were acquired with a laser scanning confocal microscope (Zeiss Exciter), and an average intensity of at least 10 cells per image was reported.

Statistical Analysis

All data expressed as mean ± standard mean of triplicate experiments. Analysis of results was completed using Graphpad Prism 5 software (Graphpad Software, La Jolla, CA). One-way and Two-way ANOVAs were used for comparisons when needed and were accompanied by multiple comparisons tests (Bonferroni post-hoc tests). Differences between means were considered significant at $P<0.05$.

5.4 Results

Treatment with EMPA Results in Elongation of HAAECs

The shape index (SI) of HAAECs treated with EMPA for 24hr in static culture or exposed to steady flow (WSS of 10dyne/cm^2) demonstrated a significant dependence on flow condition (two-way ANOVA, $P<0.001$) but not on EMPA treatment, with a significant interaction between

them (two-way ANOVA, P<0.05), Figure 1. In static culture, EMPA treated HAAECs were significantly more elongated than controls (Bonferroni post-hoc test, P<0.05)

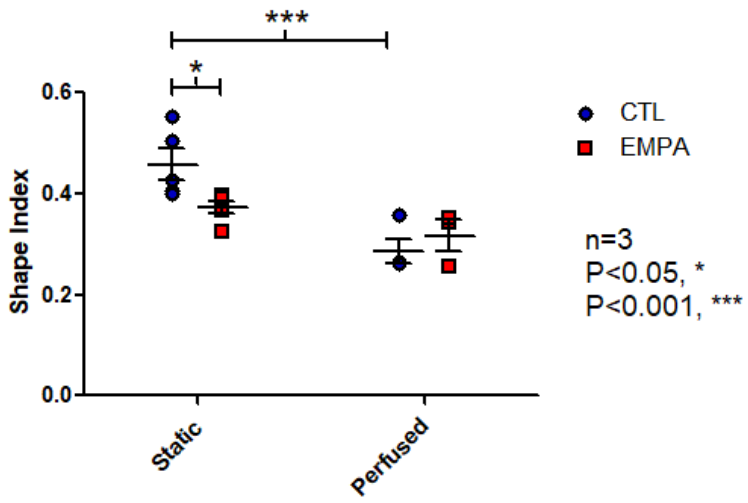

Figure 5-1: Analysis of shape index of HAAECs following 24hr of perfusion at a WSS of 10dyne/cm^2 with and without EMPA treatment (n=3, mean SI ± SEM). EMPA significantly elongated cells under static conditions (Bonferroni post-hoc test, P<0.05).

Treatment with EMPA Decreases NB4 Adhesion

NB4 cell adhesion was quantified after circulation through the models for 1hr following treatment of HAAECs for 24hr with EMPA, in static culture or exposed to steady flow (WSS of 10dyne/cm^2). Both flow condition and EMPA treatment had a significant effect on adhesion (two-way ANOVA, P<0.001 and P<0.001, respectively), including a significant interaction between them (two-way ANOVA, P<0.05), Figure 2. Following both static culture and exposure to flow, significantly lower adhesion was observed with EMPA treatment compared to controls (Bonferroni post-hoc test, P<0.01 and P<0.001, respectively).

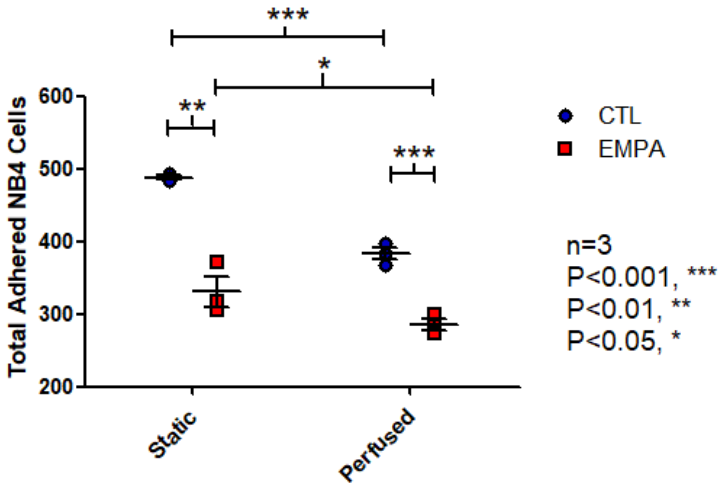

Figure 5-2: Total adhered NB4 cells after 24hr exposure to a WSS of 10dyne/cm^2 or statically cultured (n=3, mean ± SEM). EMPA treated HAAECs exhibited decreased NB4 adhesion under both static and perfused conditions (Bonferroni post-hoc test, P<0.01 and P<0.001, respectively). Further, following 24hr exposure to shear, both control and EMPA treated HAAECs exhibited significant lower NB4 adhesion (Bonferroni post-hoc test, P<0.001 and P<0.05, respectively).

CAM Expression

Cell-surface cellular adhesion molecule (CAM) expression was quantified using immunofluorescent imaging following 24hr exposure to flow (WSS of 10dyne/cm^2), with and without EMPA. For both VCAM-1 and ICAM-1, there was no significant difference between control and EMPA treated cells or an effect due to flow (two-way ANOVA). However, there was a significant decrease in both VCAM-1 and ICAM-1 in EMPA treated HAAECs following 24hr of exposure to flow compared to static culture (Bonferroni post-hoc test, both P<0.05), Figure 3a and 3b.

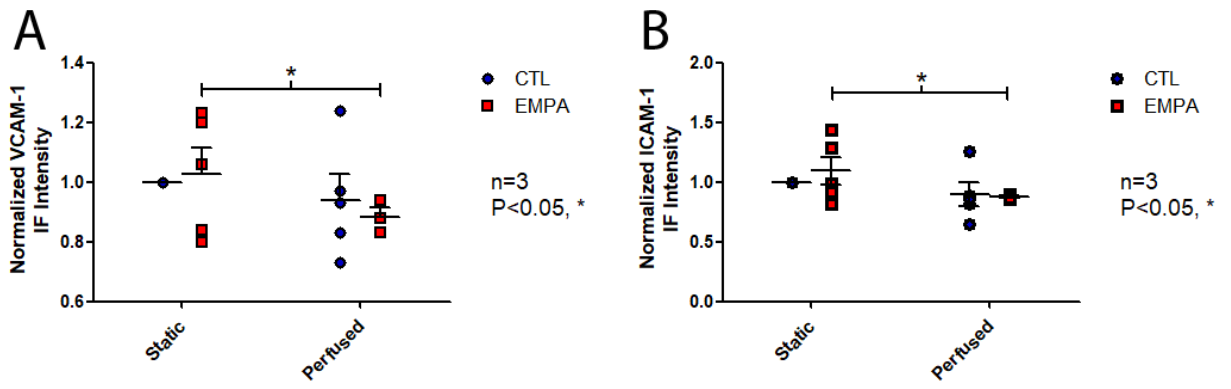

Figure 5-3: HAAEC surface A) VCAM-1 and B) ICAM-1 expression was quantified through imuunofluorescent imaging following 24hr of exposure to flow at a WSS of 10dyne/cm^2 with and without EMPA treatment (n=3, mean SI ± SEM). For both VCAM-1 and ICAM-1, a significant decrease in IF intensity was observed following perfusion on EMPA treated HAAECs (Bonferroni post-hoc test, P<0.05 and P<0.05, respectively).

Effects of HS Degradation Attenuated by EMPA

GCX health was evaluated through immunofluorescence imaging of HS on HS-degraded and control HAAECs following 24hr with EMPA treatment following either static culture or exposure to flow (WSS of 10dyne/cm^2). HS intensity was significantly affected by exposure to flow (two-way ANOVA, P<0.05) and HS-degradation (two-way ANOVA, P<0.01), Figure 4. HS-degradation significantly decreased HS intensity compared to controls and EMPA treated cultures (Bonferroni post-hoc test, P<0.001 and P<0.05, respectively). Further, HS-degraded HAAECs treated with EMPA exhibited significantly higher HS-intensity than control cultures after 24hr (Bonferroni post-hoc test, P<0.01).

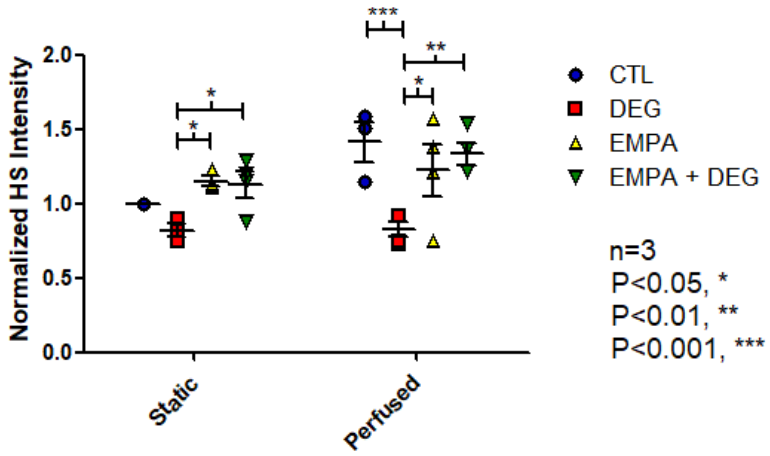

Figure 5-4: HS immunofluorescence intensity of HAAECs in either static culture or following exposure to 24hr of flow (WSS of 10dyne/cm^2) (n=3, mean IF intensity ± SEM). Experiments were performed on HAAECs immediately following HS-degradation (DEG), immediately following HS-degradation with EMPA treatment during flow conditioning/ static culture (DEG + EMPA) and controls (CTL) and EMPA treated (EMPA) cells. Both EMPA and EMPA+DEG HAAECs exhibited a significantly higher intensity than DEG in static culture (Bonferroni post-hoc test, P<0.05 and P<0.05, respectively) and following flow treatment (Bonferroni post-hoc test, P<0.05 and 0.001, respectively). After flow treatment, CTL HAAECs also exhibited a higher HS intensity than DEG (Bonferroni post-hoc test, P<0.001).

Adhesion and Morphology with Degradation

Following a 2hr enzymatic degradation of HS, HAAECs were exposed to 24hr of flow (WSS of 10dyne/cm^2) with and without EMPA treatment and analyzed for cell morphology and NB4 adhesion. The shape index of HAAECs was significantly affected by degradation and EMPA treatment as well as exposure to flow (two-way ANOVA, P<0.001 and P<0.001, respectively) with a significant interaction between them (two-way ANOVA, P<0.01). In static culture, HS-degraded and control HAAECs had a significantly higher shape index than HS-degraded cells that were also treated with EMPA (Bonferroni post-hoc test, P<0.001 and P<0.05, respectively), Figure 5a. Following 24hr exposure to flow, HS-degraded HAAECs were significantly more

rounded than both control and HS-degraded HAAECs that were also treated with EMPA (Bonferroni post-hoc test, P<0.001 and P<0.001, respectively).

Adhesion assays were performed by circulating NB4 cells for 1hr (WSS of 1dyne/cm^2) following 24hr exposure to flow (WSS of 10dyne/cm^2). HS-degraded HAAECs exhibited significantly higher NB4 adhesion compared to control and HS-degraded HAAECs that were also treated with EMPA (Bonferroni post-hoc test, P<0.001 and P<0.001, respectively), Figure 5b.

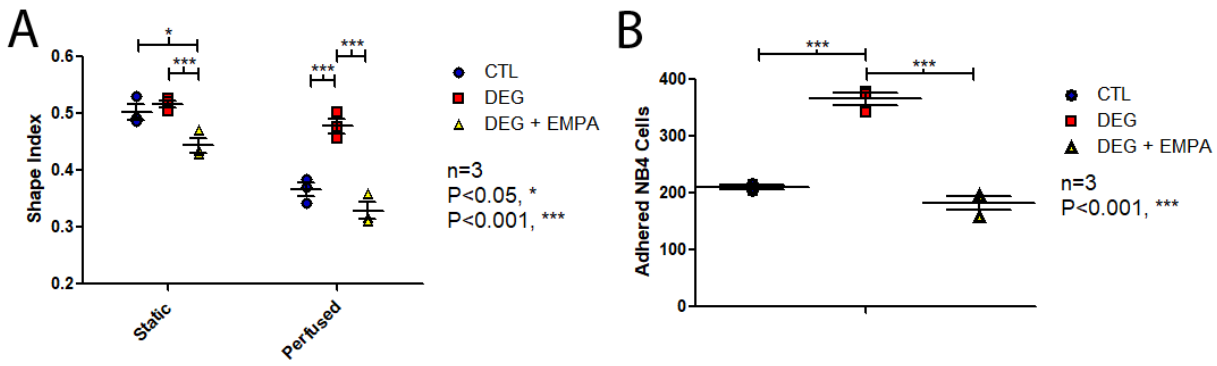

Figure 5-5: Shape index (SI) and NB4 adhesion following 24hr of exposure to flow (WSS of 10dyne/cm^2) on HAAECs immediately following HS-degradation (DEG), immediately following HS-degradation with EMPA treatment during flow conditioning/ static culture (DEG + EMPA) and controls (CTL). A) In static cultures, DEG+EMPA HAAECs exhibited a significantly lower SI than both CTL (Bonferroni post-hoc test, P<0.05) and DEG cultures (Bonferroni post-hoc test, P<0.001) (n=3, mean SI ± SEM). Both CTL and DEG+EMPA cultures exhibited a significantly lower SI than DEG HAAECs (Bonferroni post-hoc test, P<0.001). B) NB4 cells were circulated for 1hr (WSS of 1dyne/cm^2) following 24hr flow treatment CTL and DEG+EMPA HAAECs exhibited significantly lower adhesion than DEG cultures (Bonferroni post-hoc test, P<0.001) (n=3, total adhered NB4 ± SEM)

5.5 Discussion

The SGLT-2 inhibitor EMPA has been correlated with a decreased risk of cardiovascular disease in patients with T2D. This study demonstrated through *in vitro* flow experiments that EMPA improves glycocalyx health in HAAECs leading to an anti-inflammatory phenotype. Treatment of

HAAECs with EMPA showed increased HS abundance and following HS-degradation, EMPA treatment was shown to return HS levels within 24hr which also correlated with a regained mechanotransduction response.

The increased prevalence of cardiovascular disease in patients with T2D has been linked to inflammation of the endothelium [168-170]. This study demonstrated 24hr of treatment with EMPA resulted in an anti-inflammatory phenotype in ECs. In static culture, EMPA treated HAAECs exhibited significant reductions in shape index indicating cytoskeletal remodelling. Also, in both static culture and following exposure to steady WSS, a significant decrease in NB4 adhesion was observed in EMPA treated HAAECs. NB4 cells, a promyelocytic cell line, have been previously used as a surrogate for leukocyte adhesion [129] and numerous studies have shown EC inflammation is linked to increased adhesion [4, 17, 167, 171]. EMPA decreasing the quantity of adhesion therefore suggests that it promotes EC health by downregulating inflammatory phenotypes. It was observed that with flow, EMPA downregulated the quantity of the cellular adhesion molecules (CAM) VCAM-1 and ICAM-1. Exposure of ECs to moderate levels of steady WSS has previously been shown to affect CAM expression [172, 173] which correlates to decreased leukocyte adhesion [4]. However, levels of CAM expression were not significantly different between EMPA treated and control HAAECs so this does not explain the observed differences in adhesion. These findings agree with *in vivo* findings where 8 weeks of treatment with EMPA resulted in decreased serum levels of inflammatory markers such as TNF-α and IL-6 in mice [174].

Disruption of the EC GCX has been shown to increase adhesion both *in vitro* [120, 149] and *in vivo* [64, 144] and is suggested to be the result of the GCX sterically hindering adhesion [120].

Through immunofluorescent imaging, we observed a significant increase in HS abundance (a major GCX component) in static cultures of EMPA treated HAAECs. This was further confirmed by enzymatically degrading HS then demonstrating that 24hr of EMPA treatment returned the HS abundance to that of controls. This positive effect on GCX health could help explain the reduced prevalence of cardiovascular disease in T2D patients taking EMPA.

Beyond an increased abundance in HS brought on by EMPA treatment, a regained mechanotransduction response was also observed. The GCX acts as a mechanotransducer, linking the applied WSS on HAAECs to a biochemical and phenotypical cellular response. Numerous studies have documented that following enzymatic degradation of GCX components, an impaired response to WSS such as NO production [7], cellular alignment [5] and elongation [104] and NF-Kb nuclear localization [167]. In the present study, degradation of HS from HAAECs was immediately followed by assays to assess the morphological and NB4 adhesion response to exposure to 24hr of steady WSS. HS degradation abolished the typical cellular elongation and decrease in NB4 adhesion following flow treatment, which agrees with previous findings that mechanotransduction pathways were impaired [149, 167]. However, when the HS-degraded HAAECs were treated with EMPA during the flow exposure, they regained the mechanotransduction response and exhibited a similar morphology and quantity of adhesion as controls. This demonstrates that EMPA does not only promote glycocalyx health, but also can help improve the mechanotransduction properties in HAAECs.

The mechanism by which EMPA could improve vascular and GCX health is still not understood. SGLT inhibitors have been linked to membrane polarity through K+ channels [117]. GCX

structure and extension is highly dependent on charge so EMPA may be affecting membrane charge, promoting GCX health.

This study demonstrates that EMPA has a positive effect on HAAECs promoting an anti-inflammatory phenotype. We hypothesize this is due to promoting EC GCX health which is commonly impaired in patients with T2D.

Chapter 6: Discussion

The main objectives of this thesis were to: i) identify the role that the GCX plays in EC mechanotransduction, ii) determine how the GCX structure is regulated by biomolecules and mechanical forces and iii) identify the potential therapeutic benefits to the GCX from EMPA. Chapters 3 and 4 addressed the first and second objectives and Chapter 5 addressed the third.

The glycocalyx is a dynamic structure that is linked to the mechanotransduction of WSS in ECs. Its impairment in regions of WSSGs is an important factor in inflammation of the endothelium and plays a crucial role in the initiation of atherosclerosis. In our laboratory, three-dimensional tissue culture models have been developed that simulate a confluent endothelium for *in vitro* flow studies. This thesis expanded on a previously studied 50% asymmetric stenosis model (Chapter 3) and developed a model with a 180^{o} curvature (Chapter 4) to be able to examine GCX regulation in these physiological geometries. Flow-conditioning for 24hr with steady, uniform flow, corresponding to an inlet WSS of 10dyne/cm^2, was used throughout this thesis.

WSSGs have been linked to EC inflammation both *in vivo* and *in vitro* [2, 122]. Cell motility increases in response to WSSGs as ECs tend to migrate away from gradient affected areas, *in vitro* [175, 176]. Morphological analysis has shown that ECs tend to adopt a rounded shape in response to WSSGs [104, 149]. Further, cellular alignment with flow has been found to be impaired with WSSGs [177] and has been linked with a loss in actin fibre reorganization [178]. Recruitment of leukocytes has also been shown to be increased in the presence of WSSGs [4, 135]. *In vivo*, high WSS and WSSGs have been linked to atherosclerotic plaque destabilization

and intracranial aneurism formation and rupture prominently in regions of arterial curvature and bifurcation [179].

The GCX has been implicated in the mechanotransduction of WSS and its components have been linked to various inflammatory responses. HS has been linked to EC responses such as NO production [5], cellular alignment [7] and elongation [104] and leukocyte attachment [64, 121, 149]. Building on these studies, work in our lab by McDonald *et al* demonstrated that HS played a role in the regulation of NF-κB activity in response to flow [167]. Further, increased leukocyte adhesion was observed with degradation of HS which was hypothesized to be the result of a loss of steric hindrance to firm adhesion as well as a novel feedback loop involving NF-κB regulation and ICAM-1 expression. These studies were performed in regions of uniform WSS and this thesis aimed to continue this research to examine more complex flow regimes.

The first objective was to determine the role the GCX played in mechanotransduction in regions of WSSGs. HS is a primary constituent of the GCX and was therefore chosen as a target for disruption when evaluating EC mechanotransduction. Numerous studies have identified HS as vital to the flow induced regulation of a variety of biomolecules and inflammatory pathways [5-7, 38, 73, 96, 104, 118, 120, 134, 149, 180]. A protocol was developed to enzymatically degrade cell surface HS by approximately a third (as determined by immunofluorescence) using *Heparinase III*. Immediately prior to flow conditioning, this protocol was used to impair the GCX. It should be noted that HS was previously shown to not regrow within the timescale of experimentation [167]. ECs were then conditioned with flow and their response was compared to controls with an intact GCX.

Studies began on the 50% asymmetric stenosis model, Chapter 3. Rouleau *et al* previously identified inflammatory phenotypes in HAAECs in the acceleration and deceleration region of the stenosis, characterized by increased leukocyte adhesion and cellular rounding after 24hr of flow conditioning [3, 4]. When HS degradation was performed prior to flow conditioning, these response patterns were attenuated. The characteristic elongation of HAAECs in the model inlet (the internal control) were no longer observed and no increases in normalized leukocyte adhesion were observed in the acceleration and deceleration regions. This was indicative of a loss of the mechanotransduction capabilities of the ECs. HS has been implicated as a mechanotransducer of WSS, being linked to EC responses such as NO production [7], cell alignment [5] and elongation [104]. These studies were however only performed under steady WSS. Further, leukocyte adhesion patterns have been closely linked to GCX health both *in vitro* [120] and *in vivo* [64]. It is believed that it acts to provide steric hindrance, limiting the availability of adhesion molecules to circulating leukocytes [136]. Previously in our lab, McDonald *et al* proposed a mechanism where GCX impairment led to a deregulation of NF-κB nuclear localization which affected ICAM-1 expression and subsequently leukocyte adhesion [167].

Similarly, in the 180^{o} curve model, Chapter 4, experiments demonstrated an inflamed phenotype on the inner wall of curvature described by increased cellular rounding, decreased cellular alignment and a bias of leukocyte adhesion towards the inner wall of curvature. It was hypothesized that the WSSGs of the recirculating flow lead to this response. *In vitro*, inflammation has been documented with cellular rounding [154] and decreased cellular alignment [155] on the inner wall of curvature agreeing with these findings. *In vivo,* ECs in the

aortic arch have been found to have decreased alignment with flow [181] and this pattern has also been observed in other regions of curvature where complex hemodynamics exist [156]. Clinically, increased prevalence of plaque development on the inner wall of curvature has been well documented [157-159]. Leukocyte adhesion patterns have not been previously studied in regions of curvature however regions of low WSS and WSSGs have been linked to increased adhesion supporting the findings in this thesis [158]. Following enzymatic degradation of HS, the leukocyte adhesion bias was no longer observed, with patterns of HS-degraded models matching that of statically cultured controls. Both Chapters 3 and 4 therefore strengthened the hypothesis that: **1) the GCX plays a pivotal role in mechanotransduction of WSSGs**.

Next, the health of the GCX was investigated in regions of WSSGs. Previous *in vivo* studies have demonstrated that the GCX is impaired in regions of complex flow in the vasculature [63, 78, 143, 182]. To determine if this focal damage is caused by WSSGs, following flow conditioning, immunofluorescent imaging of HS and synd-1 was performed on HAAECs in the stenosis and curved models, Chapter 3 and 4, respectively. There was a significant decrease in both HS and synd-1 abundance in the regions of WSSGs proximal to the stenosis and in the Deans flow region in the curved model. Chapters 3 and 4 therefore supported the hypothesis that: **2) the GCX is focally shed in regions of WSSGs**, impairing EC health in these regions.

This finding was further investigated by determining the mechanism of GCX shedding. MMPs have been implicated in the cleavage of HS with attention being paid to the gelatinases, MMP-2 and -9 [68-70]. Increased expression and activity of gelatinases has also been found in regions of WSSGs [65, 66]. In Chapter 3, perfusion media containing a general MMP inhibitor, GM 6001, was included during flow conditioning. When HS expression was evaluated following

experimentation with GM 6001, the focal shedding was no longer observed, indicating that the inhibition of MMP activity attenuated this response. Moreover, when MMP activity was inhibited, leukocyte adhesion assays did not exhibit the same observed patterns as controls suggesting the improved GCX health resulted in decreases in adhesion in previously atheroprone regions. These findings agree with previous work by Lipowsky *et al* who observed attenuated GCX shedding and differences in leukocyte adhesion patterns following MMP inhibition, *in vitro* [143]. Mulivor *et al* observed similar affects *in vivo [144]*. In Chapter 4, gelatinase MMP activity was determined by *in situ* gel zymography, showing increased activity through the curve which correlated with HS shedding. Further, *ex situ* gel zymography demonstrated a significant increase in MMP-9 activity in the curve, again correlating with GCX shedding. Together, Chapters 3 and 4 strengthen the hypothesis: **2) the GCX is focally shed in regions of WSSGs** and proposes a mechanism of focally increased MMP activity.

Finally, a collaboration with clinicians investigating the SGLT-2 inhibitor, EMPA, demonstrated its ability to improve GCX health. EMPA is used for glycemic control in type 2 diabetics but has also been found to reduce the risk of cardiovascular disease. The mechanism of this pleiotropic effect was previously unknown, but the studies presented in Chapter 5 elucidated a possible explanation. Initial studies identified that treatment with EMPA resulted in an anti-inflammatory phenotype which was demonstrated by a less round morphology in static culture as well as decreased leukocyte adhesion in both static culture and following flow conditioning. The decreased adhesion, which we have previously shown to correlate with a healthier GCX, prompted experiments to determine if EMPA increases HS expression through immunofluorescent imaging. Following 24hr treatment with EMPA, significantly more HS was

expressed on the surface of HAAECs in static culture. Also, in both static culture and following flow conditioning, HAAECs with an enzymatically degraded GCX were able to regenerate expression of HS to levels comparable to controls when treated with EMPA. Moreover, EMPA treatment of HS degraded HAAECs demonstrated a renewed mechanotransduction response as noted by ECs regaining their elongated morphology and decreased leukocyte adhesion in response to uniform, steady WSS. Chapter 5 therefore supports the hypothesis: **3) EMPA pleiotropically promotes an anti-inflammatory EC phenotype by improving GCX health**. It also presents a clinical application where GCX health can be improved, helping decrease EC inflammation and subsequently the risk of cardiovascular disease in patients with type 2 diabetes.

Chapter 7: Conclusions

In conclusion, the work presented in this thesis demonstrated that disruption of the GCX resulted in an attenuated EC response to WSSGs, Chapter 3 and 4. It was also observed that regrowing this structure returned normal function to ECs as shown in Chapter 5. These findings support the hypothesis that **the GCX plays a pivotal role in mechanotransduction of WSSGs**. Further, the studies in Chapter 3 and 4 concluded that **the GCX is focally shed in regions of WSSGs** which mimicked the complex fluid dynamics in regions of the vasculature. The proinflammatory environment which is created in regions of disturbed flow is therefore intimately linked with GCX health, highlighting the importance of finding novel ways to protect this structure. This thesis demonstrated that EMPA, a drug designed for glycemic control in type 2 diabetics, may be one such strategy, as **EMPA pleiotropically promotes an anti-inflammatory EC phenotype by improving GCX health**.

Taken together, the work presented in this thesis highlights the role that the GCX plays in mechanotransduction and how regulation of this structure is vital to vascular health. Investigating new strategies to improve GCX health, such as drugs like EMPA, will provide researchers and clinicians effective tools to help prevent and treat cardiovascular disease.

Chapter 8: Future Work

The findings in this thesis provide a better understanding of the link between WSSGs and EC inflammation, however, they don't fully describe the fundamentals of this phenomenon. Although the WSSGs in this thesis are physiologically relevant, the "dose" response of specific WSSG magnitudes on EC response could provide a more in-depth description. Models should be developed capable of creating larger regions of specified WSSGs which can be varied based on simple flow rate or design changes. Not only could phenotypical changes such as morphology, GCX abundance and adhesion be quantified, but this could provide a larger pool of HAAECs under a specific flow condition so more compete analysis such as RNA and protein expression could be collected. This more specified approach should be done in conjunction with studies determining the pathways involved in GCX shedding. Including targeted inhibitors or gene silencing could provide a more detailed description of the role MMPs play and specify the molecules that are responsible for the disruption of different GCX components. Further, the "washdown effect" that was observed downstream of WSSGs in the stenosis and curved models could be better defined with these experiments.

The determination of GCX disruption and shedding is pivotal to this research so a more accurate way to measure this could increase the impact of findings. On the cell-surface level, a better way of imaging HS such as TEM using the RF/FS technique developed by Ebong *et al* [36] could prove to be more accurate than using immunofluorescence. LCMS quantification of HS has also been implemented which shows promise for future development [183]. Determining levels of HS in the media could also allow for a better description of the observed GCX shedding. Several

methods exist which could be implemented such as the use of enzyme-linked immunosorbent assays (ELISAs) as well as commercially developed mix-and-read assays specific to HS [184-187].

Work with EMPA is still in the early stages and needs to be advanced to elucidate how it improves cardiovascular outcomes. Although this thesis has strong evidence that EMPA helps promote GCX health, it is still unclear the mechanism that is responsible for this. Studies to investigate the ability of SGLT-2 inhibitors to alter the cell membrane and extracellular matrix should be a focus moving forward.

The evidence in this thesis that the GCX is intimately involved in the progression and initiation of atherosclerosis highlights the importance of better understanding this dynamic structure. As medical technologies advance, treatment strategies can be refined to hopefully slow or even prevent the development of atherosclerosis, helping to save millions of lives.

References

1. Weber C, Noels H. Atherosclerosis: current pathogenesis and therapeutic options. Nature medicine. 2011;17(11):1410-22. Epub 2011/11/09. doi: 10.1038/nm.2538. PubMed PMID: 22064431.
2. DeBakey ME, Lawrie GM, Glaeser DH. Patterns of atherosclerosis and their surgical significance. Annals of surgery. 1985;201(2):115-31. Epub 1985/02/01. PubMed PMID: 3155934; PubMed Central PMCID: PMCPMC1250631.
3. Rouleau L, Farcas M, Tardif JC, Mongrain R, Leask RL. Endothelial cell morphologic response to asymmetric stenosis hemodynamics: effects of spatial wall shear stress gradients. Journal of biomechanical engineering. 2010;132(8):081013. Epub 2010/07/31. doi: 10.1115/1.4001891. PubMed PMID: 20670062.
4. Rouleau L, Copland IB, Tardif JC, Mongrain R, Leask RL. Neutrophil adhesion on endothelial cells in a novel asymmetric stenosis model: effect of wall shear stress gradients. Annals of biomedical engineering. 2010;38(9):2791-804. Epub 2010/04/14. doi: 10.1007/s10439-010-0032-4. PubMed PMID: 20387119; PubMed Central PMCID: PMCPmc2915956.
5. Yao Y, Rabodzey A, Dewey CF, Jr. Glycocalyx modulates the motility and proliferative response of vascular endothelium to fluid shear stress. American journal of physiology Heart and circulatory physiology. 2007;293(2):H1023-30. Epub 2007/05/01. doi: 10.1152/ajpheart.00162.2007. PubMed PMID: 17468337.
6. Pahakis MY, Kosky JR, Dull RO, Tarbell JM. The role of endothelial glycocalyx components in mechanotransduction of fluid shear stress. Biochemical and biophysical research communications. 2007;355(1):228-33. Epub 2007/02/13. doi: 10.1016/j.bbrc.2007.01.137. PubMed PMID: 17291452; PubMed Central PMCID: PMCPmc1847369.
7. Florian JA, Kosky JR, Ainslie K, Pang Z, Dull RO, Tarbell JM. Heparan sulfate proteoglycan is a mechanosensor on endothelial cells. Circulation research. 2003;93(10):e136-42. Epub 2003/10/18. doi: 10.1161/01.res.0000101744.47866.d5. PubMed PMID: 14563712.
8. Tortora GJ. Principles of Human Anatomy. 13 ed2013.
9. Wilmer Nichols MOR, Charalambos Vlachopoulos. McDonald's Blood Flow in Arteries, Sixth Edition: Theoretical, Experimental and Clinical Principles. Sixth ed. Philadelphia: CRC Press; 2011 July 29, 2011. 768 p.
10. Waller BF, Orr CM, Slack JD, Pinkerton CA, Van Tassel JV, Peters T. Anatomy, histology, and pathology of coronary arteries: a review relevant to new interventional and imaging techniques--Part III. Clinical cardiology. 1992;15(8):607-15. Epub 1992/08/01. PubMed PMID: 1499190.
11. Crowther MA. Pathogenesis of atherosclerosis. Hematology American Society of Hematology Education Program. 2005:436-41. Epub 2005/11/24. doi: 10.1182/asheducation-2005.1.436. PubMed PMID: 16304416.
12. de Winther MP, Kanters E, Kraal G, Hofker MH. Nuclear factor kappaB signaling in atherogenesis. Arteriosclerosis, thrombosis, and vascular biology. 2005;25(5):904-14. Epub 2005/02/26. doi: 10.1161/01.atv.0000160340.72641.87. PubMed PMID: 15731497.
13. Chen F, Castranova V, Shi X. New insights into the role of nuclear factor-kappaB in cell growth regulation. The American journal of pathology. 2001;159(2):387-97. Epub 2001/08/04. PubMed PMID: 11485895; PubMed Central PMCID: PMCPMC1850555.
14. Kher N, Marsh JD. Pathobiology of atherosclerosis--a brief review. Seminars in thrombosis and hemostasis. 2004;30(6):665-72. Epub 2005/01/05. doi: 10.1055/s-2004-861509. PubMed PMID: 15630673.

15. Mehra VC, Ramgolam VS, Bender JR. Cytokines and cardiovascular disease. Journal of leukocyte biology. 2005;78(4):805-18. Epub 2005/07/12. doi: 10.1189/jlb.0405182. PubMed PMID: 16006537.
16. Hwang SJ, Ballantyne CM, Sharrett AR, Smith LC, Davis CE, Gotto AM, Jr., et al. Circulating adhesion molecules VCAM-1, ICAM-1, and E-selectin in carotid atherosclerosis and incident coronary heart disease cases: the Atherosclerosis Risk In Communities (ARIC) study. Circulation. 1997;96(12):4219-25. Epub 1998/01/07. PubMed PMID: 9416885.
17. Zhang C. The role of inflammatory cytokines in endothelial dysfunction. Basic research in cardiology. 2008;103(5):398-406. Epub 2008/07/05. doi: 10.1007/s00395-008-0733-0. PubMed PMID: 18600364; PubMed Central PMCID: PMCPMC2705866.
18. Libby P. Inflammation in atherosclerosis. Nature. 2002;420(6917):868-74. Epub 2002/12/20. doi: 10.1038/nature01323. PubMed PMID: 12490960.
19. Ross R. Atherosclerosis--an inflammatory disease. The New England journal of medicine. 1999;340(2):115-26. Epub 1999/01/14. doi: 10.1056/nejm199901143400207. PubMed PMID: 9887164.
20. Schwartz CJ, Valente AJ, Sprague EA, Kelley JL, Nerem RM. The pathogenesis of atherosclerosis: an overview. Clinical cardiology. 1991;14(2 Suppl 1):I1-16. Epub 1991/02/01. PubMed PMID: 2044253.
21. Nichols WW, Denardo SJ, Wilkinson IB, McEniery CM, Cockcroft J, O'Rourke MF. Effects of arterial stiffness, pulse wave velocity, and wave reflections on the central aortic pressure waveform. Journal of clinical hypertension (Greenwich, Conn). 2008;10(4):295-303. Epub 2008/04/11. PubMed PMID: 18401227.
22. Myers JG, Moore JA, Ojha M, Johnston KW, Ethier CR. Factors influencing blood flow patterns in the human right coronary artery. Annals of biomedical engineering. 2001;29(2):109-20. Epub 2001/04/04. PubMed PMID: 11284665.
23. Glagov S, Zarins C, Giddens DP, Ku DN. Hemodynamics and atherosclerosis. Insights and perspectives gained from studies of human arteries. Archives of pathology & laboratory medicine. 1988;112(10):1018-31. Epub 1988/10/01. PubMed PMID: 3052352.
24. Malek AM, Alper SL, Izumo S. Hemodynamic shear stress and its role in atherosclerosis. Jama. 1999;282(21):2035-42. Epub 1999/12/11. PubMed PMID: 10591386.
25. Dean WR. XVI. Note on the motion of fluid in a curved pipe. The London, Edinburgh, and Dublin Philosophical Magazine and Journal of Science. 1927;4(20):208-23. doi: 10.1080/14786440708564324.
26. Dean WR. LXXII. The stream-line motion of fluid in a curved pipe (Second paper). The London, Edinburgh, and Dublin Philosophical Magazine and Journal of Science. 1928;5(30):673-95. doi: 10.1080/14786440408564513.
27. Humphrey JAC, Iacovides H, Launder BE. Some numerical experiments on developing laminar flow in circular-sectioned bends. Journal of Fluid Mechanics. 1985;154:357-75. Epub 2006/04/20. doi: 10.1017/S0022112085001574.
28. M A M, Islam M, Rasel Sheikh M, Alam M. HIGH CURVATURE EFFECTS ON FLUID FLOW THROUGH CURVED PIPE WITH CIRCULAR CROSS-SECTION2008.
29. Nieuwdorp M, Mooij HL, Kroon J, Atasever B, Spaan JA, Ince C, et al. Endothelial glycocalyx damage coincides with microalbuminuria in type 1 diabetes. Diabetes. 2006;55(4):1127-32. Epub 2006/03/29. PubMed PMID: 16567538.
30. Zeng Y, Adamson RH, Curry FR, Tarbell JM. Sphingosine-1-phosphate protects endothelial glycocalyx by inhibiting syndecan-1 shedding. American journal of physiology Heart and circulatory physiology. 2014;306(3):H363-72. Epub 2013/11/29. doi: 10.1152/ajpheart.00687.2013. PubMed PMID: 24285115; PubMed Central PMCID: PMCPMC3920139.
31. Coombe DR, Kett WC. Heparan sulfate-protein interactions: therapeutic potential through structure-function insights. Cellular and molecular life sciences : CMLS. 2005;62(4):410-24. Epub 2005/02/19. doi: 10.1007/s00018-004-4293-7. PubMed PMID: 15719168.

32. Hileman RE, Fromm JR, Weiler JM, Linhardt RJ. Glycosaminoglycan-protein interactions: definition of consensus sites in glycosaminoglycan binding proteins. BioEssays : news and reviews in molecular, cellular and developmental biology. 1998;20(2):156-67. Epub 1998/06/19. doi: 10.1002/(sici)1521-1878(199802)20:2<156::aid-bies8>3.0.co;2-r. PubMed PMID: 9631661.
33. McGee MP, Liang J. Regulation of glycosaminoglycan function by osmotic potentials. Measurement of water transfer during antithrombin activation by heparin. The Journal of biological chemistry. 2001;276(52):49275-82. Epub 2001/10/26. doi: 10.1074/jbc.M104413200. PubMed PMID: 11677228.
34. Siegel G, Walter A, Kauschmann A, Malmsten M, Buddecke E. Anionic biopolymers as blood flow sensors. Biosensors & bioelectronics. 1996;11(3):281-94. Epub 1996/01/01. PubMed PMID: 8562009.
35. Siegel G, Malmsten M, Klussendorf D, Walter A, Schnalke F, Kauschmann A. Blood-flow sensing by anionic biopolymers. Journal of the autonomic nervous system. 1996;57(3):207-13. Epub 1996/03/07. PubMed PMID: 8964951.
36. Ebong EE, Macaluso FP, Spray DC, Tarbell JM. Imaging the endothelial glycocalyx in vitro by rapid freezing/freeze substitution transmission electron microscopy. Arteriosclerosis, thrombosis, and vascular biology. 2011;31(8):1908-15. Epub 2011/04/09. doi: 10.1161/atvbaha.111.225268. PubMed PMID: 21474821; PubMed Central PMCID: PMCPmc3141106.
37. Ihrcke NS, Wrenshall LE, Lindman BJ, Platt JL. Role of heparan sulfate in immune system-blood vessel interactions. Immunology today. 1993;14(10):500-5. Epub 1993/10/01. doi: 10.1016/0167-5699(93)90265-m. PubMed PMID: 8274190.
38. Weinbaum S, Zhang X, Han Y, Vink H, Cowin SC. Mechanotransduction and flow across the endothelial glycocalyx. Proceedings of the National Academy of Sciences of the United States of America. 2003;100(13):7988-95. Epub 2003/06/18. doi: 10.1073/pnas.1332808100. PubMed PMID: 12810946; PubMed Central PMCID: PMCPMC164700.
39. Barbee KA, Davies PF, Lal R. Shear stress-induced reorganization of the surface topography of living endothelial cells imaged by atomic force microscopy. Circulation research. 1994;74(1):163-71. Epub 1994/01/01. PubMed PMID: 8261591.
40. Wechezak AR, Wight TN, Viggers RF, Sauvage LR. Endothelial adherence under shear stress is dependent upon microfilament reorganization. Journal of cellular physiology. 1989;139(1):136-46. Epub 1989/04/01. doi: 10.1002/jcp.1041390120. PubMed PMID: 2708451.
41. Go YM, Park H, Maland MC, Jo H. In vitro system to study role of blood flow on nitric oxide production and cell signaling in endothelial cells. Methods in enzymology. 1999;301:513-22. Epub 1999/01/27. PubMed PMID: 9919599.
42. Tarbell JM, Shi ZD, Dunn J, Jo H. Fluid Mechanics, Arterial Disease, and Gene Expression. Annual review of fluid mechanics. 2014;46:591-614. Epub 2014/11/02. doi: 10.1146/annurev-fluid-010313-141309. PubMed PMID: 25360054; PubMed Central PMCID: PMCPMC4211638.
43. Chiu JJ, Wang DL, Chien S, Skalak R, Usami S. Effects of disturbed flow on endothelial cells. Journal of biomechanical engineering. 1998;120(1):2-8. Epub 1998/07/24. PubMed PMID: 9675673.
44. Li YS, Haga JH, Chien S. Molecular basis of the effects of shear stress on vascular endothelial cells. Journal of biomechanics. 2005;38(10):1949-71. Epub 2005/08/09. doi: 10.1016/j.jbiomech.2004.09.030. PubMed PMID: 16084198.
45. Levesque MJ, Nerem RM. The elongation and orientation of cultured endothelial cells in response to shear stress. Journal of biomechanical engineering. 1985;107(4):341-7. Epub 1985/11/01. PubMed PMID: 4079361.
46. Sprague AH, Khalil RA. Inflammatory cytokines in vascular dysfunction and vascular disease. Biochemical pharmacology. 2009;78(6):539-52. Epub 2009/05/06. doi: 10.1016/j.bcp.2009.04.029. PubMed PMID: 19413999; PubMed Central PMCID: PMCPMC2730638.

47. Ledebur HC, Parks TP. Transcriptional regulation of the intercellular adhesion molecule-1 gene by inflammatory cytokines in human endothelial cells. Essential roles of a variant NF-kappa B site and p65 homodimers. The Journal of biological chemistry. 1995;270(2):933-43. Epub 1995/01/13. PubMed PMID: 7822333.
48. Li YF, Xu XB, Chen XH, Wei G, He B, Wang JD. The nuclear factor-kappaB pathway is involved in matrix metalloproteinase-9 expression in RU486-induced endometrium breakdown in mice. Human reproduction (Oxford, England). 2012;27(7):2096-106. Epub 2012/05/17. doi: 10.1093/humrep/des110. PubMed PMID: 22587999.
49. Nagel T, Resnick N, Dewey CF, Jr., Gimbrone MA, Jr. Vascular endothelial cells respond to spatial gradients in fluid shear stress by enhanced activation of transcription factors. Arteriosclerosis, thrombosis, and vascular biology. 1999;19(8):1825-34. Epub 1999/08/14. PubMed PMID: 10446060.
50. Hajra L, Evans AI, Chen M, Hyduk SJ, Collins T, Cybulsky MI. The NF-kappa B signal transduction pathway in aortic endothelial cells is primed for activation in regions predisposed to atherosclerotic lesion formation. Proceedings of the National Academy of Sciences of the United States of America. 2000;97(16):9052-7. Epub 2000/08/02. PubMed PMID: 10922059; PubMed Central PMCID: PMCPMC16820.
51. Ley K, Laudanna C, Cybulsky MI, Nourshargh S. Getting to the site of inflammation: the leukocyte adhesion cascade updated. Nature reviews Immunology. 2007;7(9):678-89. Epub 2007/08/25. doi: 10.1038/nri2156. PubMed PMID: 17717539.
52. Chiu JJ, Lee PL, Chen CN, Lee CI, Chang SF, Chen LJ, et al. Shear stress increases ICAM-1 and decreases VCAM-1 and E-selectin expressions induced by tumor necrosis factor-[alpha] in endothelial cells. Arteriosclerosis, thrombosis, and vascular biology. 2004;24(1):73-9. Epub 2003/11/15. doi: 10.1161/01.atv.0000106321.63667.24. PubMed PMID: 14615388.
53. Campbell JJ, Hedrick J, Zlotnik A, Siani MA, Thompson DA, Butcher EC. Chemokines and the arrest of lymphocytes rolling under flow conditions. Science (New York, NY). 1998;279(5349):381-4. Epub 1998/02/07. PubMed PMID: 9430588.
54. Sternlicht MD, Werb Z. How matrix metalloproteinases regulate cell behavior. Annual review of cell and developmental biology. 2001;17:463-516. Epub 2001/11/01. doi: 10.1146/annurev.cellbio.17.1.463. PubMed PMID: 11687497; PubMed Central PMCID: PMCPMC2792593.
55. Van Wart HE, Birkedal-Hansen H. The cysteine switch: a principle of regulation of metalloproteinase activity with potential applicability to the entire matrix metalloproteinase gene family. Proceedings of the National Academy of Sciences of the United States of America. 1990;87(14):5578-82. Epub 1990/07/01. PubMed PMID: 2164689; PubMed Central PMCID: PMCPMC54368.
56. Nagase H, Suzuki K, Cawston TE, Brew K. Involvement of a region near valine-69 of tissue inhibitor of metalloproteinases (TIMP)-1 in the interaction with matrix metalloproteinase 3 (stromelysin 1). The Biochemical journal. 1997;325 (Pt 1):163-7. Epub 1997/07/01. PubMed PMID: 9224642; PubMed Central PMCID: PMCPMC1218541.
57. Vincenti MP, Brinckerhoff CE. Signal transduction and cell-type specific regulation of matrix metalloproteinase gene expression: can MMPs be good for you? Journal of cellular physiology. 2007;213(2):355-64. Epub 2007/07/27. doi: 10.1002/jcp.21208. PubMed PMID: 17654499.
58. Mach F, Schonbeck U, Sukhova GK, Bourcier T, Bonnefoy JY, Pober JS, et al. Functional CD40 ligand is expressed on human vascular endothelial cells, smooth muscle cells, and macrophages: implications for CD40-CD40 ligand signaling in atherosclerosis. Proceedings of the National Academy of Sciences of the United States of America. 1997;94(5):1931-6. Epub 1997/03/04. PubMed PMID: 9050882; PubMed Central PMCID: PMCPMC20020.

59. Yan C, Boyd DD. Regulation of matrix metalloproteinase gene expression. Journal of cellular physiology. 2007;211(1):19-26. Epub 2006/12/15. doi: 10.1002/jcp.20948. PubMed PMID: 17167774.
60. Kiran MS, Viji RI, Kumar SV, Prabhakaran AA, Sudhakaran PR. Changes in expression of VE-cadherin and MMPs in endothelial cells: Implications for angiogenesis. Vascular cell. 2011;3(1):6. Epub 2011/02/26. doi: 10.1186/2045-824x-3-6. PubMed PMID: 21349163; PubMed Central PMCID: PMCPMC3045352.
61. Yu Q, Stamenkovic I. Cell surface-localized matrix metalloproteinase-9 proteolytically activates TGF-beta and promotes tumor invasion and angiogenesis. Genes & development. 2000;14(2):163-76. Epub 2000/02/01. PubMed PMID: 10652271; PubMed Central PMCID: PMCPMC316345.
62. Li Q, Park PW, Wilson CL, Parks WC. Matrilysin shedding of syndecan-1 regulates chemokine mobilization and transepithelial efflux of neutrophils in acute lung injury. Cell. 2002;111(5):635-46. Epub 2002/12/05. PubMed PMID: 12464176.
63. Haldenby KA, Chappell DC, Winlove CP, Parker KH, Firth JA. Focal and regional variations in the composition of the glycocalyx of large vessel endothelium. Journal of vascular research. 1994;31(1):2-9. Epub 1994/01/01. PubMed PMID: 7506062.
64. Constantinescu AA, Vink H, Spaan JA. Endothelial cell glycocalyx modulates immobilization of leukocytes at the endothelial surface. Arteriosclerosis, thrombosis, and vascular biology. 2003;23(9):1541-7. Epub 2003/07/12. doi: 10.1161/01.atv.0000085630.24353.3d. PubMed PMID: 12855481.
65. Magid R, Murphy TJ, Galis ZS. Expression of matrix metalloproteinase-9 in endothelial cells is differentially regulated by shear stress. Role of c-Myc. The Journal of biological chemistry. 2003;278(35):32994-9. Epub 2003/06/21. doi: 10.1074/jbc.M304799200. PubMed PMID: 12816956.
66. Wang Z, Kolega J, Hoi Y, Gao L, Swartz DD, Levy EI, et al. Molecular alterations associated with aneurysmal remodeling are localized in the high hemodynamic stress region of a created carotid bifurcation. Neurosurgery. 2009;65(1):169-77; discussion 77-8. Epub 2009/07/04. doi: 10.1227/01.neu.0000343541.85713.01. PubMed PMID: 19574839; PubMed Central PMCID: PMCPMC2754173.
67. Yan L, Moses MA, Huang S, Ingber DE. Adhesion-dependent control of matrix metalloproteinase-2 activation in human capillary endothelial cells. Journal of cell science. 2000;113 (Pt 22):3979-87. Epub 2000/11/01. PubMed PMID: 11058085.
68. Hawinkels LJ, Zuidwijk K, Verspaget HW, de Jonge-Muller ES, van Duijn W, Ferreira V, et al. VEGF release by MMP-9 mediated heparan sulphate cleavage induces colorectal cancer angiogenesis. European journal of cancer (Oxford, England : 1990). 2008;44(13):1904-13. Epub 2008/08/12. doi: 10.1016/j.ejca.2008.06.031. PubMed PMID: 18691882.
69. Endo K, Takino T, Miyamori H, Kinsen H, Yoshizaki T, Furukawa M, et al. Cleavage of syndecan-1 by membrane type matrix metalloproteinase-1 stimulates cell migration. The Journal of biological chemistry. 2003;278(42):40764-70. Epub 2003/08/09. doi: 10.1074/jbc.M306736200. PubMed PMID: 12904296.
70. Manon-Jensen T, Multhaupt HA, Couchman JR. Mapping of matrix metalloproteinase cleavage sites on syndecan-1 and syndecan-4 ectodomains. The FEBS journal. 2013;280(10):2320-31. Epub 2013/02/07. doi: 10.1111/febs.12174. PubMed PMID: 23384311.
71. Gronski TJ, Jr., Martin RL, Kobayashi DK, Walsh BC, Holman MC, Huber M, et al. Hydrolysis of a broad spectrum of extracellular matrix proteins by human macrophage elastase. The Journal of biological chemistry. 1997;272(18):12189-94. Epub 1997/05/02. PubMed PMID: 9115292.
72. Li Z, Li L, Zielke HR, Cheng L, Xiao R, Crow MT, et al. Increased expression of 72-kd type IV collagenase (MMP-2) in human aortic atherosclerotic lesions. The American journal of pathology. 1996;148(1):121-8. Epub 1996/01/01. PubMed PMID: 8546199; PubMed Central PMCID: PMCPMC1861591.

73. Nieuwdorp M, van Haeften TW, Gouverneur MC, Mooij HL, van Lieshout MH, Levi M, et al. Loss of endothelial glycocalyx during acute hyperglycemia coincides with endothelial dysfunction and coagulation activation in vivo. Diabetes. 2006;55(2):480-6. Epub 2006/01/31. PubMed PMID: 16443784.
74. Caro CG, Fitz-Gerald JM, Schroter RC. Arterial wall shear and distribution of early atheroma in man. Nature. 1969;223(5211):1159-60. Epub 1969/09/13. PubMed PMID: 5810692.
75. Nieuwdorp M, Meuwese MC, Vink H, Hoekstra JB, Kastelein JJ, Stroes ES. The endothelial glycocalyx: a potential barrier between health and vascular disease. Current opinion in lipidology. 2005;16(5):507-11. Epub 2005/09/09. PubMed PMID: 16148534.
76. Mulivor AW, Lipowsky HH. Inflammation- and ischemia-induced shedding of venular glycocalyx. American journal of physiology Heart and circulatory physiology. 2004;286(5):H1672-80. Epub 2004/01/06. doi: 10.1152/ajpheart.00832.2003. PubMed PMID: 14704229.
77. Rubio-Gayosso I, Platts SH, Duling BR. Reactive oxygen species mediate modification of glycocalyx during ischemia-reperfusion injury. American journal of physiology Heart and circulatory physiology. 2006;290(6):H2247-56. Epub 2006/01/10. doi: 10.1152/ajpheart.00796.2005. PubMed PMID: 16399871.
78. Rehm M, Bruegger D, Christ F, Conzen P, Thiel M, Jacob M, et al. Shedding of the endothelial glycocalyx in patients undergoing major vascular surgery with global and regional ischemia. Circulation. 2007;116(17):1896-906. Epub 2007/10/10. doi: 10.1161/circulationaha.106.684852. PubMed PMID: 17923576.
79. Osuka A, Kusuki H, Yoneda K, Matsuura H, Matsumoto H, Ogura H, et al. Glycocalyx Shedding is Enhanced by Age and Correlates with Increased Fluid Requirement in Patients with Major Burns. Shock (Augusta, Ga). 2017. Epub 2017/10/13. doi: 10.1097/shk.0000000000001028. PubMed PMID: 29023362.
80. Rahbar E, Cardenas JC, Baimukanova G, Usadi B, Bruhn R, Pati S, et al. Endothelial glycocalyx shedding and vascular permeability in severely injured trauma patients. Journal of translational medicine. 2015;13:117. Epub 2015/04/19. doi: 10.1186/s12967-015-0481-5. PubMed PMID: 25889764; PubMed Central PMCID: PMCPMC4397670.
81. van Golen RF, van Gulik TM, Heger M. Mechanistic overview of reactive species-induced degradation of the endothelial glycocalyx during hepatic ischemia/reperfusion injury. Free radical biology & medicine. 2012;52(8):1382-402. Epub 2012/02/14. doi: 10.1016/j.freeradbiomed.2012.01.013. PubMed PMID: 22326617.
82. Singh A, Friden V, Dasgupta I, Foster RR, Welsh GI, Tooke JE, et al. High glucose causes dysfunction of the human glomerular endothelial glycocalyx. American journal of physiology Renal physiology. 2011;300(1):F40-8. Epub 2010/10/29. doi: 10.1152/ajprenal.00103.2010. PubMed PMID: 20980411; PubMed Central PMCID: PMCPMC3023224.
83. Becker BF, Chappell D, Bruegger D, Annecke T, Jacob M. Therapeutic strategies targeting the endothelial glycocalyx: acute deficits, but great potential. Cardiovascular research. 2010;87(2):300-10. Epub 2010/05/14. doi: 10.1093/cvr/cvq137. PubMed PMID: 20462866.
84. Li T, Liu X, Zhao Z, Ni L, Liu C. Sulodexide recovers endothelial function through reconstructing glycocalyx in the balloon-injury rat carotid artery model. Oncotarget. 2017;8(53):91350-61. doi: 10.18632/oncotarget.20518. PubMed PMID: PMC5710929.
85. Broekhuizen LN, Lemkes BA, Mooij HL, Meuwese MC, Verberne H, Holleman F, et al. Effect of sulodexide on endothelial glycocalyx and vascular permeability in patients with type 2 diabetes mellitus. Diabetologia. 2010;53(12):2646-55. Epub 2010/09/25. doi: 10.1007/s00125-010-1910-x. PubMed PMID: 20865240; PubMed Central PMCID: PMCPmc2974920.
86. Davies PF. Flow-mediated endothelial mechanotransduction. Physiological reviews. 1995;75(3):519-60. Epub 1995/07/01. PubMed PMID: 7624393; PubMed Central PMCID: PMCPMC3053532.

87. Olesen SP, Clapham DE, Davies PF. Haemodynamic shear stress activates a K+ current in vascular endothelial cells. Nature. 1988;331(6152):168-70. Epub 1988/01/14. doi: 10.1038/331168a0. PubMed PMID: 2448637.
88. Malek AM, Izumo S. Mechanism of endothelial cell shape change and cytoskeletal remodeling in response to fluid shear stress. Journal of cell science. 1996;109 (Pt 4):713-26. Epub 1996/04/01. PubMed PMID: 8718663.
89. Ridley AJ. Rho family proteins: coordinating cell responses. Trends in cell biology. 2001;11(12):471-7. Epub 2001/11/24. PubMed PMID: 11719051.
90. Tzima E, del Pozo MA, Shattil SJ, Chien S, Schwartz MA. Activation of integrins in endothelial cells by fluid shear stress mediates Rho-dependent cytoskeletal alignment. The EMBO journal. 2001;20(17):4639-47. Epub 2001/09/05. doi: 10.1093/emboj/20.17.4639. PubMed PMID: 11532928; PubMed Central PMCID: PMCPMC125600.
91. Yano Y, Saito Y, Narumiya S, Sumpio BE. Involvement of rho p21 in cyclic strain-induced tyrosine phosphorylation of focal adhesion kinase (pp125FAK), morphological changes and migration of endothelial cells. Biochemical and biophysical research communications. 1996;224(2):508-15. Epub 1996/07/16. doi: 10.1006/bbrc.1996.1057. PubMed PMID: 8702419.
92. Fujiwara K, Masuda M, Osawa M, Kano Y, Katoh K. Is PECAM-1 a mechanoresponsive molecule? Cell structure and function. 2001;26(1):11-7. Epub 2001/05/10. PubMed PMID: 11345499.
93. Desai G, Panick G, Zein M, Winter R, Royer CA. Pressure-jump studies of the folding/unfolding of trp repressor. Journal of molecular biology. 1999;288(3):461-75. Epub 1999/05/18. doi: 10.1006/jmbi.1999.2692. PubMed PMID: 10329154.
94. Shay-Salit A, Shushy M, Wolfovitz E, Yahav H, Breviario F, Dejana E, et al. VEGF receptor 2 and the adherens junction as a mechanical transducer in vascular endothelial cells. Proceedings of the National Academy of Sciences of the United States of America. 2002;99(14):9462-7. Epub 2002/06/25. doi: 10.1073/pnas.142224299. PubMed PMID: 12080144; PubMed Central PMCID: PMCPMC123163.
95. Hoger JH, Ilyin VI, Forsyth S, Hoger A. Shear stress regulates the endothelial Kir2.1 ion channel. Proceedings of the National Academy of Sciences of the United States of America. 2002;99(11):7780-5. Epub 2002/05/29. doi: 10.1073/pnas.102184999. PubMed PMID: 12032360; PubMed Central PMCID: PMCPMC124350.
96. Tarbell JM, Pahakis MY. Mechanotransduction and the glycocalyx. Journal of internal medicine. 2006;259(4):339-50. Epub 2006/04/06. doi: 10.1111/j.1365-2796.2006.01620.x. PubMed PMID: 16594902.
97. Secomb TW, Hsu R, Pries AR. Effect of the endothelial surface layer on transmission of fluid shear stress to endothelial cells. Biorheology. 2001;38(2-3):143-50. Epub 2001/05/31. PubMed PMID: 11381171.
98. Shi ZD, Wang H, Tarbell JM. Heparan sulfate proteoglycans mediate interstitial flow mechanotransduction regulating MMP-13 expression and cell motility via FAK-ERK in 3D collagen. PloS one. 2011;6(1):e15956. Epub 2011/01/20. doi: 10.1371/journal.pone.0015956. PubMed PMID: 21246051; PubMed Central PMCID: PMCPMC3016412.
99. Baeyens N, Mulligan-Kehoe MJ, Corti F, Simon DD, Ross TD, Rhodes JM, et al. Syndecan 4 is required for endothelial alignment in flow and atheroprotective signaling. Proceedings of the National Academy of Sciences. 2014;111(48):17308-13. doi: 10.1073/pnas.1413725111.
100. Lopes CC, Toma L, Pinhal MA, Porcionatto MA, Sogayar MC, Dietrich CP, et al. EJ-ras oncogene transfection of endothelial cells upregulates the expression of syndecan-4 and downregulates heparan sulfate sulfotransferases and epimerase. Biochimie. 2006;88(10):1493-504. Epub 2006/06/24. doi: 10.1016/j.biochi.2006.04.009. PubMed PMID: 16793191.
101. Conway DE, Breckenridge MT, Hinde E, Gratton E, Chen CS, Schwartz MA. Fluid shear stress on endothelial cells modulates mechanical tension across VE-cadherin and PECAM-1. Current biology : CB.

2013;23(11):1024-30. Epub 2013/05/21. doi: 10.1016/j.cub.2013.04.049. PubMed PMID: 23684974; PubMed Central PMCID: PMCPMC3676707.
102. Ebong EE, Depaola N. Specificity in the participation of connexin proteins in flow-induced endothelial gap junction communication. Pflugers Archiv : European journal of physiology. 2013;465(9):1293-302. Epub 2013/04/10. doi: 10.1007/s00424-013-1245-9. PubMed PMID: 23568367.
103. Helmke BP, Davies PF. The cytoskeleton under external fluid mechanical forces: hemodynamic forces acting on the endothelium. Annals of biomedical engineering. 2002;30(3):284-96. Epub 2002/06/08. PubMed PMID: 12051614.
104. Ebong EE, Lopez-Quintero SV, Rizzo V, Spray DC, Tarbell JM. Shear-induced endothelial NOS activation and remodeling via heparan sulfate, glypican-1, and syndecan-1. Integrative biology : quantitative biosciences from nano to macro. 2014;6(3):338-47. Epub 2014/02/01. doi: 10.1039/c3ib40199e. PubMed PMID: 24480876; PubMed Central PMCID: PMCPMC3996848.
105. Kalra S. Sodium Glucose Co-Transporter-2 (SGLT2) Inhibitors: A Review of Their Basic and Clinical Pharmacology. Diabetes Therapy. 2014;5(2):355-66. doi: 10.1007/s13300-014-0089-4. PubMed PMID: PMC4269649.
106. Gerich JE. Role of the kidney in normal glucose homeostasis and in the hyperglycaemia of diabetes mellitus: therapeutic implications. Diabetic medicine : a journal of the British Diabetic Association. 2010;27(2):136-42. Epub 2010/06/16. doi: 10.1111/j.1464-5491.2009.02894.x. PubMed PMID: 20546255; PubMed Central PMCID: PMCPMC4232006.
107. Vemula S, Roder KE, Yang T, Bhat GJ, Thekkumkara TJ, Abbruscato TJ. A Functional Role for Sodium-Dependent Glucose Transport across the Blood-Brain Barrier during Oxygen Glucose Deprivation. The Journal of Pharmacology and Experimental Therapeutics. 2009;328(2):487-95. doi: 10.1124/jpet.108.146589. PubMed PMID: PMC2630371.
108. DeFronzo RA, Ferrannini E, Groop L, Henry RR, Herman WH, Holst JJ, et al. Type 2 diabetes mellitus. Nature reviews Disease primers. 2015;1:15019. Epub 2015/01/01. doi: 10.1038/nrdp.2015.19. PubMed PMID: 27189025.
109. Dixit D, Yoon Y, Volino LR, Mansukhani RP. Empagliflozin: a sodium-glucose cotransporter 2 inhibitor for treatment of type 2 diabetes. American journal of health-system pharmacy : AJHP : official journal of the American Society of Health-System Pharmacists. 2015;72(22):1943-54. Epub 2015/11/07. doi: 10.2146/ajhp150071. PubMed PMID: 26541949.
110. Liakos A, Karagiannis T, Athanasiadou E, Sarigianni M, Mainou M, Papatheodorou K, et al. Efficacy and safety of empagliflozin for type 2 diabetes: a systematic review and meta-analysis. Diabetes, obesity & metabolism. 2014;16(10):984-93. Epub 2014/04/29. doi: 10.1111/dom.12307. PubMed PMID: 24766495.
111. Yoon KH, Nishimura R, Lee J, Crowe S, Salsali A, Hach T, et al. Efficacy and safety of empagliflozin in patients with type 2 diabetes from Asian countries: pooled data from four phase III trials. Diabetes, obesity & metabolism. 2016;18(10):1045-9. Epub 2016/06/07. doi: 10.1111/dom.12699. PubMed PMID: 27265507.
112. Devi R, Mali G, Chakraborty I, Unnikrishnan MK, Abdulsalim S. Efficacy and safety of empagliflozin in type 2 diabetes mellitus: a meta-analysis of randomized controlled trials. Postgraduate medicine. 2017;129(3):382-92. Epub 2016/11/15. doi: 10.1080/00325481.2017.1259544. PubMed PMID: 27841714.
113. Zinman B, Wanner C, Lachin JM, Fitchett D, Bluhmki E, Hantel S, et al. Empagliflozin, Cardiovascular Outcomes, and Mortality in Type 2 Diabetes. The New England journal of medicine. 2015;373(22):2117-28. Epub 2015/09/18. doi: 10.1056/NEJMoa1504720. PubMed PMID: 26378978.
114. Patel A, MacMahon S, Chalmers J, Neal B, Billot L, Woodward M, et al. Intensive blood glucose control and vascular outcomes in patients with type 2 diabetes. The New England journal of medicine. 2008;358(24):2560-72. Epub 2008/06/10. doi: 10.1056/NEJMoa0802987. PubMed PMID: 18539916.

115. Buse JB, Bigger JT, Byington RP, Cooper LS, Cushman WC, Friedewald WT, et al. Action to Control Cardiovascular Risk in Diabetes (ACCORD) trial: design and methods. The American journal of cardiology. 2007;99(12a):21i-33i. Epub 2007/07/12. doi: 10.1016/j.amjcard.2007.03.003. PubMed PMID: 17599422.
116. Holman RR, Paul SK, Bethel MA, Matthews DR, Neil HA. 10-year follow-up of intensive glucose control in type 2 diabetes. The New England journal of medicine. 2008;359(15):1577-89. Epub 2008/09/12. doi: 10.1056/NEJMoa0806470. PubMed PMID: 18784090.
117. Han Y, Cho Y-E, Ayon R, Guo R, Youssef KD, Pan M, et al. SGLT inhibitors attenuate NO-dependent vascular relaxation in the pulmonary artery but not in the coronary artery. American Journal of Physiology - Lung Cellular and Molecular Physiology. 2015;309(9):L1027-L36. doi: 10.1152/ajplung.00167.2015. PubMed PMID: PMC4628985.
118. Chappell D, Dorfler N, Jacob M, Rehm M, Welsch U, Conzen P, et al. Glycocalyx protection reduces leukocyte adhesion after ischemia/reperfusion. Shock (Augusta, Ga). 2010;34(2):133-9. Epub 2010/07/17. doi: 10.1097/SHK.0b013e3181cdc363. PubMed PMID: 20634656.
119. Lopez AD, Mathers CD, Ezzati M, Jamison DT, Murray CJ. Global and regional burden of disease and risk factors, 2001: systematic analysis of population health data. Lancet. 2006;367(9524):1747-57. Epub 2006/05/30. doi: 10.1016/s0140-6736(06)68770-9. PubMed PMID: 16731270.
120. Mulivor AW, Lipowsky HH. Role of glycocalyx in leukocyte-endothelial cell adhesion. American journal of physiology Heart and circulatory physiology. 2002;283(4):H1282-91. Epub 2002/09/18. doi: 10.1152/ajpheart.00117.2002. PubMed PMID: 12234777.
121. Giuffre L, Cordey AS, Monai N, Tardy Y, Schapira M, Spertini O. Monocyte adhesion to activated aortic endothelium: role of L-selectin and heparan sulfate proteoglycans. J Cell Biol. 1997;136(4):945-56. Epub 1997/02/24. PubMed PMID: 9049258; PubMed Central PMCID: PMCPmc2132500.
122. Alon R, Ley K. Cells on the run: shear-regulated integrin activation in leukocyte rolling and arrest on endothelial cells. Curr Opin Cell Biol. 2008;20(5):525-32. Epub 2008/05/24. doi: 10.1016/j.ceb.2008.04.003. PubMed PMID: 18499427.
123. Nerem RM, Levesque MJ, Cornhill JF. Vascular endothelial morphology as an indicator of the pattern of blood flow. Journal of biomechanical engineering. 1981;103(3):172-6. Epub 1981/08/01. PubMed PMID: 7278195.
124. van Haaren PM, VanBavel E, Vink H, Spaan JA. Localization of the permeability barrier to solutes in isolated arteries by confocal microscopy. American journal of physiology Heart and circulatory physiology. 2003;285(6):H2848-56. Epub 2003/08/09. doi: 10.1152/ajpheart.00117.2003. PubMed PMID: 12907418.
125. Lewis JC, Taylor RG, Jones ND, St Clair RW, Cornhill JF. Endothelial surface characteristics in pigeon coronary artery atherosclerosis. I. Cellular alterations during the initial stages of dietary cholesterol challenge. Laboratory investigation; a journal of technical methods and pathology. 1982;46(2):123-38. Epub 1982/02/01. PubMed PMID: 7062718.
126. Vink H, Duling BR. Identification of distinct luminal domains for macromolecules, erythrocytes, and leukocytes within mammalian capillaries. Circulation research. 1996;79(3):581-9. Epub 1996/09/01. PubMed PMID: 8781491.
127. Castier Y, Brandes RP, Leseche G, Tedgui A, Lehoux S. p47phox-dependent NADPH oxidase regulates flow-induced vascular remodeling. Circulation research. 2005;97(6):533-40. Epub 2005/08/20. doi: 10.1161/01.res.0000181759.63239.21. PubMed PMID: 16109921.
128. Farcas MA, Rouleau L, Fraser R, Leask RL. The development of 3-D, in vitro, endothelial culture models for the study of coronary artery disease. Biomedical engineering online. 2009;8:30. Epub 2009/10/30. doi: 10.1186/1475-925x-8-30. PubMed PMID: 19863806; PubMed Central PMCID: PMCPMC2773771.

129. Marchetti M, Falanga A, Giovanelli S, Oldani E, Barbui T. All-trans-retinoic acid increases adhesion to endothelium of the human promyelocytic leukaemia cell line NB4. British journal of haematology. 1996;93(2):360-6. Epub 1996/05/01. PubMed PMID: 8639429.
130. Brown DC, Tsuji H, Larson RS. All-trans retinoic acid regulates adhesion mechanism and transmigration of the acute promyelocytic leukaemia cell line NB-4 under physiologic flow. British journal of haematology. 1999;107(1):86-98. Epub 1999/10/16. PubMed PMID: 10520028.
131. McDonald KK, Cooper S, Danielzak L, Leask RL. Glycocalyx Degradation Induces a Proinflammatory Phenotype and Increased Leukocyte Adhesion in Cultured Endothelial Cells under Flow. PloS one. 2016;11(12). doi: 10.1371/journal.pone.0167576. PubMed PMID: 27907146; PubMed Central PMCID: PMCPmc5132265.
132. Lawrence MB, Kansas GS, Kunkel EJ, Ley K. Threshold levels of fluid shear promote leukocyte adhesion through selectins (CD62L,P,E). The Journal of cell biology. 1997;136(3):717-27. Epub 1997/02/10. PubMed PMID: 9024700; PubMed Central PMCID: PMCPmc2134292.
133. Grobelny D, Poncz L, Galardy RE. Inhibition of human skin fibroblast collagenase, thermolysin, and Pseudomonas aeruginosa elastase by peptide hydroxamic acids. Biochemistry. 1992;31(31):7152-4. Epub 1992/08/11. PubMed PMID: 1322694.
134. Thi MM, Tarbell JM, Weinbaum S, Spray DC. The role of the glycocalyx in reorganization of the actin cytoskeleton under fluid shear stress: a "bumper-car" model. Proceedings of the National Academy of Sciences of the United States of America. 2004;101(47):16483-8. Epub 2004/11/17. doi: 10.1073/pnas.0407474101. PubMed PMID: 15545600; PubMed Central PMCID: PMCPmc534550.
135. Uzarski JS, Scott EW, McFetridge PS. Adaptation of endothelial cells to physiologically-modeled, variable shear stress. PLoS One. 2013;8(2):e57004. Epub 2013/03/05. doi: 10.1371/journal.pone.0057004. PubMed PMID: 23457646; PubMed Central PMCID: PMCPmc3573044.
136. Lipowsky HH. The endothelial glycocalyx as a barrier to leukocyte adhesion and its mediation by extracellular proteases. Annals of biomedical engineering. 2012;40(4):840-8. Epub 2011/10/11. doi: 10.1007/s10439-011-0427-x. PubMed PMID: 21984514; PubMed Central PMCID: PMCPmc3306510.
137. Tamatani T, Miyasaka M. Identification of monoclonal antibodies reactive with the rat homolog of ICAM-1, and evidence for a differential involvement of ICAM-1 in the adherence of resting versus activated lymphocytes to high endothelial cells. International immunology. 1990;2(2):165-71. Epub 1990/01/01. PubMed PMID: 2088483.
138. Pries AR, Secomb TW, Gaehtgens P. The endothelial surface layer. Pflugers Archiv : European journal of physiology. 2000;440(5):653-66. Epub 2000/09/28. PubMed PMID: 11007304.
139. Bonetti PO, Lerman LO, Lerman A. Endothelial dysfunction: a marker of atherosclerotic risk. Arteriosclerosis, thrombosis, and vascular biology. 2003;23(2):168-75. Epub 2003/02/18. PubMed PMID: 12588755.
140. Hsieh HJ, Liu CA, Huang B, Tseng AH, Wang DL. Shear-induced endothelial mechanotransduction: the interplay between reactive oxygen species (ROS) and nitric oxide (NO) and the pathophysiological implications. Journal of biomedical science. 2014;21:3. Epub 2014/01/15. doi: 10.1186/1423-0127-21-3. PubMed PMID: 24410814; PubMed Central PMCID: PMCPMC3898375.
141. van den Berg BM, Spaan JA, Rolf TM, Vink H. Atherogenic region and diet diminish glycocalyx dimension and increase intima-to-media ratios at murine carotid artery bifurcation. American journal of physiology Heart and circulatory physiology. 2006;290(2):H915-20. Epub 2005/09/13. doi: 10.1152/ajpheart.00051.2005. PubMed PMID: 16155109.
142. Gouverneur M, Berg B, Nieuwdorp M, Stroes E, Vink H. Vasculoprotective properties of the endothelial glycocalyx: effects of fluid shear stress. Journal of internal medicine. 2006;259(4):393-400. Epub 2006/04/06. doi: 10.1111/j.1365-2796.2006.01625.x. PubMed PMID: 16594907.

143. Lipowsky HH, Lescanic A. The effect of doxycycline on shedding of the glycocalyx due to reactive oxygen species. Microvascular research. 2013;90:80-5. Epub 2013/08/01. doi: 10.1016/j.mvr.2013.07.004. PubMed PMID: 23899417; PubMed Central PMCID: PMCPMC3852187.
144. Mulivor AW, Lipowsky HH. Inhibition of glycan shedding and leukocyte-endothelial adhesion in postcapillary venules by suppression of matrixmetalloprotease activity with doxycycline. Microcirculation (New York, NY : 1994). 2009;16(8):657-66. Epub 2009/11/13. doi: 10.3109/10739680903133714. PubMed PMID: 19905966.
145. Dewey CF, Jr., Bussolari SR, Gimbrone MA, Jr., Davies PF. The dynamic response of vascular endothelial cells to fluid shear stress. Journal of biomechanical engineering. 1981;103(3):177-85. Epub 1981/08/01. PubMed PMID: 7278196.
146. Goode TB, Davies PF, Reidy MA, Bowyer DE. Aortic endothelial cell morphology observed in situ by scanning electron microscopy during atherogenesis in the rabbit. Atherosclerosis. 1977;27(2):235-51. Epub 1977/06/01. PubMed PMID: 71155.
147. Berger SA. Flow in Curved Pipes. Annual Review of Fluid Mechanics. 1983;15:461-512. doi: 10.1146/annurev.fl.15.010183.002333.
148. Nichols W, O'Rourke M, Vlachopoulos C. McDonald's Blood Flow in Arteries: Theoretical, Experimental and Clinical Principles. Sixth ed: CRC Press 2011 July 29, 2011. 768 p.
149. Cooper S, McDonald K, Burkat D, Leask RL. Stenosis Hemodynamics Disrupt the Endothelial Cell Glycocalyx by MMP Activity Creating a Proinflammatory Environment. Annals of biomedical engineering. 2017. Epub 2017/05/06. doi: 10.1007/s10439-017-1846-0. PubMed PMID: 28474270.
150. Zang C, Liu H, Ries C, Ismair MG, Petrides PE. Enhanced migration of the acute promyelocytic leukemia cell line NB4 under in vitro conditions during short-term all-trans-retinoic acid treatment. Journal of cancer research and clinical oncology. 2000;126(1):33-40. Epub 2000/01/21. PubMed PMID: 10641747.
151. Frankowski H, Gu YH, Heo JH, Milner R, Del Zoppo GJ. Use of gel zymography to examine matrix metalloproteinase (gelatinase) expression in brain tissue or in primary glial cultures. Methods in molecular biology (Clifton, NJ). 2012;814:221-33. Epub 2011/12/07. doi: 10.1007/978-1-61779-452-0_15. PubMed PMID: 22144310; PubMed Central PMCID: PMCPmc3670093.
152. Potter CM, Lundberg MH, Harrington LS, Warboys CM, Warner TD, Berson RE, et al. Role of shear stress in endothelial cell morphology and expression of cyclooxygenase isoforms. Arteriosclerosis, thrombosis, and vascular biology. 2011;31(2):384-91. Epub 2010/12/04. doi: 10.1161/atvbaha.110.214031. PubMed PMID: 21127291.
153. Wang Y, Mannino RG, Myers DR, Li W, Joiner CH, Lam WA. vessel geometry interacts with red blood cell stiffness to promote endothelial cell dysfunction in sickle cell disease Blood. 2015;126:965.
154. Potter CM, Schobesberger S, Lundberg MH, Weinberg PD, Mitchell JA, Gorelik J. Shape and compliance of endothelial cells after shear stress in vitro or from different aortic regions: scanning ion conductance microscopy study. PloS one. 2012;7(2):e31228. Epub 2012/02/24. doi: 10.1371/journal.pone.0031228. PubMed PMID: 22359578; PubMed Central PMCID: PMCPMC3281062.
155. Ghriallais RN, McNamara L, Bruzzi M. Comparison of in vitro human endothelial cell response to self-expanding stent deployment in a straight and curved peripheral artery simulator. Journal of the Royal Society, Interface. 2013;10(81):20120965. Epub 2013/02/01. doi: 10.1098/rsif.2012.0965. PubMed PMID: 23365191; PubMed Central PMCID: PMCPmc3627103.
156. Alloush MM, Oweis GF, Nasr R, Zeidan A, editors. An aortic arch flow loop for the study of hemodynamic-induced endothelial cell injury and inflammation. 2nd Middle East Conference on Biomedical Engineering; 2014 17-20 Feb. 2014.
157. Suo J, Ferrara DE, Sorescu D, Guldberg RE, Taylor WR, Giddens DP. Hemodynamic shear stresses in mouse aortas: implications for atherogenesis. Arteriosclerosis, thrombosis, and vascular biology.

2007;27(2):346-51. Epub 2006/11/24. doi: 10.1161/01.atv.0000253492.45717.46. PubMed PMID: 17122449.
158. Wahle A, Lopez JJ, Olszewski ME, Vigmostad SC, Chandran KB, Rossen JD, et al. Plaque development, vessel curvature, and wall shear stress in coronary arteries assessed by X-ray angiography and intravascular ultrasound. Med Image Anal. 2006;10(4):615-31. Epub 2006/04/29. doi: 10.1016/j.media.2006.03.002. PubMed PMID: 16644262; PubMed Central PMCID: PMCPmc2590653.
159. Smedby O, Johansson J, Molgaard J, Olsson AG, Walldius G, Erikson U. Predilection of atherosclerosis for the inner curvature in the femoral artery. A digitized angiography study. Arteriosclerosis, thrombosis, and vascular biology. 1995;15(7):912-7. Epub 1995/07/01. PubMed PMID: 7600123.
160. VanderLaan PA, Reardon CA, Getz GS. Site specificity of atherosclerosis: site-selective responses to atherosclerotic modulators. Arteriosclerosis, thrombosis, and vascular biology. 2004;24(1):12-22. Epub 2003/11/08. doi: 10.1161/01.ATV.0000105054.43931.f0. PubMed PMID: 14604830.
161. Moore JE, Jr., Ku DN, Zarins CK, Glagov S. Pulsatile flow visualization in the abdominal aorta under differing physiologic conditions: implications for increased susceptibility to atherosclerosis. Journal of biomechanical engineering. 1992;114(3):391-7. Epub 1992/08/11. PubMed PMID: 1295493.
162. Scheen AJ. Pathophysiology of type 2 diabetes. Acta clinica Belgica. 2003;58(6):335-41. Epub 2004/04/08. doi: 10.1179/acb.2003.58.6.001. PubMed PMID: 15068125.
163. Isaji M. Sodium-glucose cotransporter inhibitors for diabetes. Current opinion in investigational drugs (London, England : 2000). 2007;8(4):285-92. Epub 2007/04/27. PubMed PMID: 17458177.
164. Grempler R, Thomas L, Eckhardt M, Himmelsbach F, Sauer A, Sharp DE, et al. Empagliflozin, a novel selective sodium glucose cotransporter-2 (SGLT-2) inhibitor: characterisation and comparison with other SGLT-2 inhibitors. Diabetes, obesity & metabolism. 2012;14(1):83-90. Epub 2011/10/12. doi: 10.1111/j.1463-1326.2011.01517.x. PubMed PMID: 21985634.
165. Kannel WB, Hjortland M, Castelli WP. Role of diabetes in congestive heart failure: the Framingham study. The American journal of cardiology. 1974;34(1):29-34. Epub 1974/07/01. PubMed PMID: 4835750.
166. Salmon AH, Satchell SC. Endothelial glycocalyx dysfunction in disease: albuminuria and increased microvascular permeability. The Journal of pathology. 2012;226(4):562-74. Epub 2011/11/22. doi: 10.1002/path.3964. PubMed PMID: 22102407.
167. McDonald KK, Cooper S, Danielzak L, Leask RL. Glycocalyx Degradation Induces a Proinflammatory Phenotype and Increased Leukocyte Adhesion in Cultured Endothelial Cells under Flow. PloS one. 2016;11(12):e0167576. Epub 2016/12/03. doi: 10.1371/journal.pone.0167576. PubMed PMID: 27907146; PubMed Central PMCID: PMCPMC5132265.
168. Onat D, Brillon D, Colombo PC, Schmidt AM. Human vascular endothelial cells: a model system for studying vascular inflammation in diabetes and atherosclerosis. Current diabetes reports. 2011;11(3):193-202. Epub 2011/02/22. doi: 10.1007/s11892-011-0182-2. PubMed PMID: 21337131; PubMed Central PMCID: PMCPMC3311155.
169. Watts GF, O'Brien SF, Silvester W, Millar JA. Impaired endothelium-dependent and independent dilatation of forearm resistance arteries in men with diet-treated non-insulin-dependent diabetes: role of dyslipidaemia. Clinical science (London, England : 1979). 1996;91(5):567-73. Epub 1996/11/01. PubMed PMID: 8942395.
170. Tabit CE, Chung WB, Hamburg NM, Vita JA. Endothelial dysfunction in diabetes mellitus: molecular mechanisms and clinical implications. Reviews in endocrine & metabolic disorders. 2010;11(1):61-74. Epub 2010/02/27. doi: 10.1007/s11154-010-9134-4. PubMed PMID: 20186491; PubMed Central PMCID: PMCPMC2882637.
171. Cooper S, Dick M, Emmott A, Jonak P, Leask RL. In Vitro Leukocyte Adhesion in Endothelial Tissue Culture Models Under Flow. Biomedical Engineering. 3: InTech; 2011.

172. Tsuboi H, Ando J, Korenaga R, Takada Y, Kamiya A. Flow stimulates ICAM-1 expression time and shear stress dependently in cultured human endothelial cells. Biochemical and biophysical research communications. 1995;206(3):988-96. Epub 1995/01/26. doi: 10.1006/bbrc.1995.1140. PubMed PMID: 7832815.
173. Morigi M, Zoja C, Figliuzzi M, Foppolo M, Micheletti G, Bontempelli M, et al. Fluid shear stress modulates surface expression of adhesion molecules by endothelial cells. Blood. 1995;85(7):1696-703. Epub 1995/04/01. PubMed PMID: 7535583.
174. Han JH, Oh TJ, Lee G, Maeng HJ, Lee DH, Kim KM, et al. The beneficial effects of empagliflozin, an SGLT2 inhibitor, on atherosclerosis in ApoE (-/-) mice fed a western diet. Diabetologia. 2017;60(2):364-76. Epub 2016/11/21. doi: 10.1007/s00125-016-4158-2. PubMed PMID: 27866224.
175. Tardy Y, Resnick N, Nagel T, Gimbrone MA, Jr., Dewey CF, Jr. Shear stress gradients remodel endothelial monolayers in vitro via a cell proliferation-migration-loss cycle. Arteriosclerosis, thrombosis, and vascular biology. 1997;17(11):3102-6. Epub 1997/12/31 23:48. PubMed PMID: 9409299.
176. Ostrowski Maggie A, Huang Ngan F, Walker Travis W, Verwijlen T, Poplawski C, Khoo Amanda S, et al. Microvascular Endothelial Cells Migrate Upstream and Align Against the Shear Stress Field Created by Impinging Flow. Biophysical Journal. 2014;106(2):366-74. doi: https://doi.org/10.1016/j.bpj.2013.11.4502.
177. Sato M, Saito N, Sakamoto N, Ohashi T. High Wall Shear Stress Gradient Suppress Morphological Responses of Endothelial Cells to Fluid Flow. In: Dössel O, Schlegel WC, editors. World Congress on Medical Physics and Biomedical Engineering, September 7 - 12, 2009, Munich, Germany: Vol 25/4 Image Processing, Biosignal Processing, Modelling and Simulation, Biomechanics. Berlin, Heidelberg: Springer Berlin Heidelberg; 2010. p. 312-3.
178. Sakamoto N, Saito N, Han X, Ohashi T, Sato M. Effect of spatial gradient in fluid shear stress on morphological changes in endothelial cells in response to flow. Biochemical and biophysical research communications. 2010;395(2):264-9. Epub 2010/04/08. doi: 10.1016/j.bbrc.2010.04.002. PubMed PMID: 20371223.
179. Dolan JM, Kolega J, Meng H. High wall shear stress and spatial gradients in vascular pathology: a review. Annals of biomedical engineering. 2013;41(7):1411-27. Epub 2012/12/12. doi: 10.1007/s10439-012-0695-0. PubMed PMID: 23229281; PubMed Central PMCID: PMCPMC3638073.
180. Chappell D, Hofmann-Kiefer K, Jacob M, Rehm M, Briegel J, Welsch U, et al. TNF-alpha induced shedding of the endothelial glycocalyx is prevented by hydrocortisone and antithrombin. Basic research in cardiology. 2009;104(1):78-89. Epub 2008/10/07. doi: 10.1007/s00395-008-0749-5. PubMed PMID: 18836678.
181. Potter DR, Damiano ER. The hydrodynamically relevant endothelial cell glycocalyx observed in vivo is absent in vitro. Circulation research. 2008;102(7):770-6. Epub 2008/02/09. doi: 10.1161/circresaha.107.160226. PubMed PMID: 18258858.
182. Koo A, Dewey CF, Jr., Garcia-Cardena G. Hemodynamic shear stress characteristic of atherosclerosis-resistant regions promotes glycocalyx formation in cultured endothelial cells. Am J Physiol Cell Physiol. 2013;304(2):C137-46. Epub 2012/11/02. doi: 10.1152/ajpcell.00187.2012. PubMed PMID: 23114962; PubMed Central PMCID: PMCPmc3546807.
183. Dimitrievska S, Gui L, Weyers A, Lin T, Cai C, Wu W, et al. New Functional Tools for Antithrombogenic Activity Assessment of Live Surface Glycocalyx. Arteriosclerosis, thrombosis, and vascular biology. 2016;36(9):1847-53. Epub 2016/07/09. doi: 10.1161/atvbaha.116.308023. PubMed PMID: 27386939; PubMed Central PMCID: PMCPMC5283952.
184. Shafat I, Zcharia E, Nisman B, Nadir Y, Nakhoul F, Vlodavsky I, et al. An ELISA method for the detection and quantification of human heparanase. Biochemical and biophysical research communications. 2006;341(4):958-63. doi: 10.1016/j.bbrc.2006.01.048. PubMed PMID: PMC1484501.

185. Release of heparan sulfate from endothelial cells. Implications for pathogenesis of hyperacute rejection. The Journal of Experimental Medicine. 1990;171(4):1363-8. PubMed PMID: PMC2187844.
186. Rappold M, Warttinger U, Kramer R. A Fluorescent Probe for Glycosaminoglycans Applied to the Detection of Dermatan Sulfate by a Mix-and-Read Assay. Molecules (Basel, Switzerland). 2017;22(5). Epub 2017/05/10. doi: 10.3390/molecules22050768. PubMed PMID: 28486420.
187. Warttinger U, Giese C, Harenberg J, Holmer E, Kramer R. A fluorescent probe assay (Heparin Red) for direct detection of heparins in human plasma. Analytical and bioanalytical chemistry. 2016;408(28):8241-51. Epub 2016/10/22. doi: 10.1007/s00216-016-9940-y. PubMed PMID: 27655335.